BELL AEROSYSTEMS COMPANY
DIVISION OF BELL AEROSPACE CORPORATION

NOZZLE PERFORMANCE EVALUATION PROGRAM

BELL MODEL 8289

CONTRACT NAS9-1467

FINAL REPORT

REPORT NO. 8289-933002 DATE: 2-24-64

CONTENTS

Section		Page
I	INTRODUCTION	1
II	SUMMARY	2
III	HARDWARE DESIGN	4
	A. Over-all Design Considerations	4
	B. Injector	4
	C. Chamber Sections	6
	D. Start Nozzle (Sea Level)	9
	E. Altitude Nozzles	9
IV	SEA-LEVEL INJECTOR TEST PROGRAM	20
	A. General	20
	B. Cell 1AW Testing	20
	C. Cell 2ES Testing	22
	D. Discussion of Sea-Level Test Data	23
V	ALTITUDE TEST PROGRAM	37
	A. General	37
	B. 15° Conical Nozzle Testing, $\epsilon = 40$	38
	C. 15° Conical Nozzle Testing, $\epsilon = 60$	39
	D. Rao Nozzle Testing, $\epsilon = 40$	40
	E. 80% Bell Nozzle Testing, $\epsilon = 40$	40
	F. Discussion of Altitude Test Data	40
VI	DISCUSSION OF DATA ACCURACIES	67
	A. General	67
	B. Accuracy of Measured Thrust	68
	C. Accuracy of Measured Chamber Pressure	70
	D. Accuracy of Measured Flowrate	70
	E. Accuracy of Measured Throat Area	71
	F. Accuracy of Measured Altitude Pressure	71
	G. Accuracy of Computed Performance Parameters	72
	H. Performance Parameter Accuracy as Established from Errors in Independent Variables	73
VII	CONCLUSIONS AND RECOMMENDATIONS	76

CONTENTS (Cont'd)

Section		Page
VIII	APPENDIX	76
	A. Instrumentation	79
	B. Data-Reduction Procedures	82
	C. Statistical Data Analysis Methods	87
	D. Heat Transfer Data	92
	E. Injector Design Analysis	96
	F. N_2O_4 Flowmeter Calibrations	100
	G. Altitude Nozzles	102

ILLUSTRATIONS

Figure		Page
1	Injector Assembly	5
2	Injector Front View (Before Testing)	7
3	Water-Cooled Chamber Assembly Drawing	8
4	Start Hardware Composite	11
5	15° Conical Nozzle Throat Section Assembly Drawing	12
6	80% Bell Nozzle Throat Section Assembly Drawing	13
7	Rao Nozzle Throat Section Assembly Drawing	14
8	15° Conical Nozzle Extension Assembly Drawing	15
9	80% Bell Nozzle Extension Assembly Drawing	16
10	Rao Nozzle Extension Assembly Drawing	17
11	Water-Cooled Nozzle Throat Sections	18
12	Uncooled Nozzle Extensions	19
13	Test Cell 1AW Setup	26
14	Test Cell 2ES Sea-Level Setup	29
15	Cell 2ES Thrust Yoke and Load Cell Installation	30
16	Injector Characteristic Velocity (Sea-Level Data)	31
17	Injector Combustion Efficiency (Sea-Level Data)	32
18	Thrust Chamber Sea-Level Thrust Coefficient Corrected to Vacuum Conditions	33
19	Thrust Chamber Nozzle Efficiency (Start Nozzle)	34

Figure		Page
20	Thrust Chamber Sea-Level Specific Impulse Corrected to Vacuum Conditions	35
21	Thrust Chamber Over-all Efficiency (Sea-Level Data)	36
22	Altitude Test Facility	41
23	15° Conical Nozzle (ϵ=40) Installation	42
24	Altitude Facility Interior (Duct Section)	43
25	15° Conical Nozzle (ϵ=60) Duct Installation	44
26	Injector Characteristic Velocity (Combined Sea-Level and Altitude Data)	52
27	Injector Combustion Efficiency (Combined Sea-Level and Altitude Data)	53
28	Altitude Nozzle Vacuum Thrust Coefficients	54
29	Altitude Nozzle Efficiency	55
30	Thrust Chamber Altitude Specific Impulse Corrected to Vacuum Conditions (Actual Data)	56
31	Thrust Chamber Vacuum Specific Impulse Corrected to Vacuum Conditions (Average Data)	57
32	Thrust Chamber Over-all Efficiency - 15° Conical Nozzles (Altitude Data)	58
33	Thrust Chamber Over-all Efficiency - Contour Nozzles (Altitude Data)	59
34	Corrected Vacuum Specific Impulse - 15° Conical Nozzle, ϵ=40	60
35	Corrected Vacuum Specific Impulse - 15° Conical Nozzle, ϵ=60	61
36	Corrected Vacuum Specific Impulse - 80% Bell Nozzle, ϵ=40	62

Figure		Page
37	Corrected Vacuum Specific Impulse - Rao Nozzle, ϵ=40	63
38	Injector Front View (After Testing)	77
39	Injection Velocity Ratio Effects on Injector Combustion Efficiency	98
40	Injection Momentum Ratio Effects on Injector Combustion Efficiency	99
41	Altitude Nozzle Contours	104

TABLES

Table		
I	Sea-Level Injector Test Data - Cell 1AW	27
II	Sea-Level Injector Test Data - Cell 2ES	28
III	Altitude Test Data - 15° Conical Nozzles	45
IV	Altitude Test Data - Rao, 80% Bell Nozzles	46
V	Correction Factors for Vacuum Specific Impulse	64
VI	Corrected Vacuum Specific Impulse Data	65
VII	Undefined Nozzle Losses	66
VIII	Water-Cooled Hardware Heat Transfer Data	94
IX	Nozzle Extension Outer Surface Temperatures	95
X	Summary of Nozzle Aerodynamic Analysis	103

I. INTRODUCTION

Presented in this final report is the sea-level and altitude testing accomplished by the Bell Aerosystems Company on the Nozzle Performance Evaluation Program. The work was performed in accordance with Contract NAS9-1467 under the sponsorship and technical guidance of the National Aeronautics and Space Administration, Manned Spacecraft Center, Houston, Texas.

The primary program objective was to determine experimentally the altitude performance of four nozzles; three having exit area ratios (ϵ) of 40 and one having an area ratio of 60. The ϵ = 40 nozzles are a 15° conical, an 80% bell (Agena-type), and a Rao optimum contour. The ϵ = 60 nozzle was also a 15° conical type. Testing was conducted at a nominal thrust level and chamber pressure of 1000 pounds and 100 psia, respectively, over a nominal reactant ratio ($R_{o/f}$) range of 1.60 to 2.00. The propellants were N_2O_4 and a 50/50 blend of N_2H_4-UDMH.

The sea-level injector testing was conducted to evaluate injector performance (characteristic velocity) and to determine hardware durability.

The altitude test program was conducted to determine the performance of the previously mentioned nozzles at the nominal test conditions.

II. SUMMARY

The final report covers both the sea-level and altitude testing on the Nozzle Performance Evaluation Program. Testing was conducted at a nominal chamber pressure of 100 psia and over a nominal reactant ratio range of 1.60 to 2.00 using N_2O_4 and 50/50 N_2H_4-UDMH as propellants.

Fifty-eight test runs were conducted during this program: 28 during the sea-level injector testing and 30 during the altitude test program.

The injector demonstrated high performance and good stability during the entire test program. The durability of the injector and water-cooled chamber was also demonstrated with an accumulated sea-level firing duration of 442.5 seconds.

The altitude testing included 11 tests on the 15° conical (ϵ=40) nozzle, 6 tests each on the 15° conical (ϵ=60) and Rao (ϵ=40) nozzles, and 7 tests on the 80% Bell (ϵ=40) nozzle.

The injector combustion efficiency (based upon both sea-level and altitude data) varied linearly from approximately 0.965 to 0.976 over the reactant ratio range of 1.60 to 2.00 (based on theoretical equilibrium composition).

The experimental vacuum thrust coefficients (C_{f_∞}) follow the theoretical frozen composition data for all four nozzles evaluated.

The experimentally determined vacuum specific impulse (I_{sp_∞}) data have the following maximum values occurring at a reactant ratio of approximately 1.75:

Nozzle Type	I_{sp_∞} (sec)
15° Conical, ϵ=40	304.0
15° Conical, ϵ=60	307.5
80% Bell, ϵ=40	302.2
Rao, ϵ=40	300.4

The experimental vacuum specific impulse data were corrected for nozzle three dimensional, heat transfer, and friction losses. These data were then compared with theoretical performance data which had to be corrected for actual combustion efficiency. The experimental data were between the theoretical frozen composition and Bray analytical data in all cases except the low reactant ratio data on the 15° conical nozzles. These data lie slightly above the revised Bray curves. The corrected experimental data are (in all cases) within approximately 2% of the Bray analytical data.

The injector accumulated a total test duration of 1327.9 seconds during the over-all program without a measurable variation in performance.

III. HARDWARE DESIGN

A. OVER-ALL DESIGN CONSIDERATIONS

Consistent with meeting the over-all program objectives, the injector had to be capable of delivering high performance (combustion efficiency) with the N_2O_4 and 50/50 N_2H_4-UDMH propellants. Operating conditions would be at the nominal thrust and chamber pressure of 1000 pounds and 100 psia, respectively, over the reactant ratio range of 1.6 to 2.0. The injector must also have sufficient durability to maintain the consistent high-performance level throughout the projected test program. The over-all performance requirements indicated the desirability of utilizing a relatively large combustion chamber volume.

The data accuracy requirements indicated the desirability of having a relatively large thrust chamber contraction ratio, thus minimizing the corrections to measured chamber pressures (to obtain the total nozzle entrance pressure).

The durability of the nozzle extensions must be sufficient to permit the run durations required to obtain altitude system stabilization.

B. INJECTOR

The injector is a flat-face triplet design having a square grid pattern and fabricated from 6061 aluminum alloy. The oxidizer orifices are the central element of each triplet and are fed from a drilled grid pattern which is parallel to the injector face. The fuel is fed from the fuel manifold to the fuel orifices through pockets milled into the back surface of the orifice plate. The assembly drawing of the injector is shown in Figure 1.

The injector orifice plate design is based upon data from previous injectors and is essentially the primary (central) zone

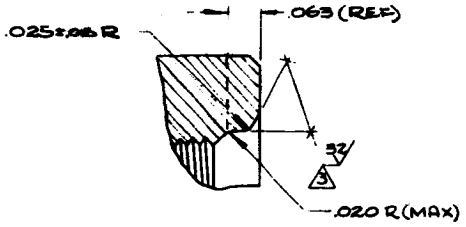

DETAIL B
(SCALE: NONE)

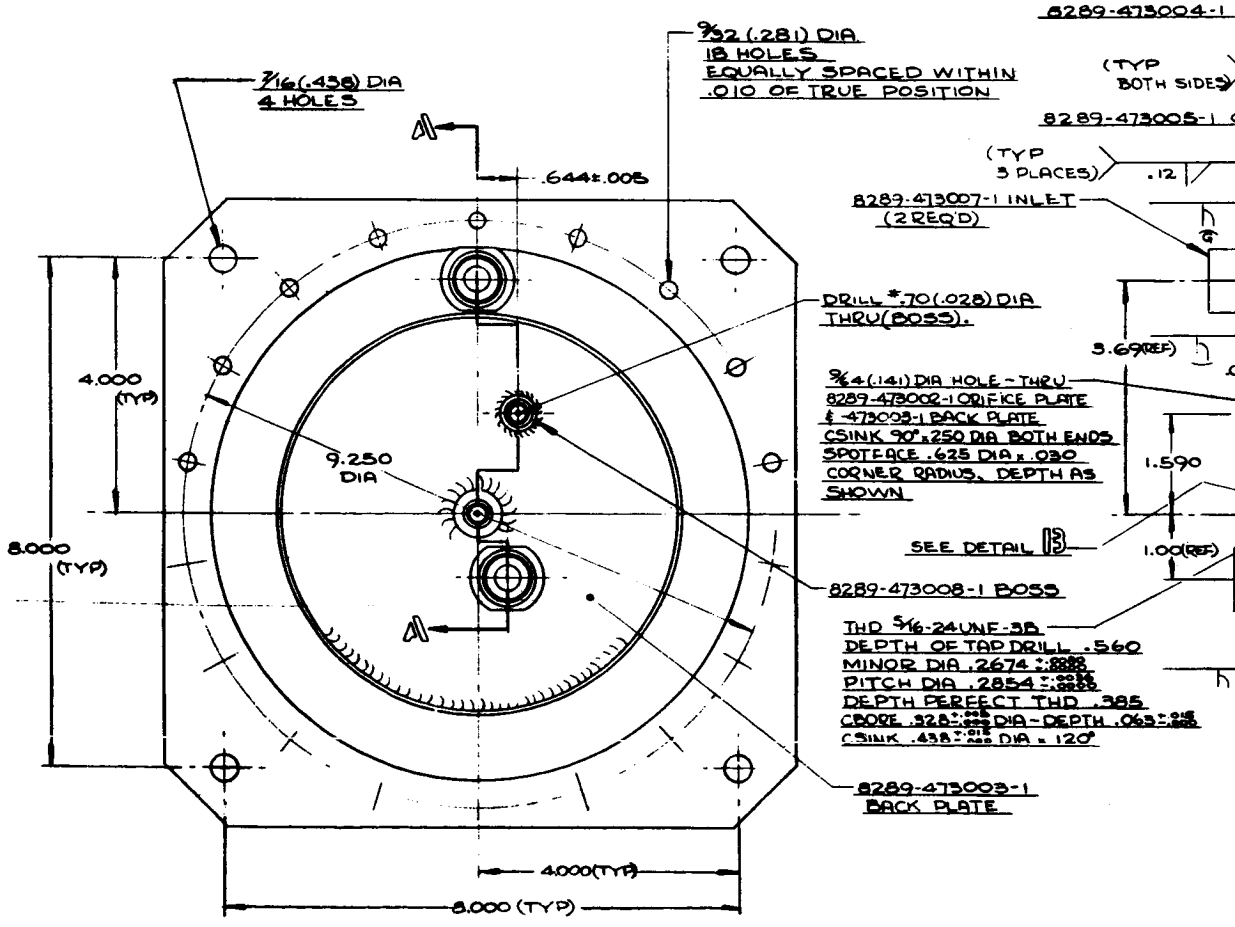

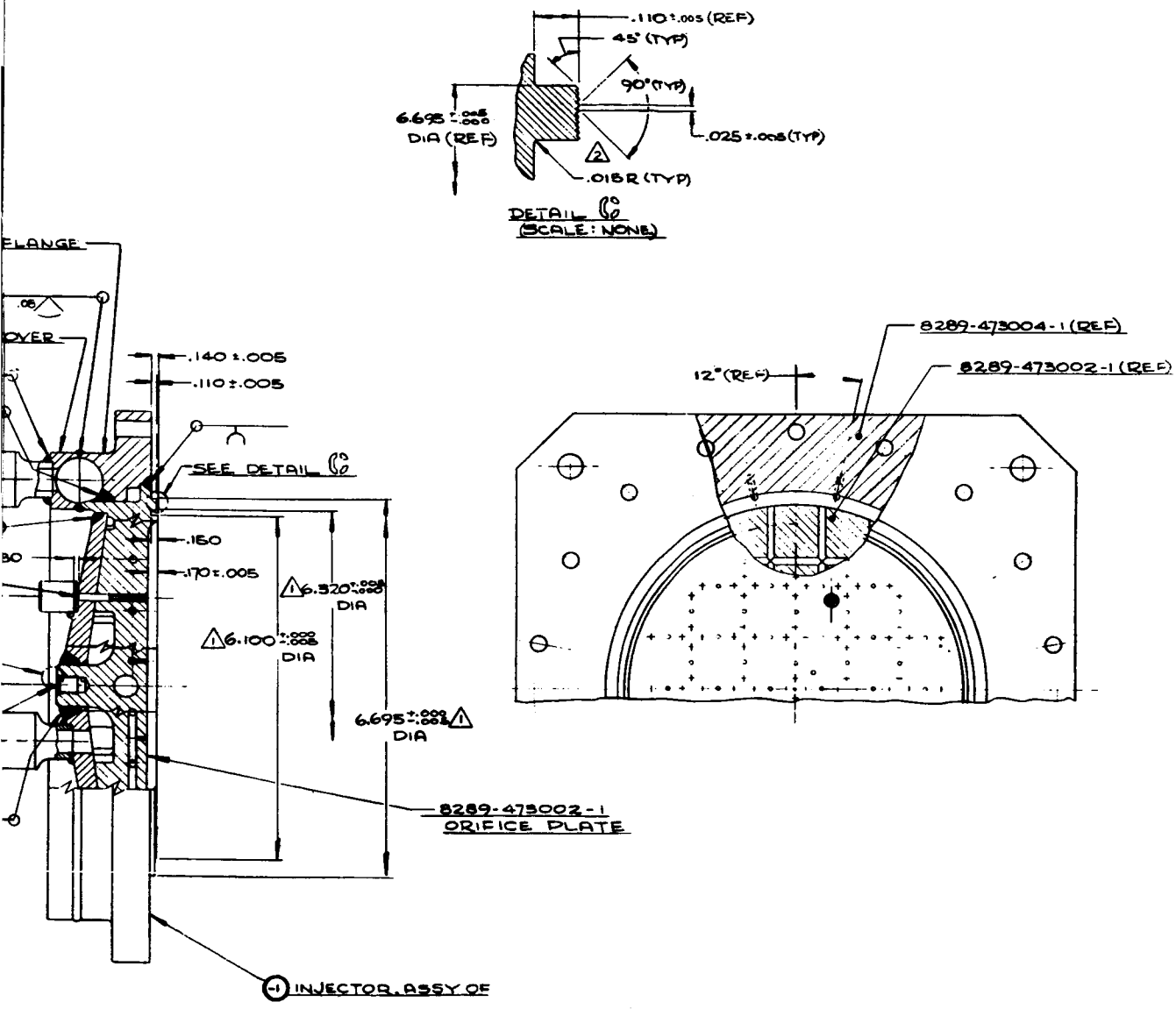

INJECTOR ASSEMBLY DRAWING

FIGURE 1

of the Agena-type injectors. The injector orifice plate has 52 triplets; the impingement half-angle and the distance from the injector face is 28° and 0.532 inch, respectively. The oxidizer and fuel orifices diameters are 0.037 and 0.022 inch, respectively, and have design pressure drops of 50 psi at the 1.80 reactant ratio. At this reactant ratio, the axial oxidizer-to-fuel velocity ratio (V_O/V_{FA}) is 0.901 and the axial oxidizer-to-fuel momentum ratio (M_O/M_{FA}) is 1.62. Figure 2 shows the front view of the injector before testing.

Consideration was given during the design of the injector to obtaining the required durability with a very low injector loading (propellant flow rate per unit surface area). Because of the relatively large contraction ratio, the injector loading of 0.11 pounds total flow/sec/in.^{2} is approximately one-fifth the value normally associated with this type of injector. The injector face cooling requirement indicated the desirability of having as large a number of triplet elements as possible. The number of triplet elements is limited, however, by the practical consideration of maintaining a reasonable orifice pressure drop (to obtain the desired combustion efficiency and stability) with orifice holes of sufficient size from the manufacturing consideration.

C. CHAMBER SECTIONS

Two chamber sections were utilized during the testing program. An uncooled, mild-steel start chamber was employed for the injector testing in Cell 1AW and a drilled aluminum water-cooled chamber was used during the Cell 2ES sea-level and altitude testing. Figure 3 shows the assembly drawing of the water-cooled chamber section utilized in the Cell 2ES testing.

All chamber sections have a characteristic length (L*) of approximately 63 inches and a cylindrical length/diameter ratio of 1.75. The gas side surfaces of all chambers were plasma-sprayed

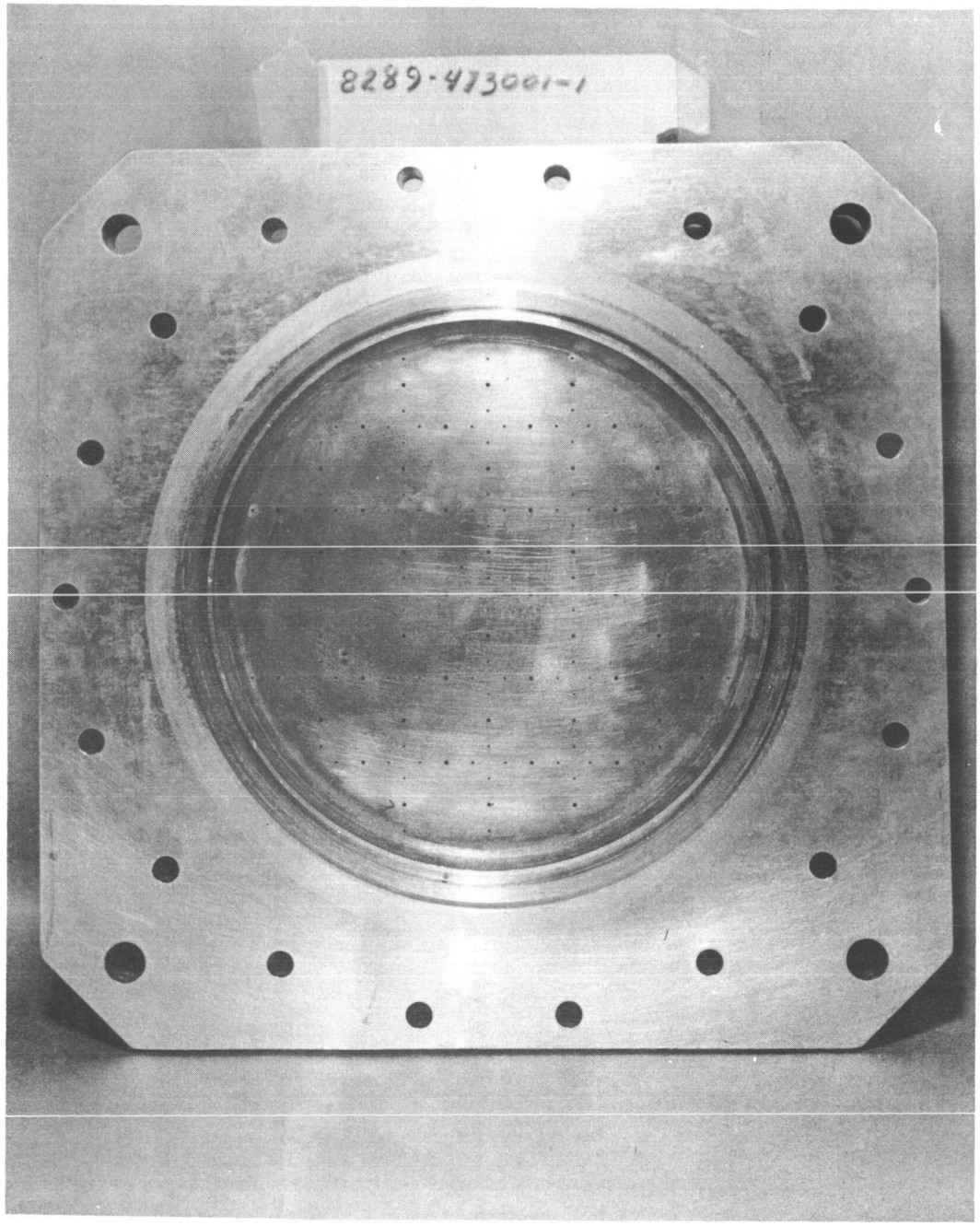

INJECTOR FRONT VIEW (BEFORE TESTING)

FIGURE 2

MODEL _____

DATE _____

BELL AERO

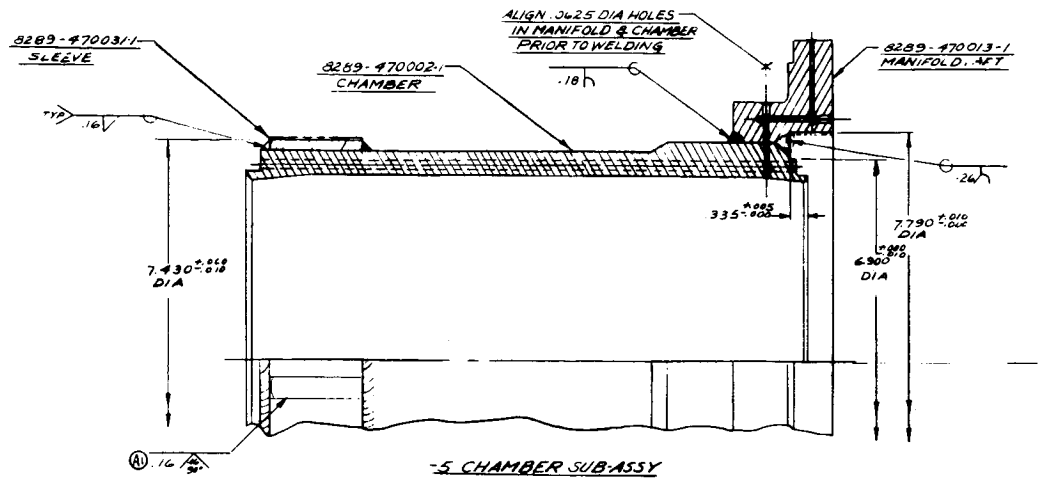

-5 CHAMBER SUB-ASSY

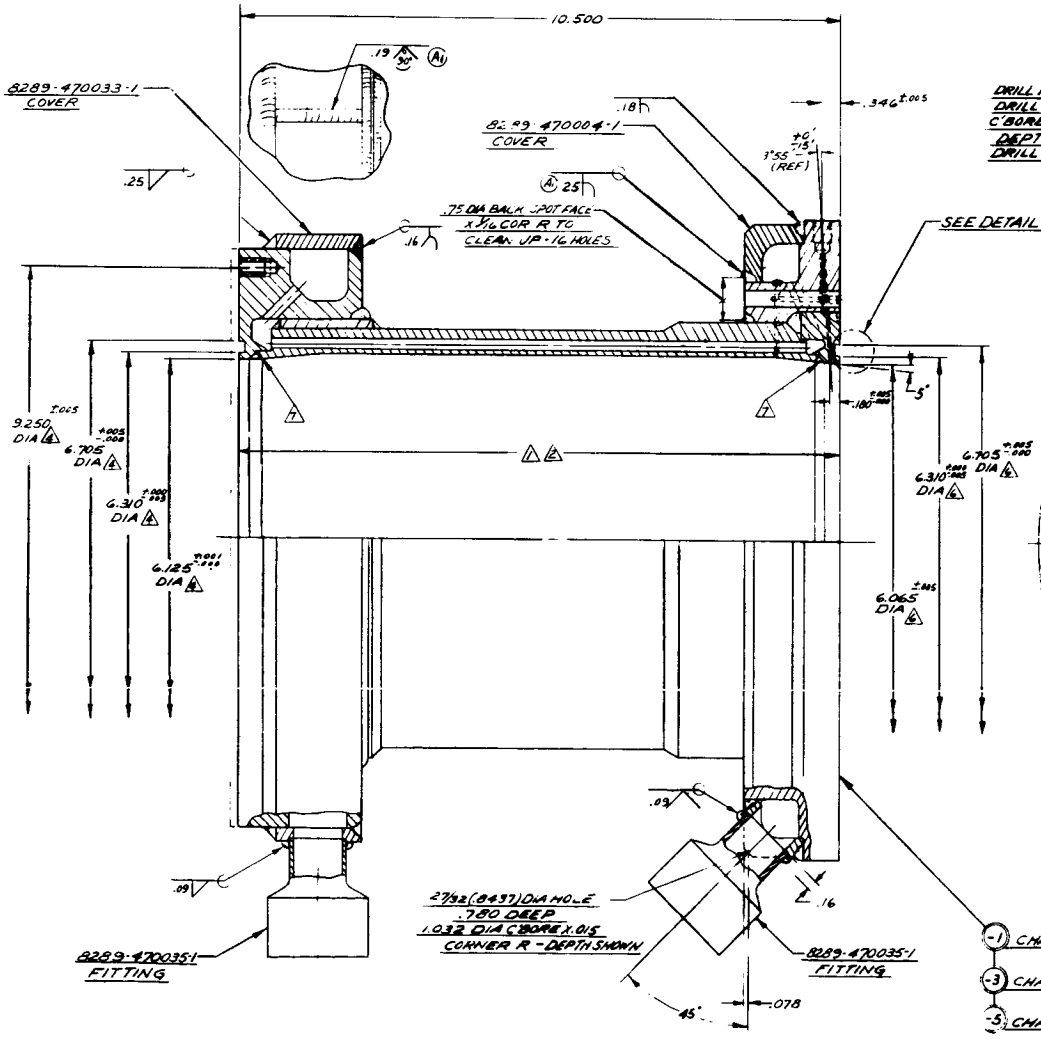

Form 0345 Rev. 1258 Sheet 1

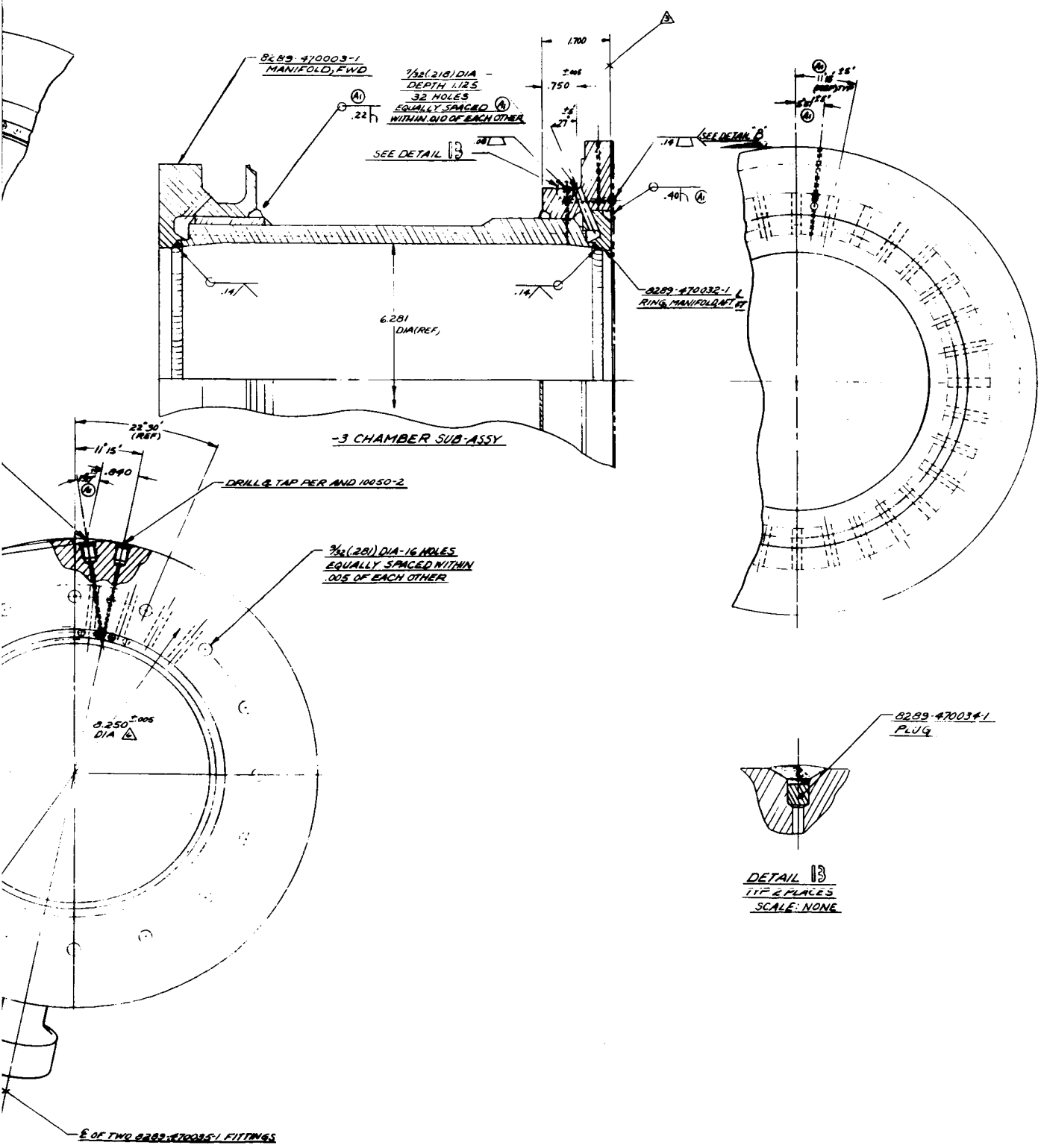

WATER COOLED CHAMBER ASSEMBLY

FIGURE 3

to increase durability by minimizing wall erosion effects. The mild-steel chamber was coated with aluminum oxide and the two water-cooled aluminum chambers with tungsten carbide. (Two water-cooled chamber sections were fabricated, but only one was utilized during the test program).

D. START NOZZLE (SEA LEVEL)

The start nozzle consisted of a milled aluminum liner and a mild-steel holder-manifold assembly. The nozzle has an exit area ratio (ϵ) of 1.00. The coolant water enters the nozzle at the chamber end and exhausts from the individual cooling slots at an area ratio of 1.00.

Figure 4 is a composite photograph showing the hardware utilized during the initial Cell 1AW testing. The Cell 2ES sea-level hardware is identical except that the uncooled chamber section is replaced with the water-cooled chamber section. The same water-cooled chamber section was utilized throughout the altitude testing program.

E. ALTITUDE NOZZLES

The altitude nozzles (see details in Section G of Appendix) tested have water-cooled throat sections and uncooled stainless-steel nozzle extensions. The throat section-to-extension joint was located at an area ratio of seven on all nozzles.

Three water-cooled throat sections were designed and fabricated from 6061 aluminum alloy: one 15° conical, one 80% Bell, and one Rao contour. All the nozzles are of similar construction, having milled coolant passages fed from inlet and outlet manifolds. Figures 5, 6 and 7 show the assembly drawings of the 15° conical, 80% Bell, and Rao nozzle throat sections, respectively.

The following nozzle extensions were designed and fabricated:

Type	Area Ratio (ϵ)
15° Conical	40
15° Conical	60
80% Bell	40
Rao	40

The nozzle extensions were formed from three 0.125-inch-thick stainless steel segments, welded together, and with suitable attachment flanges and exit rings for stiffening. The assembly drawings of the nozzle extensions are shown in Figures 8, 9, and 10.

Figure 11 shows the three water-cooled nozzle sections. The four stainless steel nozzle extensions are shown in Figure 12. Both photographs were taken at the completion of testing.

A flat Velbestos gasket was used to seal the various water-cooled throat sections to their respective nozzle extensions.

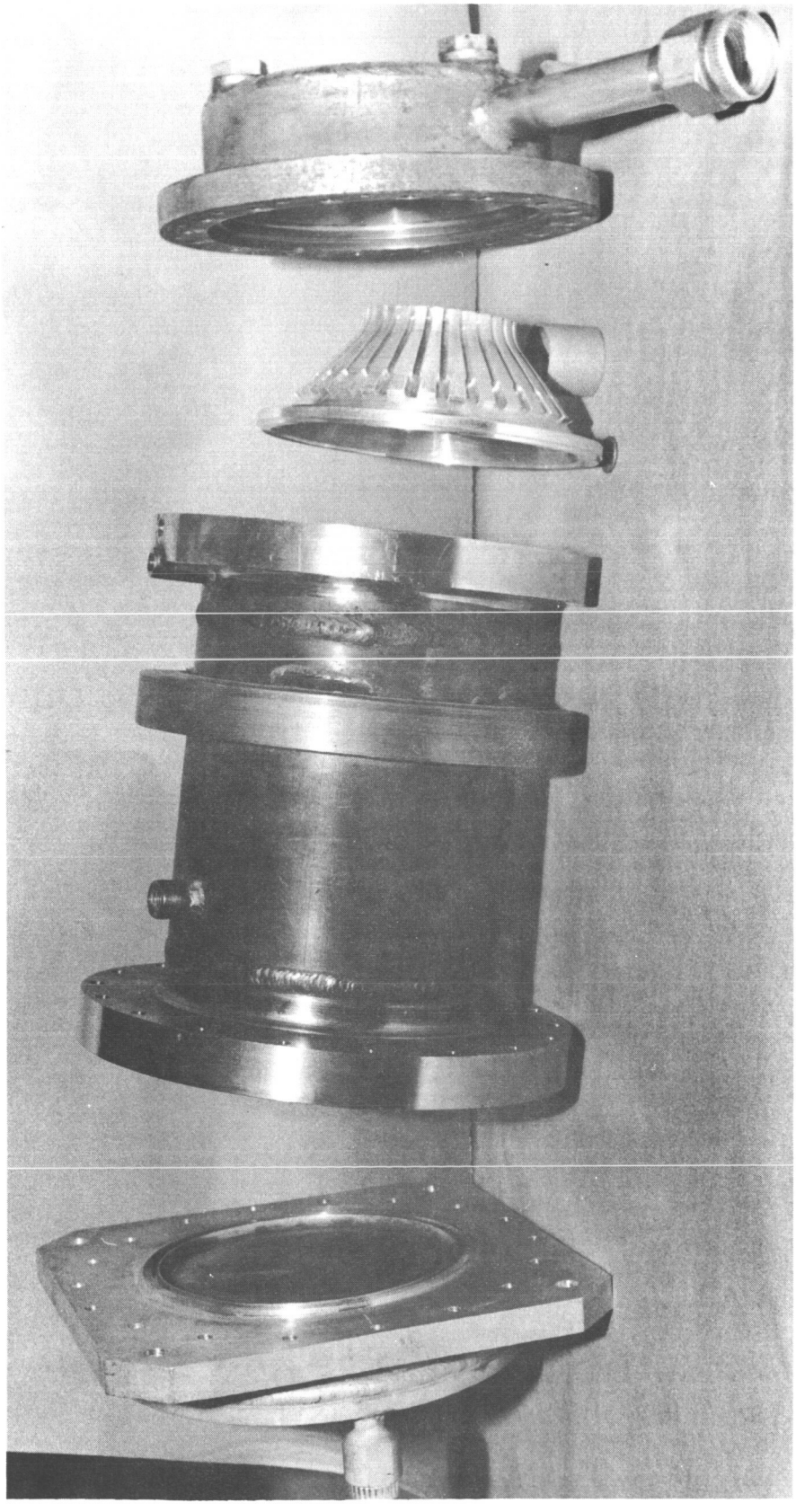

START HARDWARE COMPOSITE

FIGURE 4

MODEL _____

DATE _____

BELL AERO

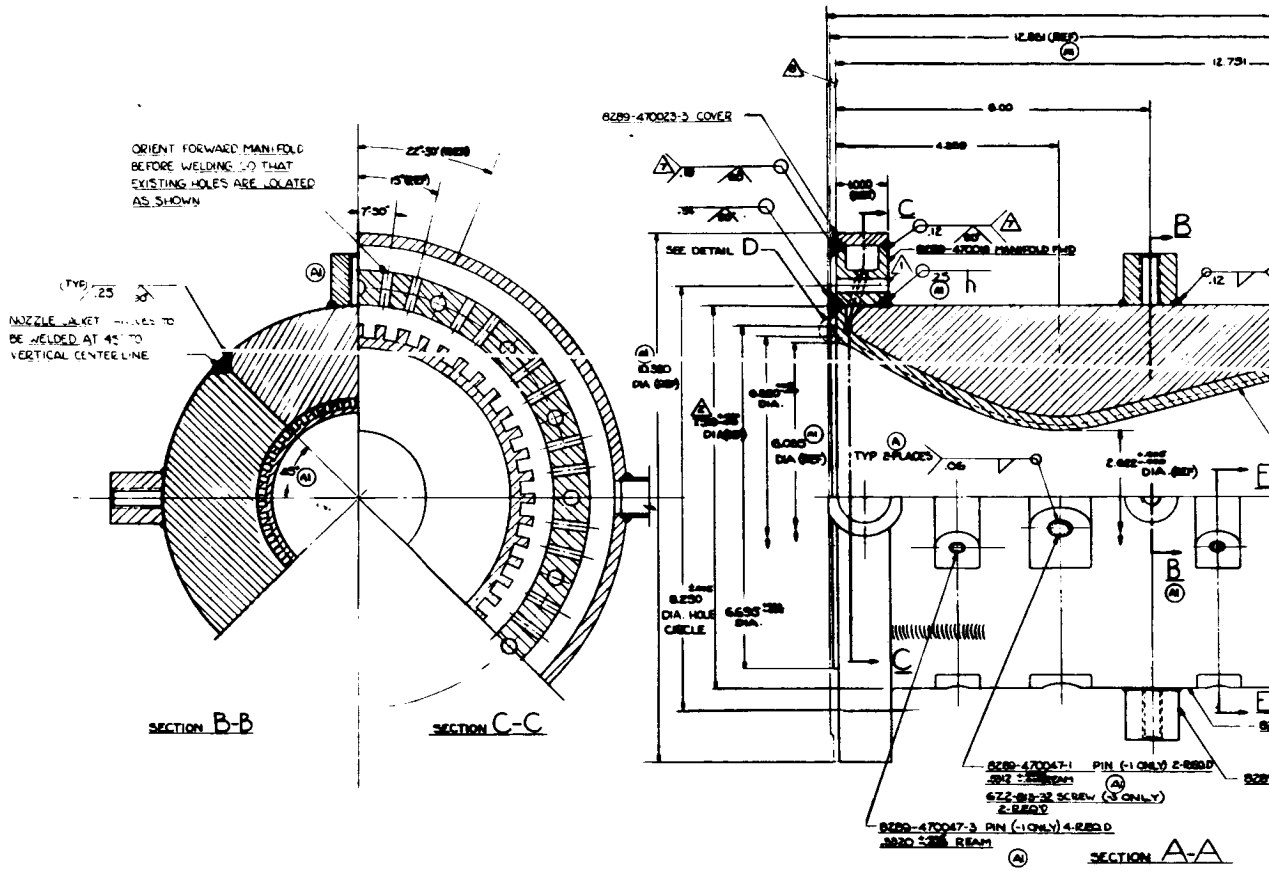

Form 0345 Rev. 1258 Sheet 1

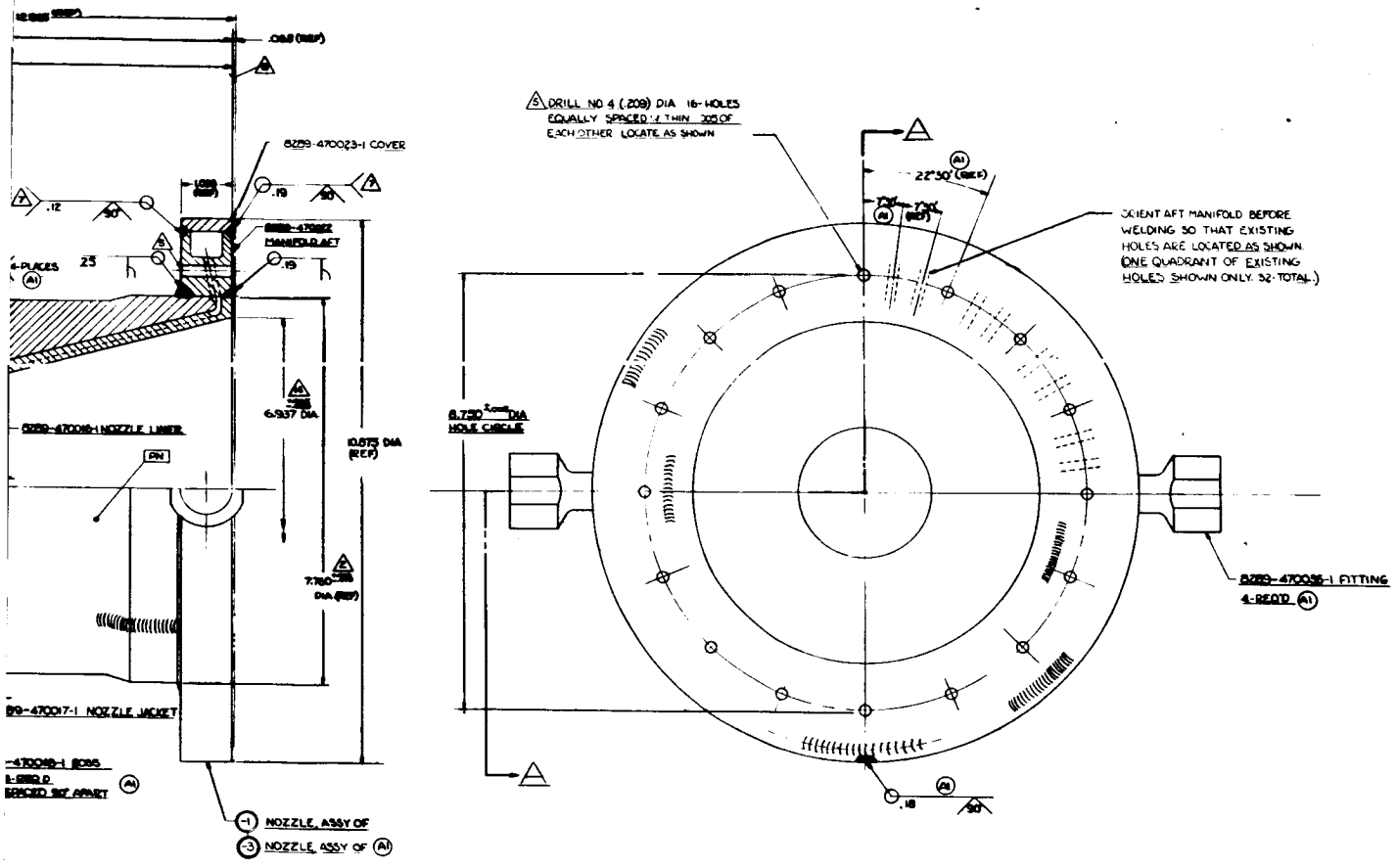

15° CONICAL NOZZLE THROAT ASSEMBLY

FIGURE 5

MODEL _____

DATE _____

BELL AERO

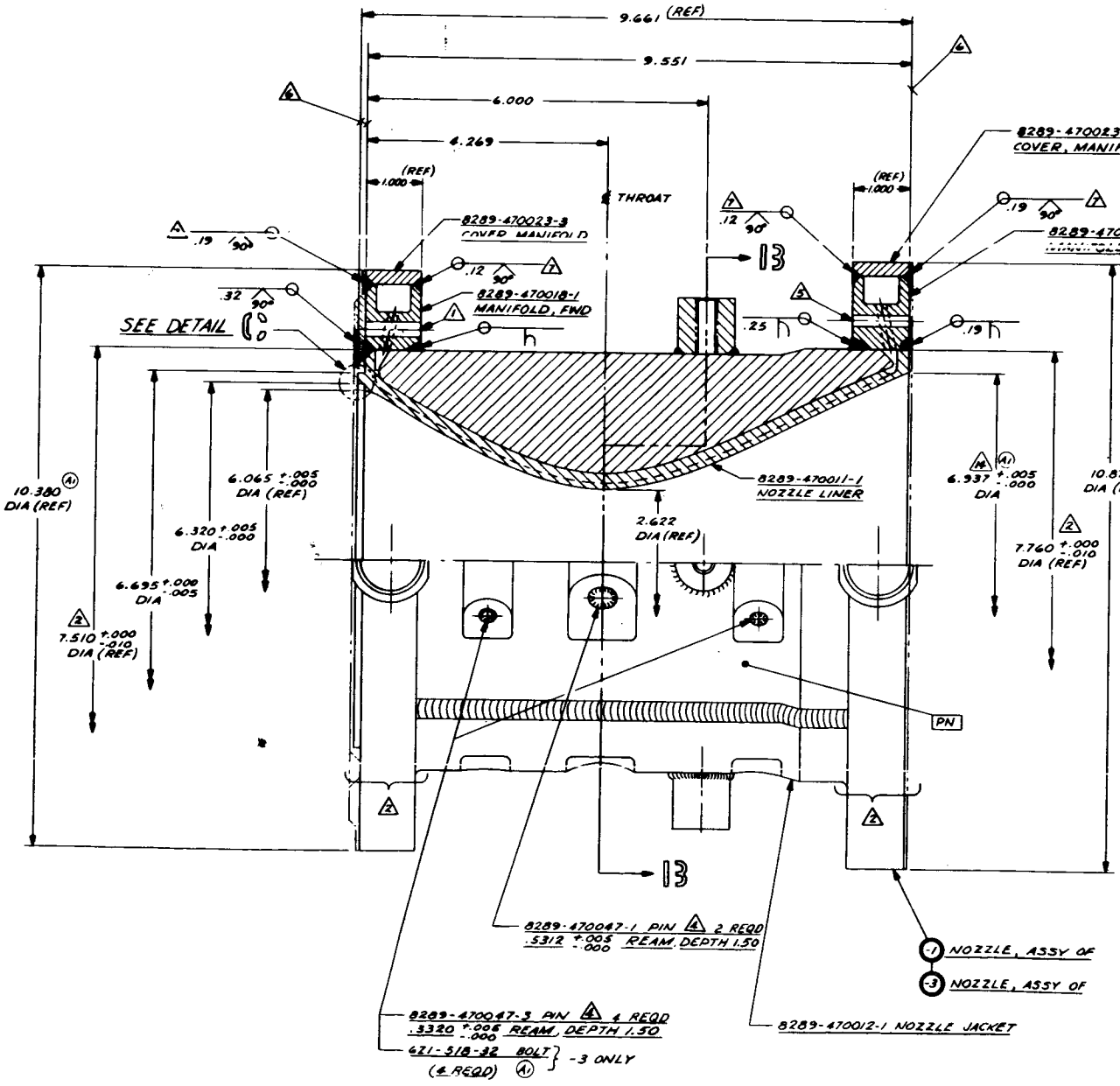

SECTION B-B

Form 0345 (rev. 1258) Sheet 1

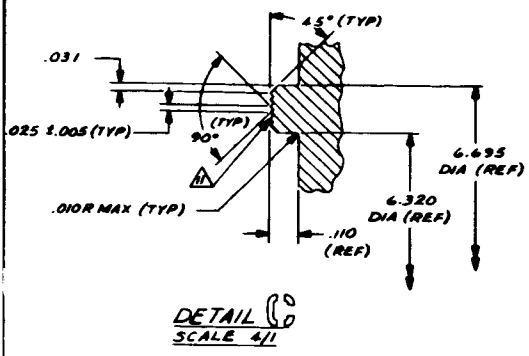

DETAIL C
SCALE 4/1

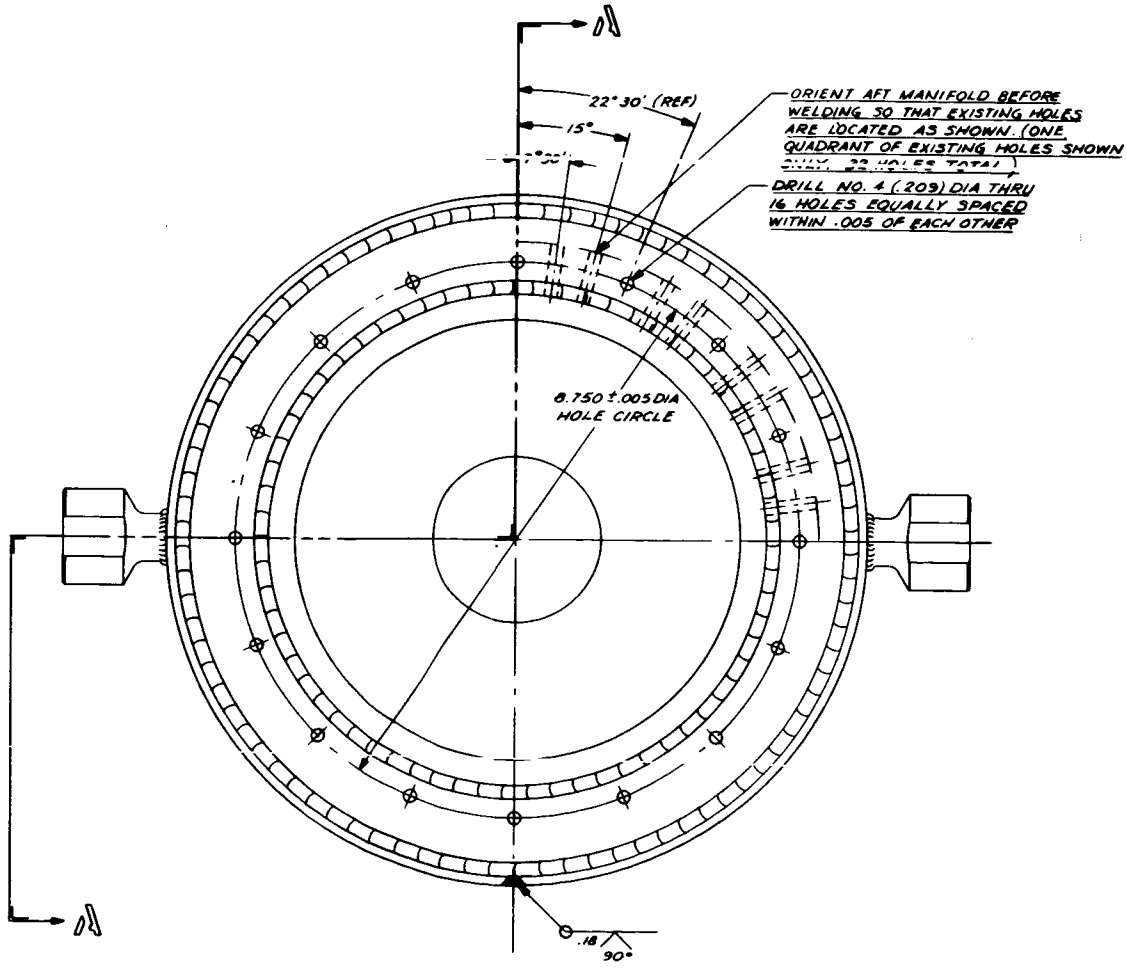

80% BELL NOZZLE THROAT ASSEMBLY

FIGURE 6

MODEL _____

DATE _____

BELL AERO

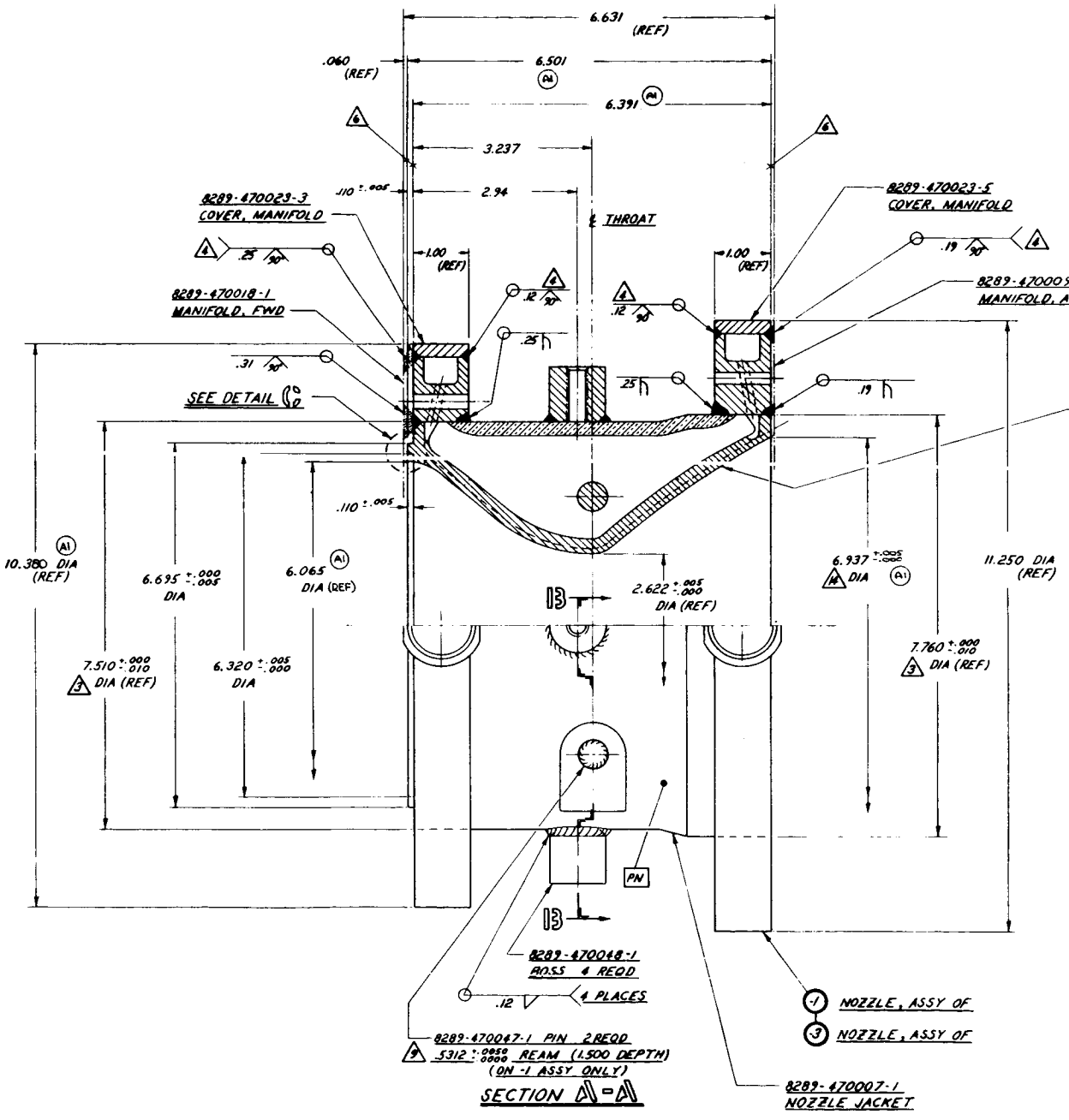

Form 0345 Rev. 1258 Sheet 1

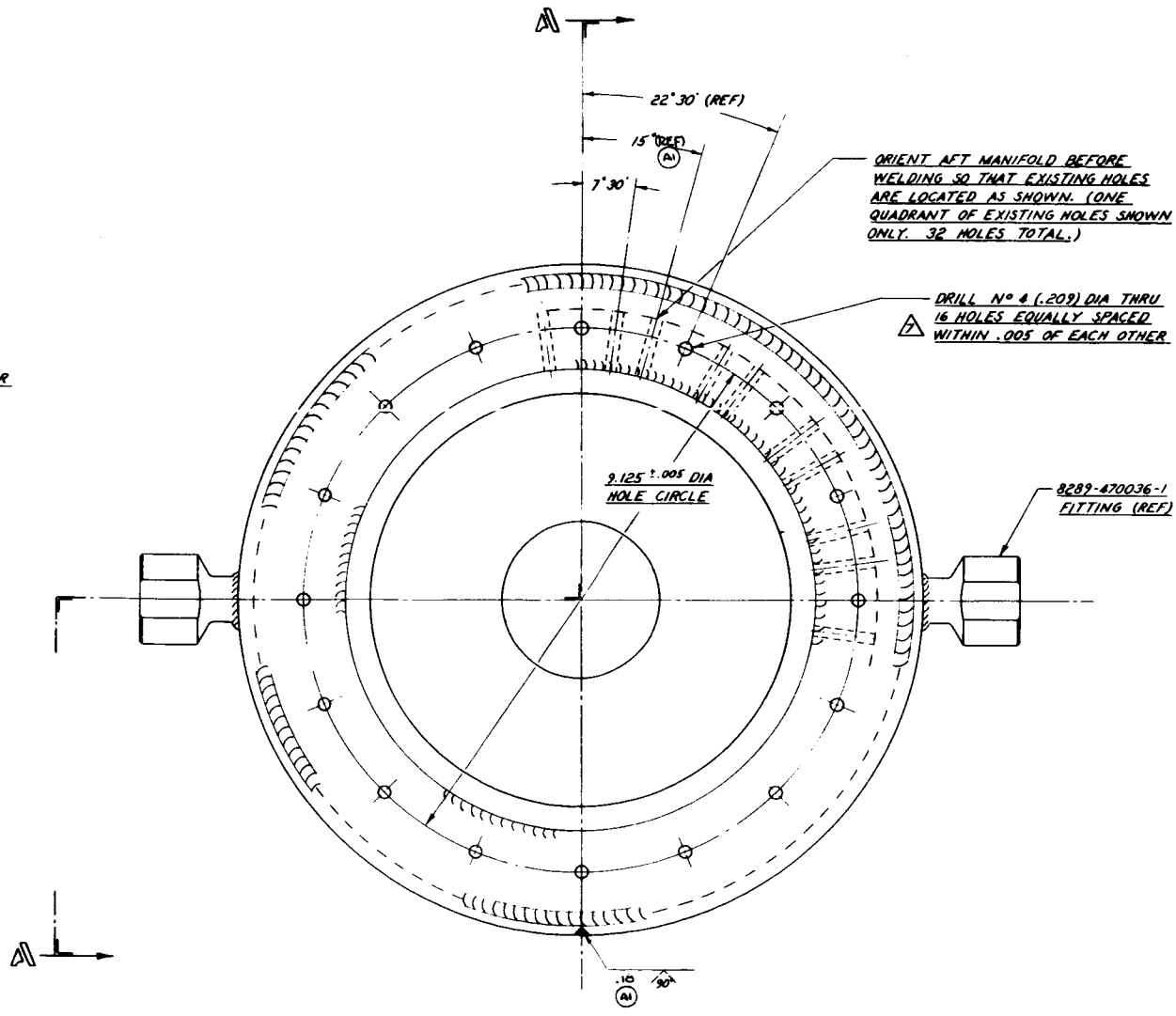

RAO NOZZLE THROAT ASSEMBLY

FIGURE 7

MODEL _____

DATE _____

BELL AEROS

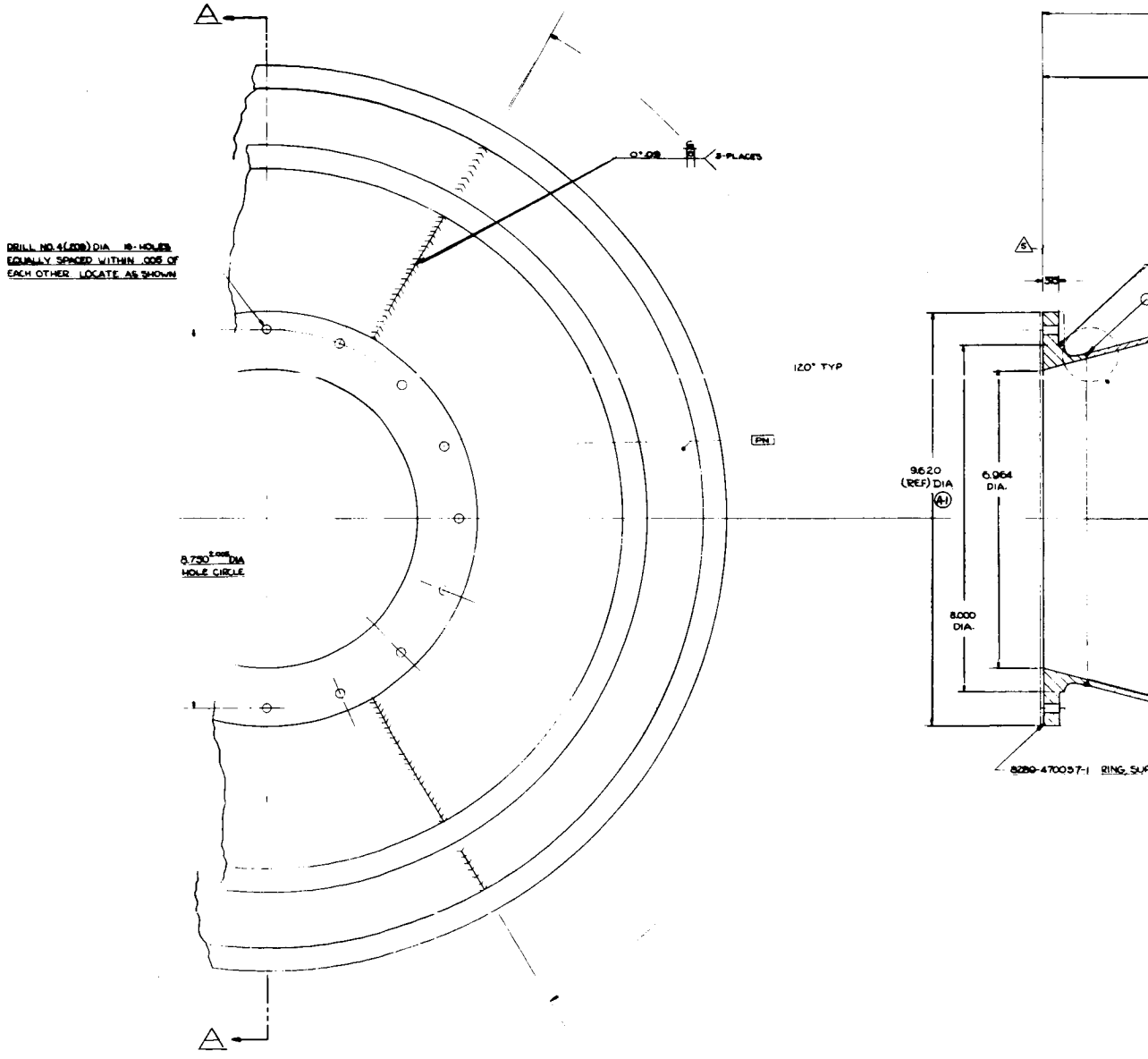

Form 0345 Rev. 1258 Sheet 1

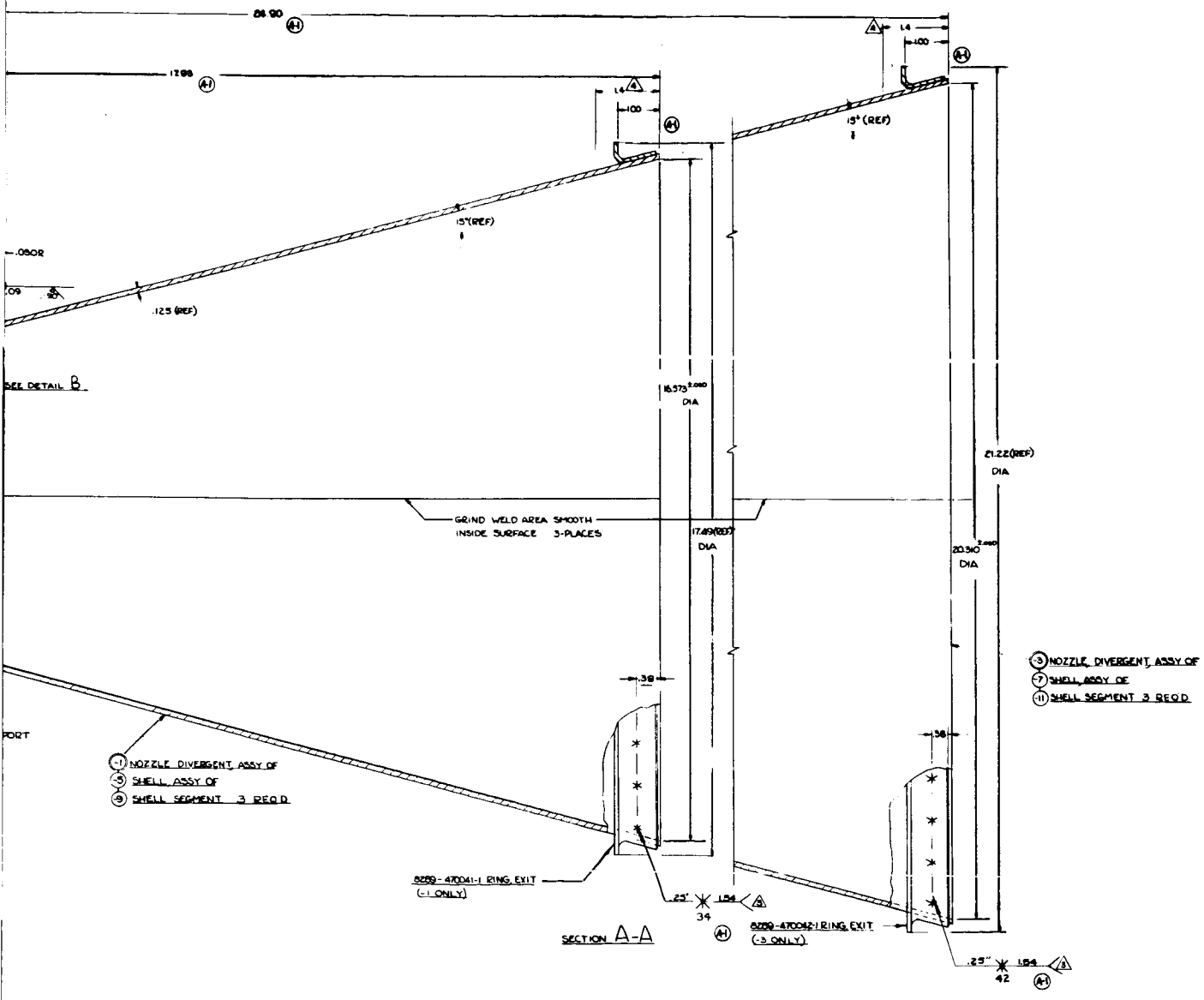

15° CONICAL NOZZLE EXTENTION ASSEMBLY
FIGURE 8

MODEL _____

DATE _____

BELL AERO

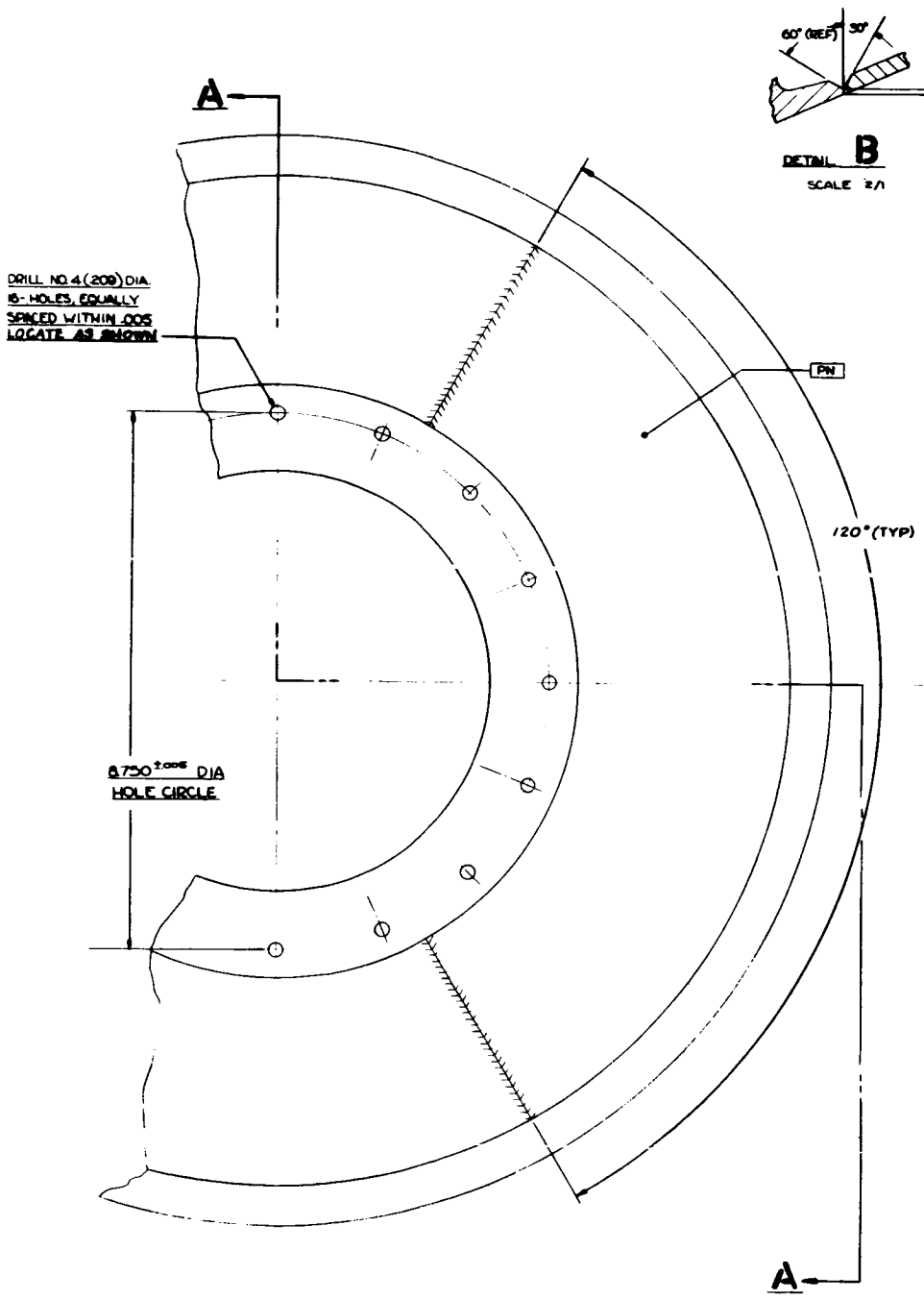

DETAIL B
SCALE 2/1

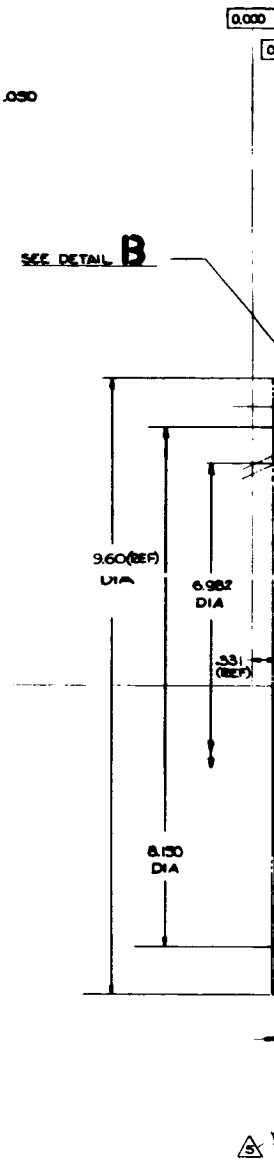

Form 0345 Rev. 1258 Sheet 1

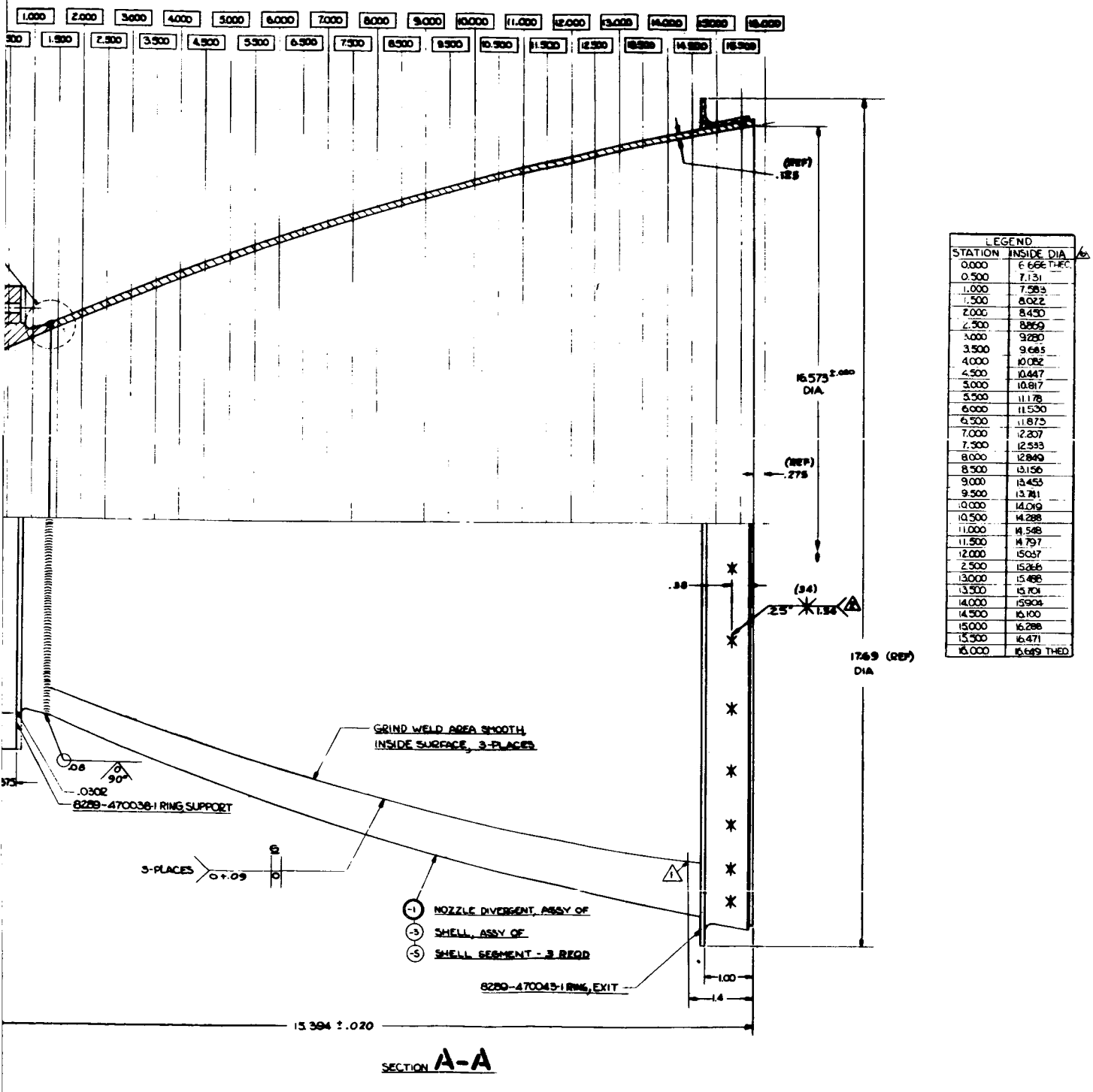

SECTION A-A

LEGEND	
STATION	INSIDE DIA
0.000	6.666 THEO.
0.500	7.131
1.000	7.583
1.500	8.022
2.000	8.450
2.500	8.869
3.000	9.280
3.500	9.685
4.000	10.082
4.500	10.447
5.000	10.817
5.500	11.178
6.000	11.530
6.500	11.875
7.000	12.207
7.500	12.533
8.000	12.849
8.500	13.156
9.000	13.453
9.500	13.741
10.000	14.019
10.500	14.288
11.000	14.548
11.500	14.797
12.000	15.037
12.500	15.266
13.000	15.488
13.500	15.701
14.000	15.904
14.500	16.100
15.000	16.288
15.500	16.471
16.000	16.649 THEO

80% BELL NOZZLE EXTENTION ASSEMBLY

FIGURE 9

MODEL _____

DATE _____

BELL AERO

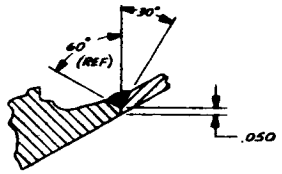

DETAIL 13
SCALE 2/1

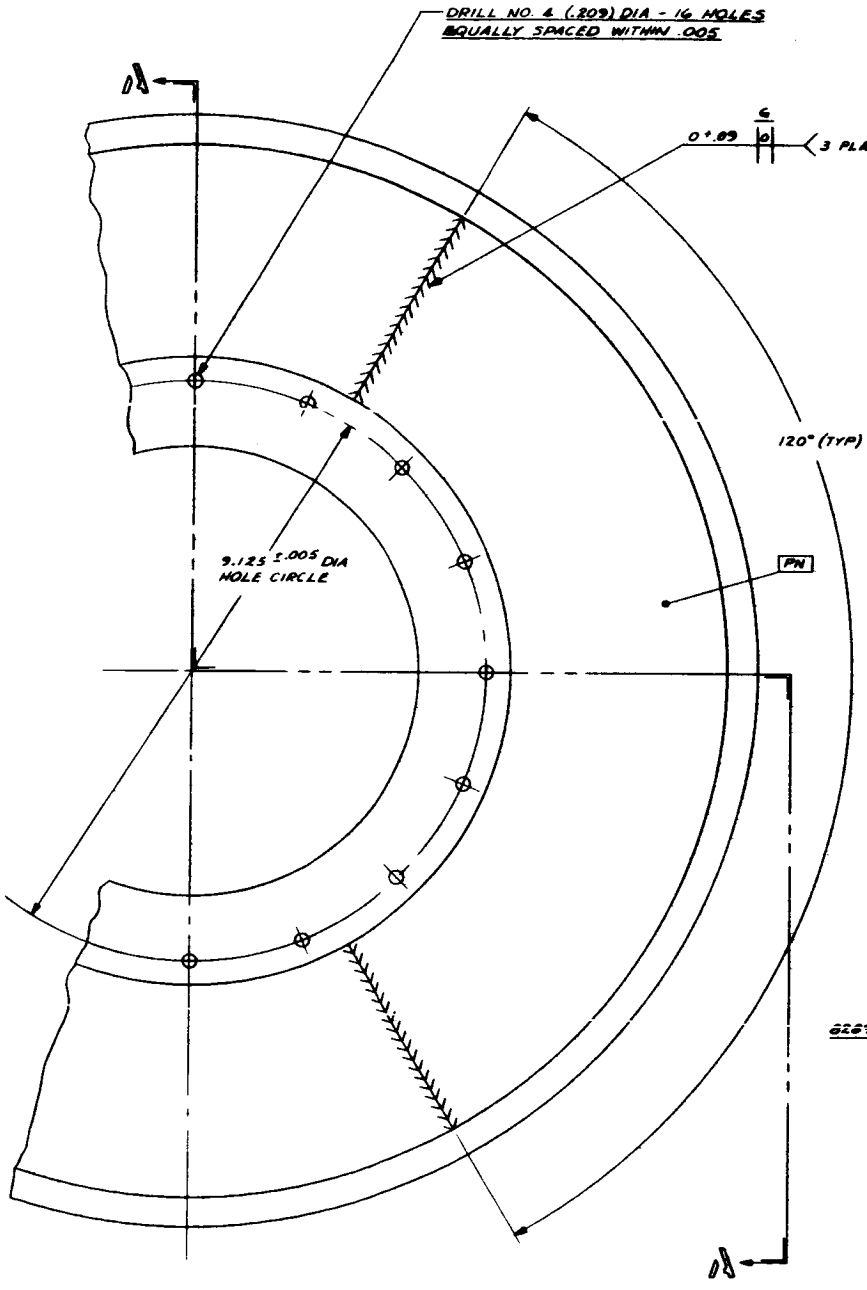

SEE DETAIL 13

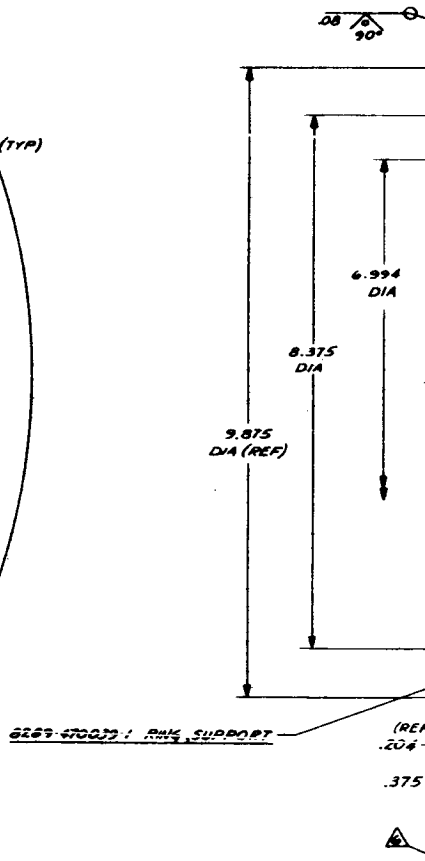

Form 0345 Rev. 1258 Sheet 1

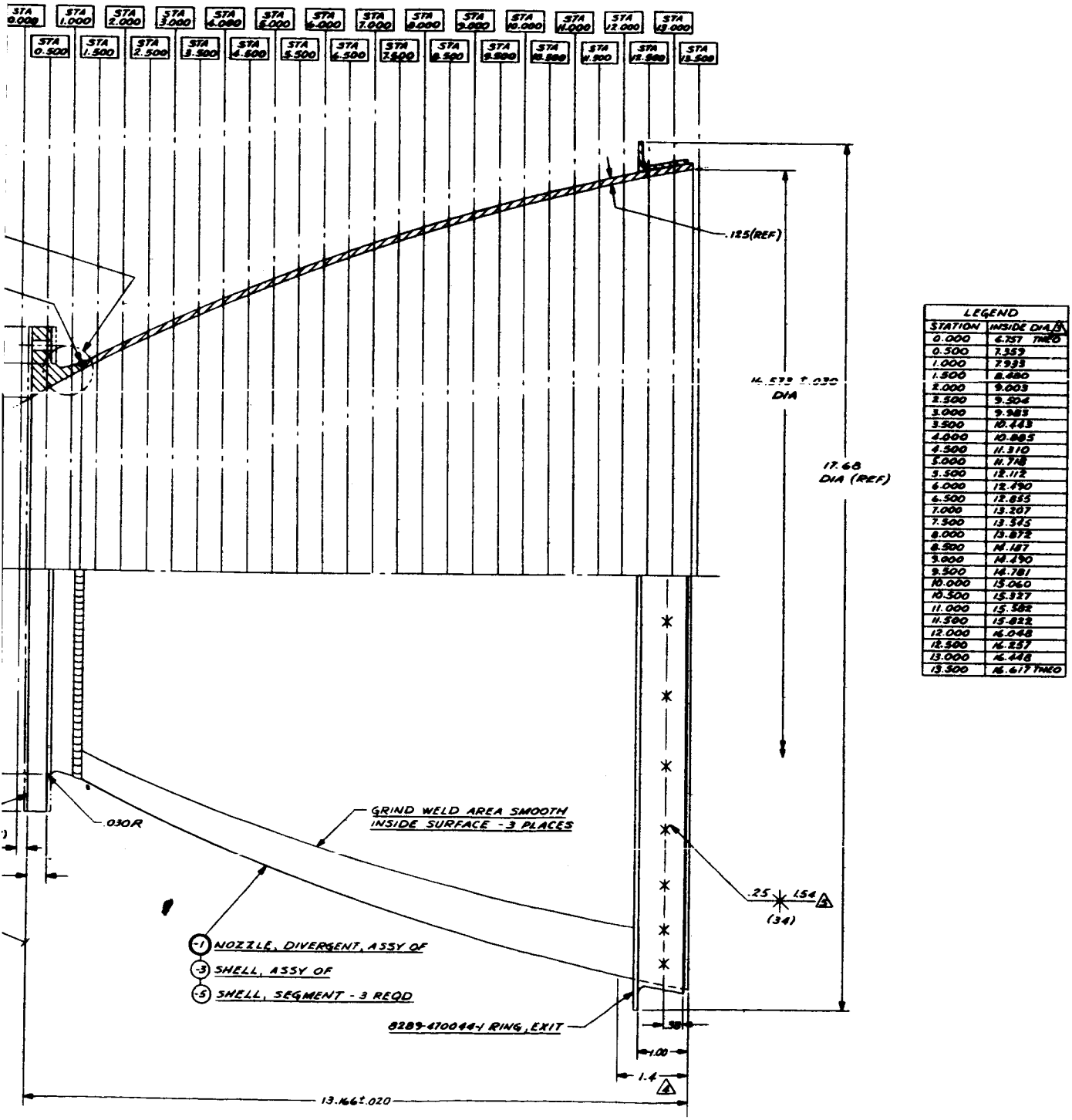

LEGEND	
STATION	INSIDE DIA
0.000	6.257 THEO
0.500	7.359
1.000	7.938
1.500	8.480
2.000	9.003
2.500	9.504
3.000	9.983
3.500	10.443
4.000	10.885
4.500	11.310
5.000	11.718
5.500	12.112
6.000	12.490
6.500	12.855
7.000	13.207
7.500	13.545
8.000	13.872
8.500	14.187
9.000	14.490
9.500	14.781
10.000	15.060
10.500	15.327
11.000	15.582
11.500	15.822
12.000	16.048
12.500	16.257
13.000	16.448
13.300	16.617 THEO

SECTION A-A

RAO NOZZLE EXTENTION ASSEMBLY

FIGURE 10

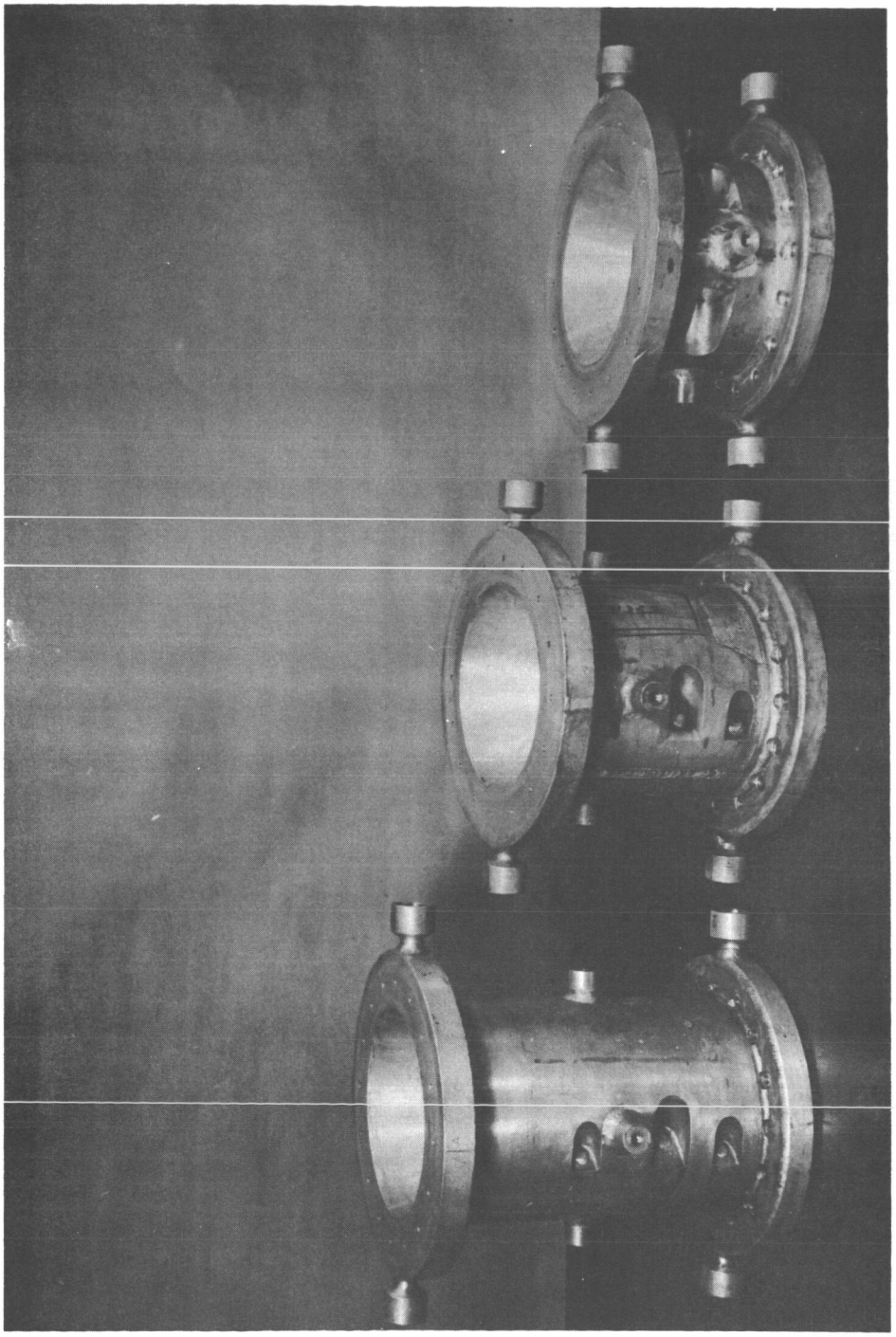

WATER COOLED NOZZLE THROAT SECTIONS

FIGURE 11

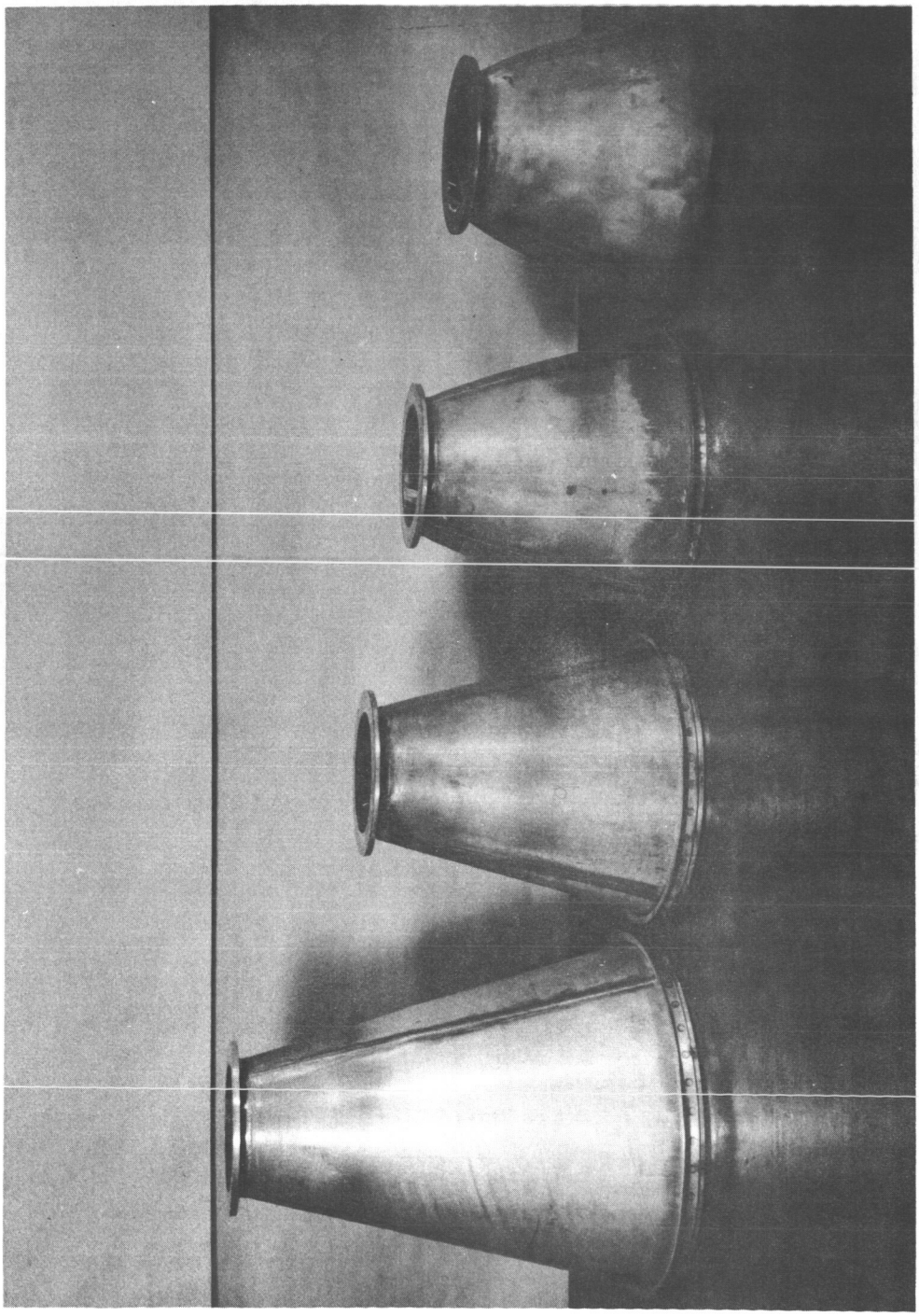

UNCOOLED NOZZLE EXTENTIONS

FIGURE 12

IV. SEA LEVEL INJECTOR TEST PROGRAM

A. GENERAL

The primary objective of the sea-level testing was to determine the injector characteristic velocity (c*) over the reactant ratio ($R_{o/f}$) range of 1.60 to 2.00. The testing, in both test cells, employed conventional pressurized test cell systems. In addition to the normal instrumentation required for cell and thrust chamber operation, the following thrust chamber performance instrumentation was utilized:

Parameter	No. of Primary Instruments
Chamber Pressure	6 (3 stations)
Propellant Flow Rates	4 (2 ox + 2 fuel)
Propellant Line Temperature	4 (2 ox + 2 fuel)
Thrust	1 (Cell 1AW)
	2 (Cell 2ES)

In addition, thrust chamber heat rejection instrumentation was utilized on the water-cooled chamber section during the Cell 2ES testing. Two sets of propellant flowmeters (8 total) and chamber pressure transducers (8 total) were employed during the testing to minimize errors due to the individual instrument calibrations. Close-coupled chamber pressure instrumentation was employed during the initial four Cell 1AW tests to evaluate combustion stability.

B. TEST CELL 1AW TESTING

Twelve test firings were conducted in Cell 1AW. Figure 13 shows the test cell installation for this testing. Except for the first two start tests, the testing was conducted at nominal chamber pressures and durations of 100 psia and 5 seconds, re-

respectively. Testing was initiated in Cell 1AW since the Cell 2ES facility (and also the associated test equipment) was not available.

Delays were encountered in the correlation of these data because of:

(1) Difficulties with the cell bleed procedures causing possible uncertainties in propellant flowmeter readings and injector performance.

(2) Non-agreement of the two oxidizer flowmeters based upon normal water calibrations (more pronounced with second flowmeter set).

(3) Inability to control propellant temperatures (no circulation system) and the possible effect of this on flowmeters (primary oxidizer) and injector performance.

Earlier in the program, the best correlation of these data was obtained by calculating the oxidizer flowrate (for each test) based upon an average oxidizer system impedance (ΔP). This method allowed correlation of the test data, but made it difficult to determine the accuracy of the performance (c^*) data obtained by this procedure. A more-accurate procedure incorporated in Cell 2ES was to conduct in-cell calibrations of the oxidizer flowmeters using N_2O_4. This will be discussed in greater detail later in this report.

The final test data obtained in Cell 1AW are shown in Table I. These data include the N_2O_4 calibrations of the oxidizer flowmeters.

Stable combustion was obtained over the reactant ratio range of interest.

C. TEST CELL 2ES SEA-LEVEL TESTING

Sixteen sea-level test firings were conducted in Cell 2ES. The test cell installation for this testing is shown in Figure 14. Figure 15 shows the thrust yoke and load cell installation. Of the 16 tests conducted, two tests were terminated by the cell malfunction safety circuit;* therefore, no data were obtained. During all tests, the propellant temperatures were maintained at a nominal 60°F. The nominal run duration for this testing was 30 seconds except for Runs 2ES-1587 and 2ES-1590. Run 2ES-1587 was a nominal 5-second system checkout and the duration of 2ES-1590 was reduced to evaluate chamber coating losses encountered in the previous test run.

Ten tests (2ES-1587 through 2ES-1596) were conducted and the data reduced utilizing the normal water calibrations of both the fuel and oxidizer flowmeters. Difficulties were still being encountered correlating data; not only with the previously obtained Cell 1AW data, but also with the Cell 2ES test data obtained with the two different flowmeter sets. The primary difficulty still appeared to be in the oxidizer flowrate measurements.

Because of the lack of correlation of the test data and the questionability of utilizing water calibrations for the N_2O_4 flowmeters, a series of calibrations was performed on both sets of oxidizer flowmeters (in the test cell system) using N_2O_4. (These calibrations are discussed in greater detail in Section F of the Appendix.)

The additional test runs were then conducted (tests 2ES-1597 through 2ES-1602) and these data and the previously obtained Cell

*NOTE: The malfunction safety circuit is designed to shut down the test cell system if the desired chamber pressure level is not achieved in a preset time interval. This is primarily for protection of the test hardware from system malfunctions and at no time during the program was attributable to test hardware difficulties.

2ES date were reduced using the N_2O_4 oxidizer calibrations. Table II lists the injector sea-level test data obtained in Cell 2ES.

D. DISCUSSION OF SEA-LEVEL TEST DATA

Twenty-eight injector test firings were conducted: 12 in Cell 1AW and 16 in Cell 2ES. The final data from these tests are presented in Tables I and II.

As previously mentioned, the N_2O_4 calibration factors obtained in Cell 2ES were utilized to reduce all of the test data (including Cell 1AW data). This was done because the utilization of these calibrations represents the most accurate data reduction method even though the test cells do not have identical oxidizer flow system piping.

Owing to the difficulties encountered during the Cell 1AW testing (primarily with the oxidizer flow measurements), it was not possible to utilize all the test results obtained in this cell.

In the determination of injector characteristic velocity (c*), Runs 1AW-581 through 1AW-584 were used since the system bleed procedures were modified prior to run 1AW-581. (However, some of the earlier test data correlates with the final injector performance (c*) data, but there was no valid reason for selecting only these tests and not all other tests.)

In the determination of thrust chamber sea-level thrust coefficients, all the Cell 1AW data were utilized except Runs 1AW-573, 1AW-576, and 1AW-580. Runs 1AW-573 and 1AW-580 were not used because of the high injector pressure drops and Run 1AW-576 was out of the reactant ratio range of primary interest.

All run data from the Cell 2ES testing were utilized except the two tests where a malfunction shutdown occurred (and no data were obtained) and Run 2ES-1598. During test run 2ES-1598,

difficulties were encountered with the oxidizer purge system (the injector nitrogen purge flow did not shut off completely). The oscillograph record was lost during Run 2ES-1593; however, because of the high consistency of the over-all flow data, it was possible to calculate propellant flow system impedances (ΔP) and utilize the measured system pressure drop data to calculate the propellant flows during this test.

The injector performance data in Tables I and II are shown plotted as a function of reactant ratio ($R_{O/f}$) in Figures 16 through 21. In all cases, the data point was taken approximately 0.5 to 1 second from the end of each test run. Seventeen test runs were utilized as valid injector performance (c*) data and 22 test runs for nozzle ($C_{f\infty}$) performance data.

Figures 16 and 17 show the injector characteristic velocity (c*) and combustion efficiency (η c*) plotted as a function of reactant ratio ($R_{O/f}$). The theoretical equilibrium and frozen characteristic velocities are also shown in Figure 16 for comparative purposes. The measured injector characteristic velocity has a peak value of 5536 ft/sec. at a reactant ratio of approximately 1.65. The best fit curve through the data in Figure 17 shows the injector combustion efficiency increasing from 0.967 at a reactant ratio of 1.60 to 0.979 at a reactant ratio of 2.00. These data are based on theoretical equilibrium composition performance calculations. (All theoretical propellant performance data utilized was supplied by NASA-MSC.)

Figures 18 and 19 contain the sea-level thrust coefficient and nozzle efficiency data for the area ratio of 1.0 sea-level nozzle corrected to vacuum conditions. The corrected thrust coefficient is shown to decrease from a value of 1.223 at a reactant ratio of 1.60 to 1.219 at a 2.00 reactant ratio. The nozzle efficiency (based upon the theoretical equilibrium composition data for ϵ=1.0) is shown in Figure 19 to be essentially

a constant value of 0.9907 over the entire reactant ratio range.

The corrected thrust chamber specific impulse ($I_{sp\infty}$) and over-all efficiency ($\eta I_{sp\infty}$) data are shown in Figures 20 and 21, respectively. The corrected specific impulse is seen to have a maximum value of 212 seconds at a reactant ratio of approximately 1.60. The over-all thrust chamber efficiency ($\eta I_{sp\infty}$) has essentially the same trend as the combustion efficiency curve (Figure 17) because the nozzle efficiency is independent of reactant ratio. Figure 21 shows that the over-all efficiency varies from approximately 0.958 to 0.970 over the reactant ratio range of 1.60 to 2.00, respectively.

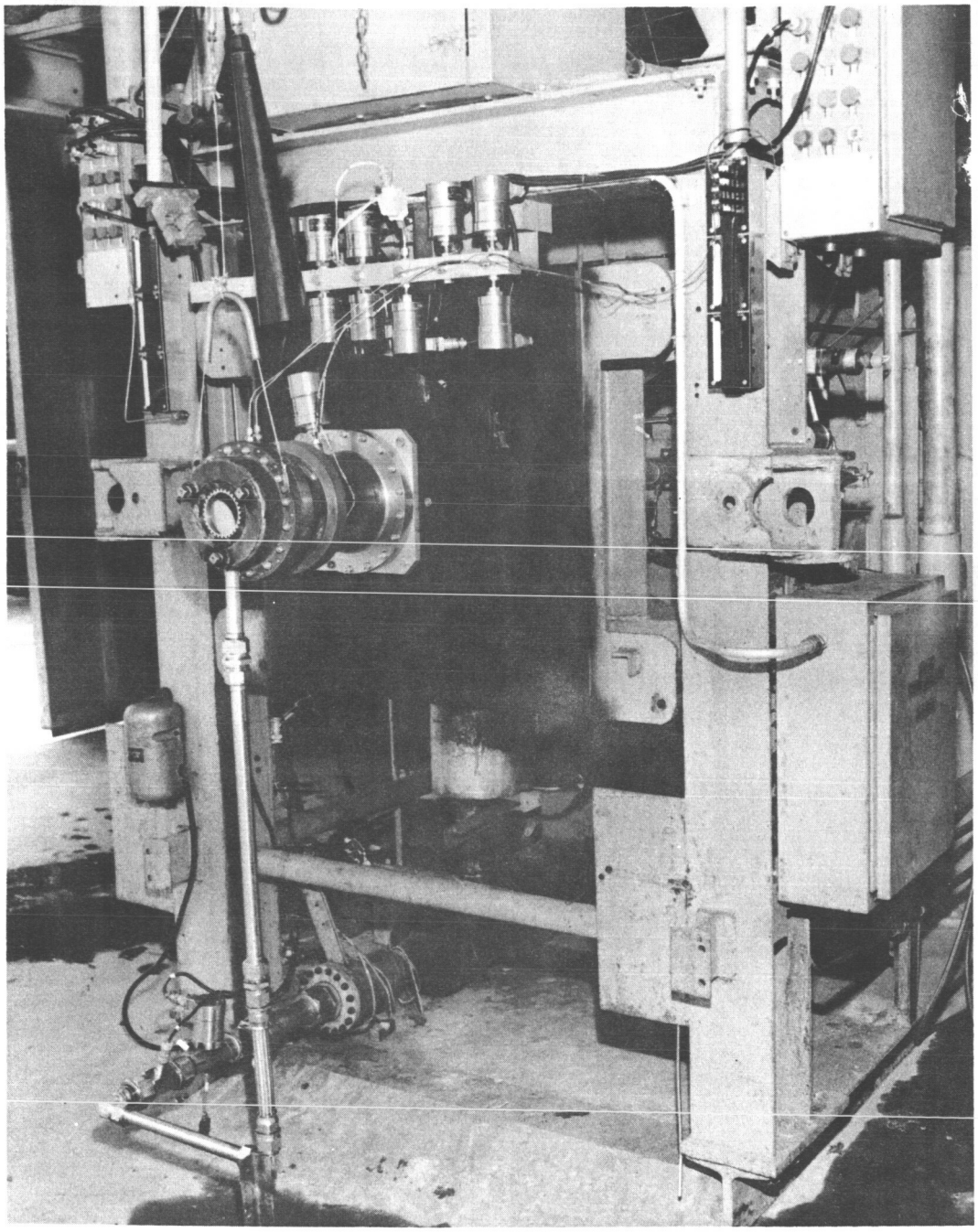

TEST CELL 1AW SETUP

FIGURE 13

MODEL _____

DATE 2-24-64

BELL AERO

TA

SEA-LEVEL INJECTOR

Test Number		Duration (sec.)	$\overline{P}_o$ (psia)	R_o/f	W_T (lb/sec.)	F_m (lb
1	1AW-573	3.5	85.6	1.593	2.728	481
2	-574	4.3	117.3	1.851	3.718	689
3	-575	5.1	99.3	1.930	3.157	576
4	-576	4.7	96.9	1.222	3.097	567
5	-577	5.2	100.7	1.615	3.184	589
6	-578	5.1	100.1	1.711	3.149	584
7	-579	5.9	101.0	2.129	3.232	587
8	-580	5.5	94.6	1.615	3.023	545
9	-581	4.8	101.8	1.972	3.224	591
10	-582	5.0	101.8	1.760	3.196	594
11	-583	5.0	100.7	2.004	3.202	584
12	-584	5.2	101.5	1.784	3.196	598

Form 0345 Rev. 1258 Sheet 1

BLE I

TEST DATA - CELL 1AW

)	c* (ft/sec)	$C_{f\infty}$	$I_{sp\infty}$ (sec)	η_{c*}	$\eta_{C_{f\infty}}$	$\eta_{I_{sp\infty}}$	Remarks
.9	5461	1.212	205.7	0.955	0.981	0.937	High injector ΔP - apparent two-phase flow
.5	5489	1.212	206.8	0.969	0.983	0.952	
.0	5471	1.220	207.4	0.970	0.990	0.960	
.3	5445	1.233	208.7	0.967	0.994	0.961	Tank pressure setting error
.2	5503	1.227	209.8	0.962	0.993	0.955	
.6	5537	1.225	210.8	0.971	0.993	0.964	
.2	5442	1.219	206.2	0.978	0.990	0.968	
.9	5443	1.222	206.7	0.952	0.989	0.941	High injector ΔP - apparent two-phase flow
.7	5505	1.218	208.4	0.979	0.989	0.968	
.7	5538	1.223	210.5	0.973	0.992	0.965	
.9	5476	1.218	207.3	0.976	0.989	0.965	
.4	5531	1.217	209.2	0.973	0.987	0.960	

MODEL _____

DATE 2-24-64

BELL AERO

SEA-LEVEL INJECT

Test Number		Duration (sec)	$\overline{P}_o$ (psia)	R_o/f	W_T (lb/sec)	F_m (lb)
13	2ES-1587	4.8	98.00	1.920	3.095	565.0
14	-1588	---------- MALFUNCTION SHUTDOWN ----------				
15	-1589	30.3	101.40	1.662	3.200	593.7
16	-1590	15.5	99.00	1.807	3.105	575.8
17	-1591	30.0	99.77	1.975	3.154	579.2
18	-1592	30.4	100.10	1.545	3.146	583.7
19	-1593	30.3	100.11	2.048	3.173	585.1
20	-1594	30.4	100.70	2.136	3.218	584.4
21	-1595	30.4	98.40	1.673	3.095	571.2
22	-1596	30.9	100.60	1.877	3.176	583.4
23	-1597	---------- MALFUNCTION SHUTDOWN ----------				
24	-1598	30.5	87.57	1.304	2.832	496.2
25	-1599	29.9	97.25	1.574	3.063	567.7
26	-1600	29.9	99.36	2.021	3.154	575.8
27	-1601	29.9	99.03	1.566	3.123	573.1
28	-1602	30.0	99.54	1.711	3.137	583.5

Form 0345 Rev. 1258 Sheet 1

TABLE II

OR TEST DATA - CELL 2ES

	c^* (ft/sec)	C_{f_∞}	I_{sp_∞} (sec)	η_{c^*}	$\eta_{C_{f_\infty}}$	$\eta_{I_{sp_\infty}}$	Remarks
	5510	1.216	208.2	0.977	0.987	0.964	
	5515	1.226	210.1	0.966	0.994	0.960	
	5549	1.224	211.1	0.977	0.993	0.970	
	5504	1.220	208.7	0.979	0.991	0.970	
	5540	1.224	210.7	0.968	0.991	0.959	
	5492	1.227	209.4	0.982	0.996	0.978	Oscillograph flows lost
	5444	1.220	206.4	0.979	0.991	0.970	
	5531	1.224	210.4	0.968	0.991	0.959	
	5509	1.219	208.7	0.974	0.991	0.965	
	5379	1.216	203.3	0.944	0.982	0.927	High injector ΔP - apparent two-phase flow
	5526	1.229	211.1	0.966	0.995	0.961	
	5484	1.218	207.6	0.978	0.989	0.967	
	5520	1.218	209.0	0.965	0.986	0.951	
	5526	1.231	211.4	0.969	0.998	0.967	

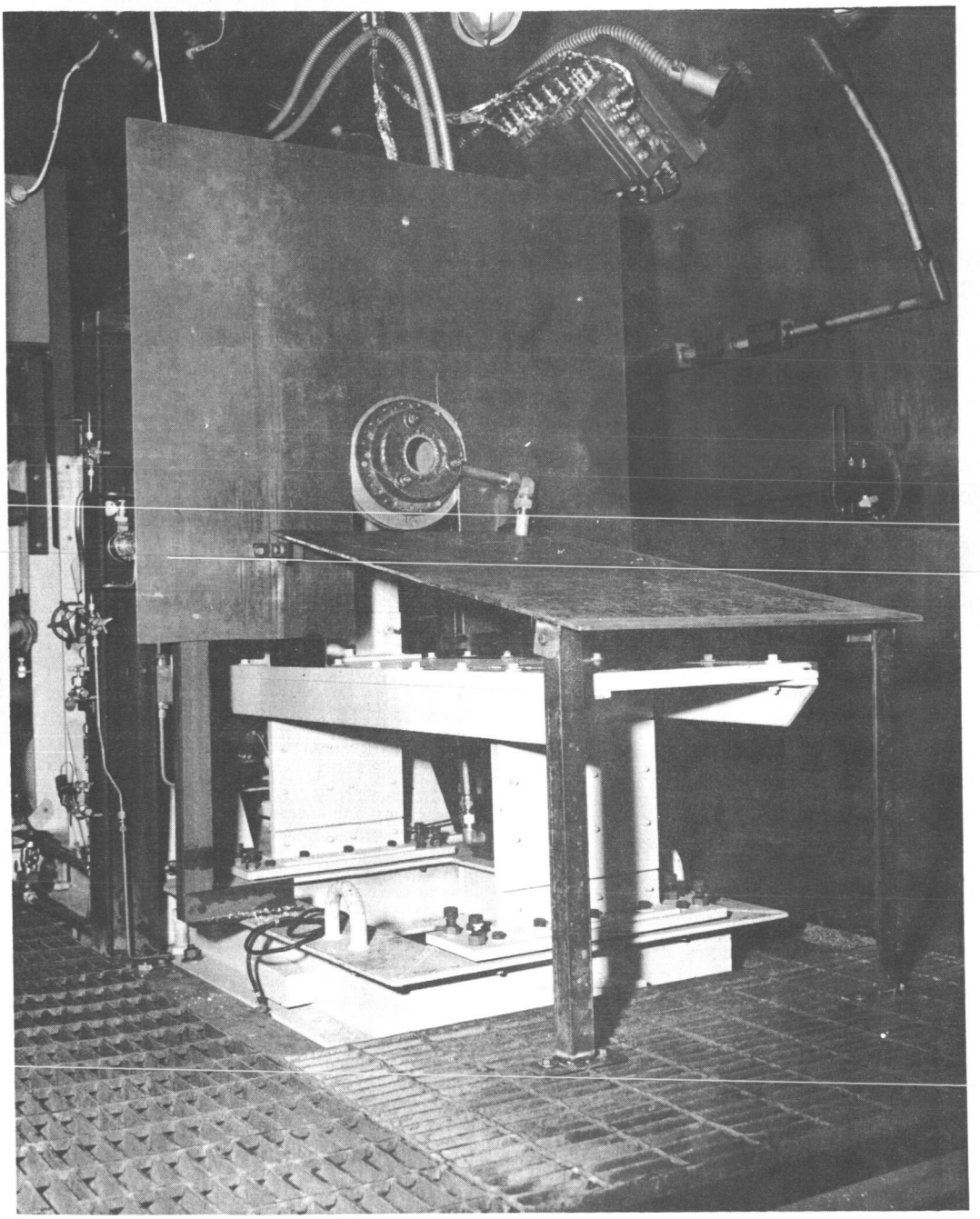

TEST CELL 2ES SEA LEVEL SETUP

FIGURE 14

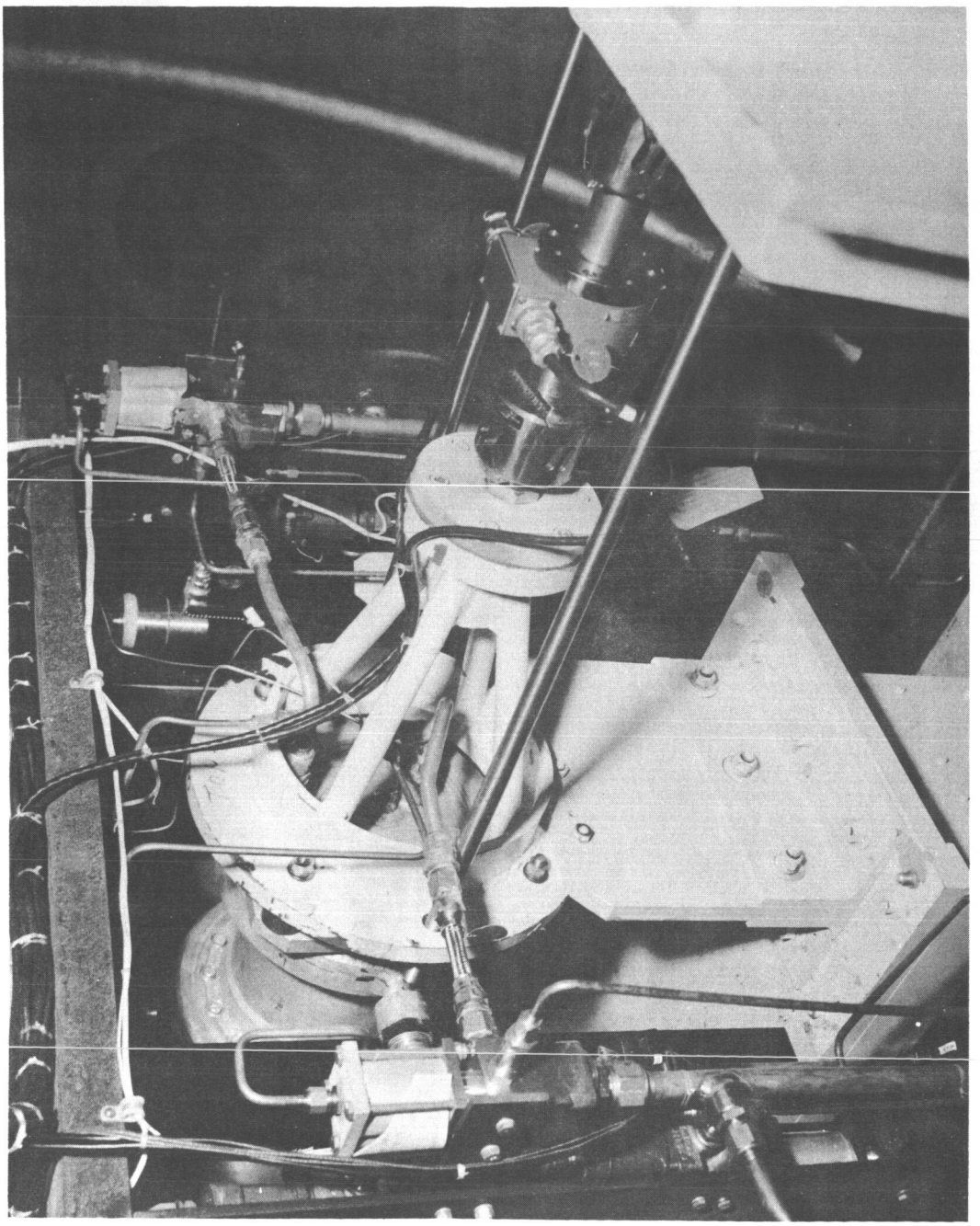

TEST CELL 2ES THRUST YOKE AND LOAD CELL INSTALLATION

FIGURE 15

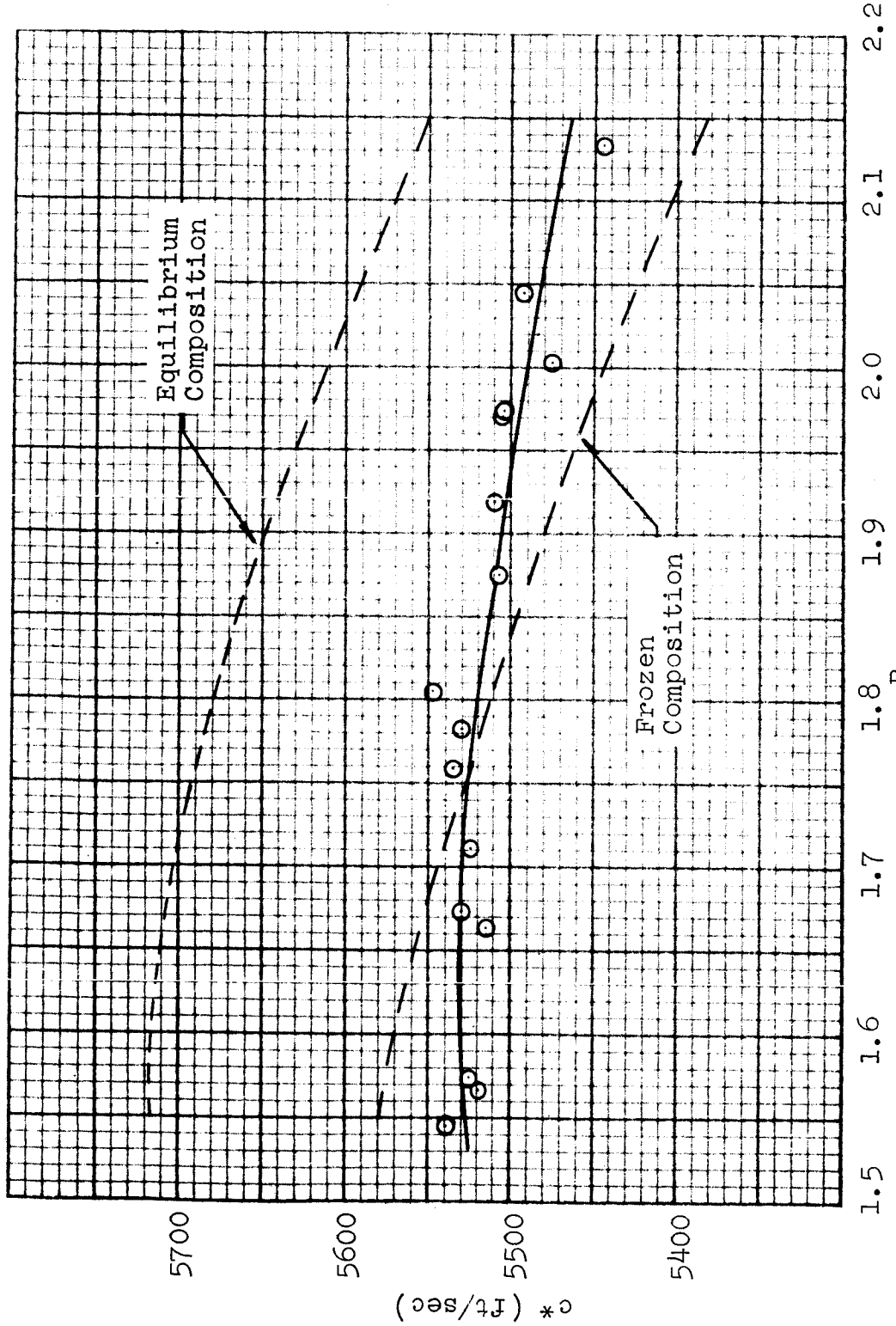

INJECTOR CHARACTERISTIC VELOCITY (Sea Level Data)

FIGURE 16

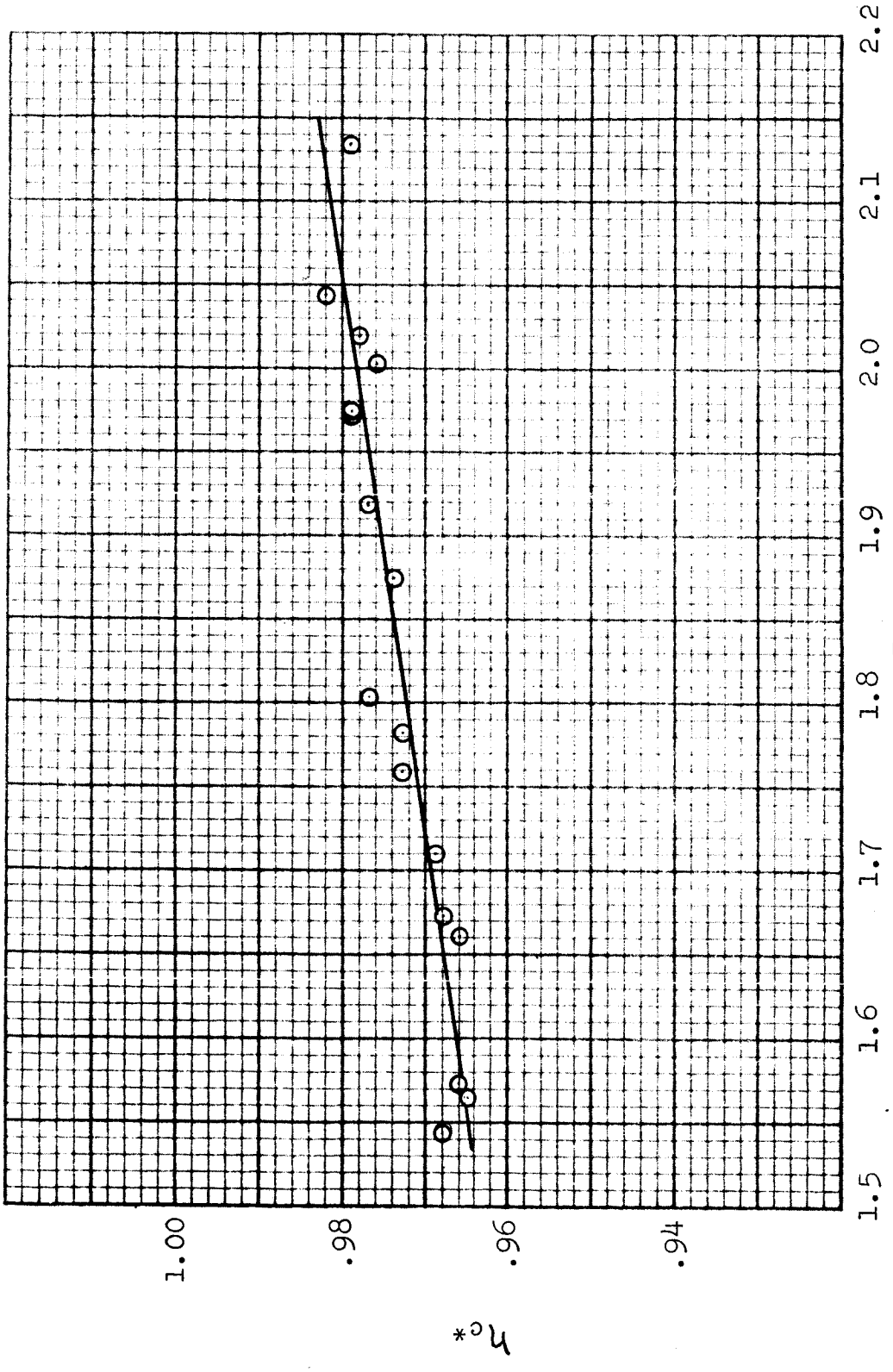

INJECTOR COMBUSTION EFFICIENCY (Sea Level Data
Based On Theoretical Equilibrium Composition)

FIGURE 17

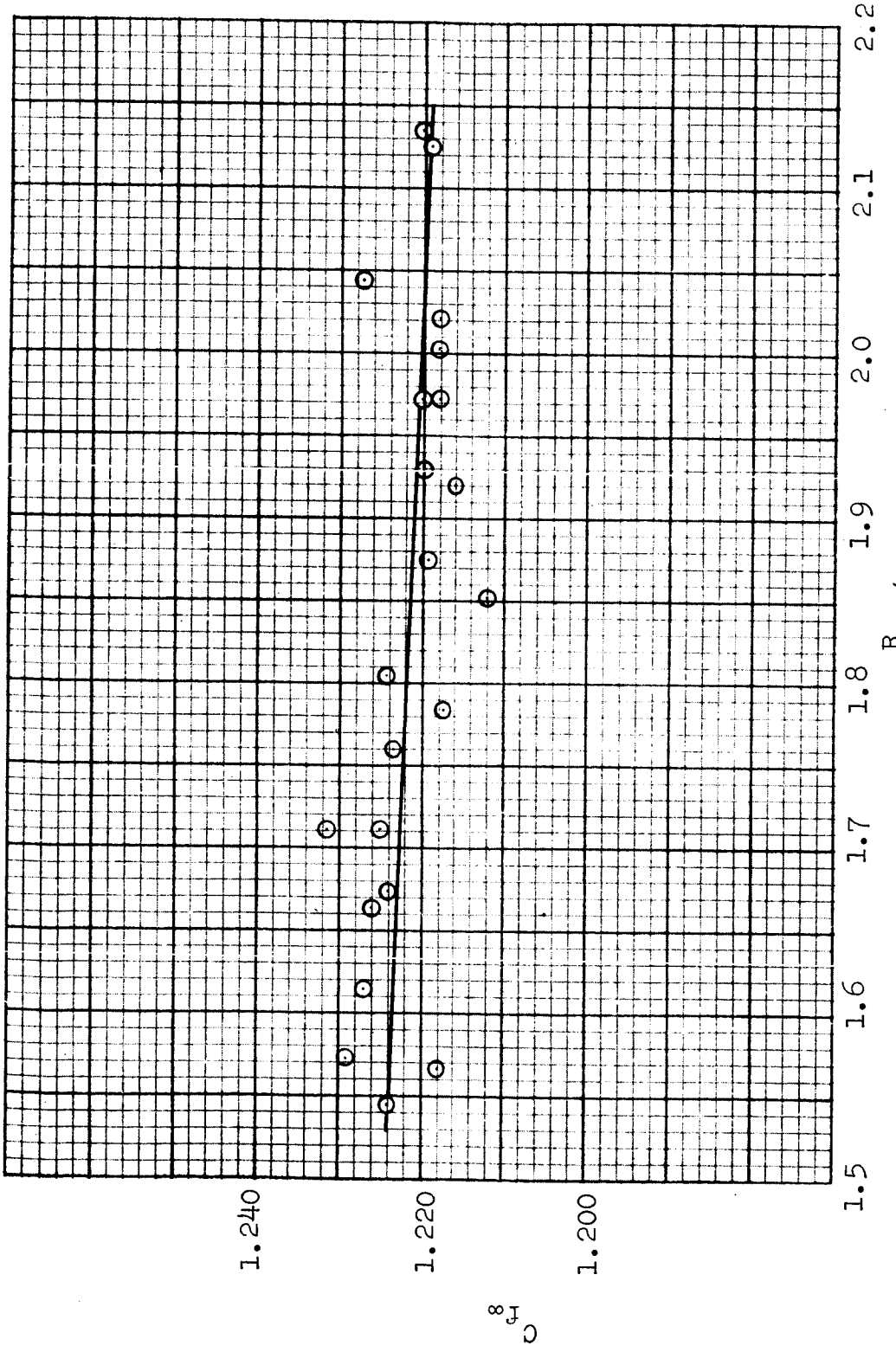

THRUST CHAMBER SEA LEVEL THRUST COEFFICIENT
CORRECTED TO VACUUM CONDITIONS

FIGURE 18

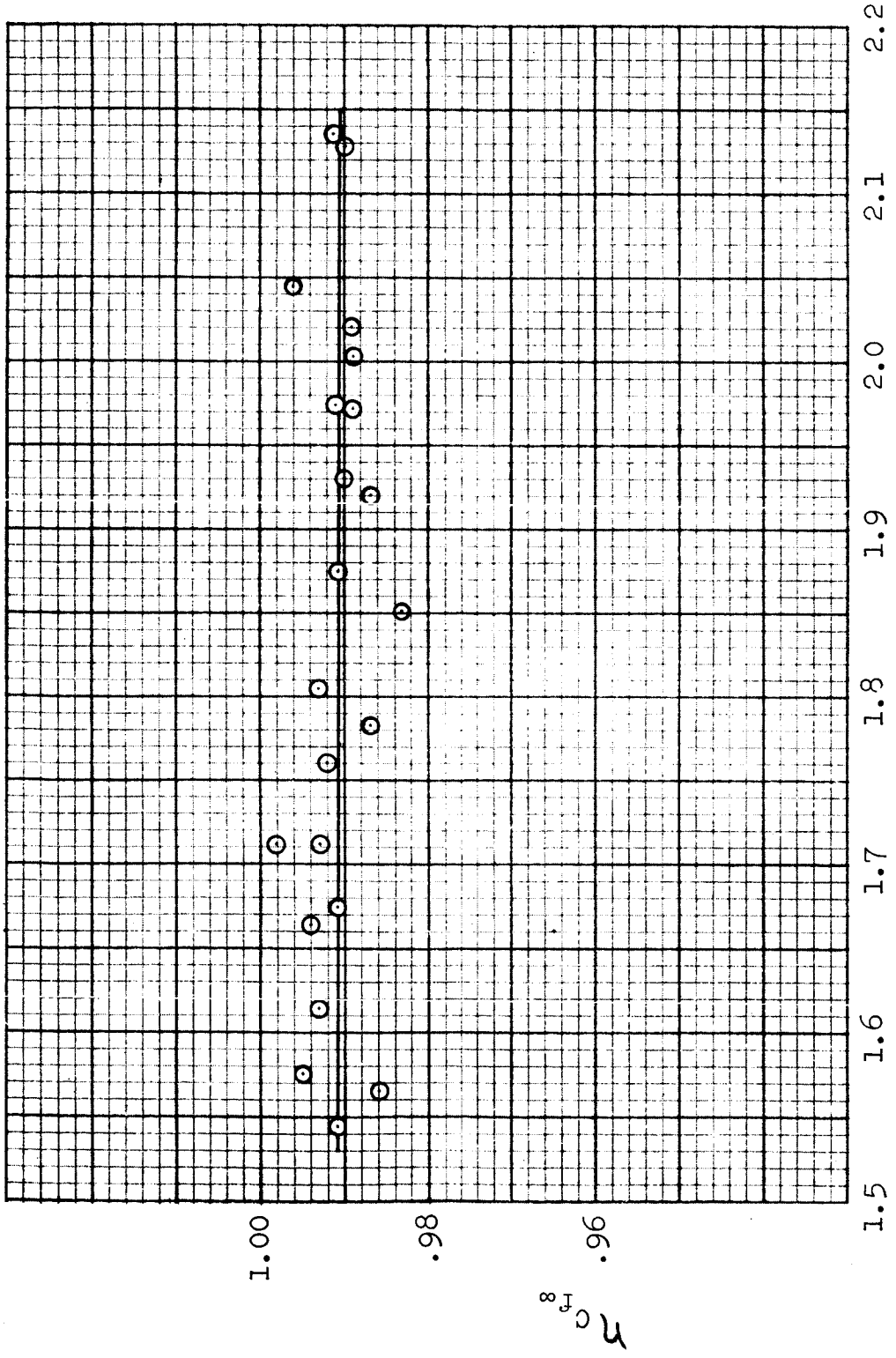

THRUST CHAMBER NOZZLE EFFICIENCY (Start Nozzle Based On Theoretical Equilibrium Composition)

FIGURE 19

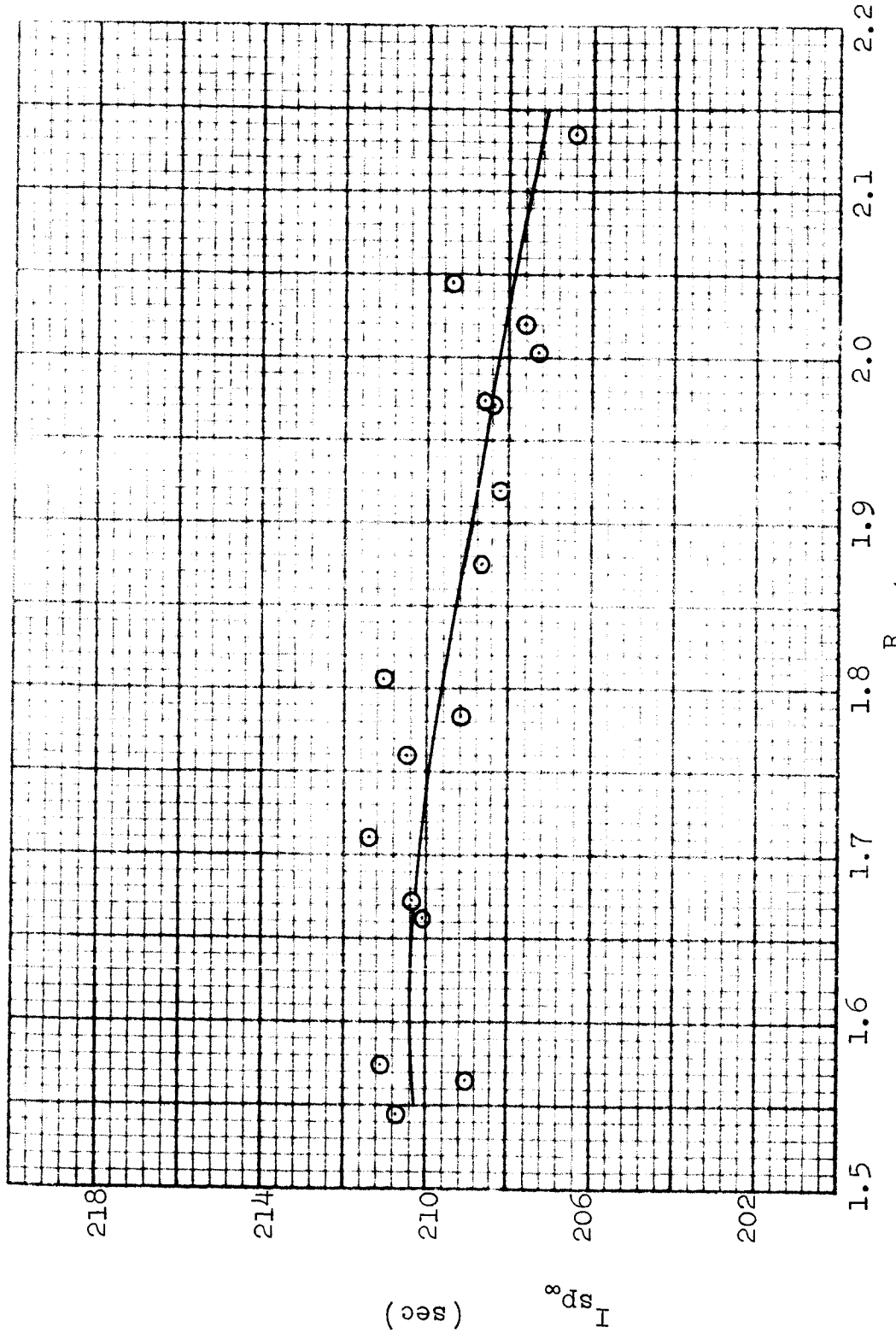

THRUST CHAMBER SEA LEVEL SPECIFIC IMPULSE CORRECTED TO VACUUM CONDITIONS

FIGURE 20

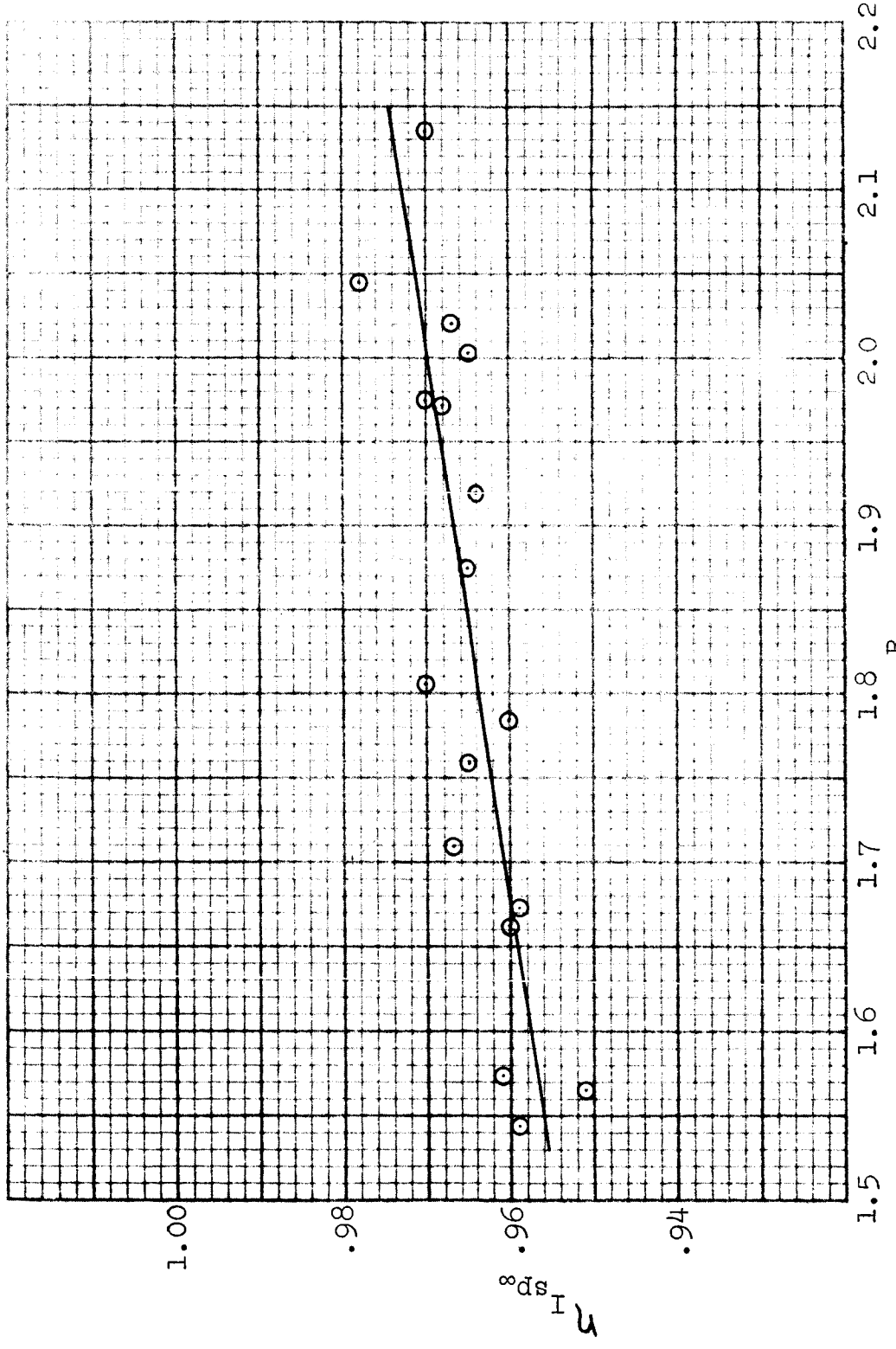

THRUST CHAMBER OVER-ALL EFFICIENCY (Sea Level Data
Based On Theoretical Equilibrium Composition)

FIGURE 21

V. ALTITUDE TEST PROGRAM

A. GENERAL

All altitude testing was conducted in Cell 2ES shown in Figure 22. This altitude facility employs a dual steam ejector system, a low-capacity ejector that can be operated continuously, and a high-capacity ejector that has a limited operating duration (approximately 5 minutes).

A water-cooled exhaust duct was installed inside the altitude facility, with a sealing bulkhead between this duct and the altitude chamber walls. Thus, all thrust chamber exhaust gases must pass through the water-cooled inner duct. The duct has an inside diameter of approximately 21 inches and an over-all length of about 18 feet (L/D = 10.3).

Figure 23 shows that 15° conical nozzle (ϵ=40) installation during final cell buildup (prior to sealing up of facility). This nozzle is shown in Figure 24 with the duct in place prior to the initial altitude test firing. The duct was mounted on a roller assembly, thus allowing for sufficient travel to mate with the various nozzle extensions. The exit plane of the nozzles with area ratio of 40 was inserted into the duct approximately 1.5 to 2.0 inches, having an annular gap between the nozzle exit support ring and the duct inside diameter of approximately 1.75 inches.

The conical nozzle extension with area ratio of 60 required a special adapter section since its over-all exit diameter was too large to be inserted directly into the duct. An 8° conical adapter section was fabricated for attachment to the end of the duct. Thus, the annular gap (about the nozzle exit) could be maintained similar to the 1.75 inches used for the ϵ=40 nozzles. Figure 25 shows the 15° conical nozzle (ϵ=60) installed with the duct adapter section in place.

The only additional instrumentation required for determining altitude thrust chamber performance (in addition to that utilized for the Cell 2ES sea-level testing) was two pressure transducers utilized for measuring the altitude during testing. Additional instrumentation was also employed to determine the water-cooled nozzle heat rejection rates and to monitor the nozzle extension skin temperatures.

The normal altitude testing sequence utilized was as follows:

(1) Once all prefire checks are completed, close facility and go to altitude using the small steam ejector system.

(2) Upon obtaining an altitude of approximately 100,000 feet, set up the desired tank and purge pressures.

(3) Conduct prerun thrust calibration.

(4) Turn on large steam ejector system and fire thrust chamber when altitude stabilizes (it usually takes about 30 seconds to stabilize at approximately 120,000 feet).

(5) Turn off the large steam ejector system on completion of test, leaving small system on to maintain altitude.

(6) Conduct postrun thrust calibration.

(7) Secure tank pressures.

(8) Conduct postrun procedures.

The nominal altitude test duration is set at approximately 30 seconds. The altitude (at the thrust chamber region) decreases slowly during the first 15 to 20 seconds of the test and then remains essentially constant for the remainder of the test (at a level of approximately 105,000 feet).

B. 15° CONICAL NOZZLE TESTING , ϵ=40

Eleven altitude tests were conducted with the 15° conical

nozzle, area ratio of 40. (Runs 2ES-1603 through 2ES-1613). All test runs were of a nominal duration of 30 seconds except Runs 2ES-1603 and 2ES-1605. Run 2ES-1603 was 44.3 seconds and useful in evaluating the over-all altitude system capability. Run 2ES-1605 was for 13.2 seconds duration because of overheating of the altitude chamber walls (at the corner where the gas flow turns 90°). A flame deflector was then installed at this location and no further facility overheating difficulties were encountered.

The tests covered the reactant ratio range of 1.573 to 2.089 at the nominal chamber pressure of 100 psia. Data were reduced at approximately 1 second from the end of the run on all tests except Run 2ES-1603. A data point was taken at 29 seconds during this test to correspond with the nominal 30-second run data point.

Performance data from these tests are listed in Table III and are discussed in greater detail later in this report.

C. 15° CONICAL NOZZLE TESTING, ϵ=60

Six altitude tests were conducted with the 15° conical nozzle, area ratio of 60 (Runs 2ES-1614 through 2ES-1619). All tests were of a nominal duration of 30 seconds and data points taken were approximately 1 second before shutdown.

The tests covered a reactant ratio range of 1.56 to 2.016 at a nominal chamber pressure of 100 psia. Data from these tests are listed on Table III.

As previously mentioned, a conical duct adapter section was required for testing this nozzle extension.

D. RAO NOZZLE TESTING, ϵ =40

Six (6) altitude tests were conducted with Rao nozzle with an area ratio of 40 (Runs 2ES-1620 through 2ES-1625). These tests, at the nominal chamber pressure of 100 psia, covered a reactant ratio range of 1.626 to 2.021. Again, data points were taken approximately 1 second from the shutdown of the 30-second tests.

Data from this series of tests are listed on Table IV.

E. 80% BELL NOZZLE TESTING, ϵ =40

Seven altitude tests were conducted with the 80% Bell nozzle, ϵ=40 (Runs 2ES-1626 through 2ES-1632). At the nominal 100 psia chamber pressure, testing was conducted over the reactant ratio range of 1.608 to 2.011. All tests had the same nominal 30-second duration except Runs 2ES-1628 and 2ES-1629.

During Run 2ES-1628, a loss of altitude occurred after approximately 7 seconds and the test was terminated at 16.6 seconds because of the excessive decrease in altitude. The altitude loss was apparently due to water freezing in one or more of the large steam system condensers. Exhaust flame flashback damaged electrical wiring and some instrumentation in the thrust chamber area. The thrust chamber hardware was undamaged and, therefore, testing was resumed after the damaged wiring and instrumentation were replaced. Run 2ES-1629 was terminated after 21.1 seconds because a nozzle extension surface thermocouple erroneously indicated extension overheating.

Data points were taken at the normal times (1 second from shutdown) except Run 2ES-1618. Data for this test were taken at the 5-second point (2 seconds before the altitude trend changed). Data from these tests are listed on Table IV.

F. DISCUSSION OF ALTITUDE TEST DATA

Thirty altitude test runs were conducted to define experimentally the performance of the nozzles. Chamber pressure transducers and propellant flowmeter sets were switched at least once during each series of tests on a particular nozzle. This permitted obtaining experimental data at a given reactant ratio with independently calibrated sets of instrumentation.

Figure 26 shows the injector characteristic velocity plotted as a function of reactant ratio (R_o/f). The curve includes both the sea-level and altitude data. The peak characteristic velocity of 5521 ft/sec is obtained at a reactant ratio of approximately 1.68.

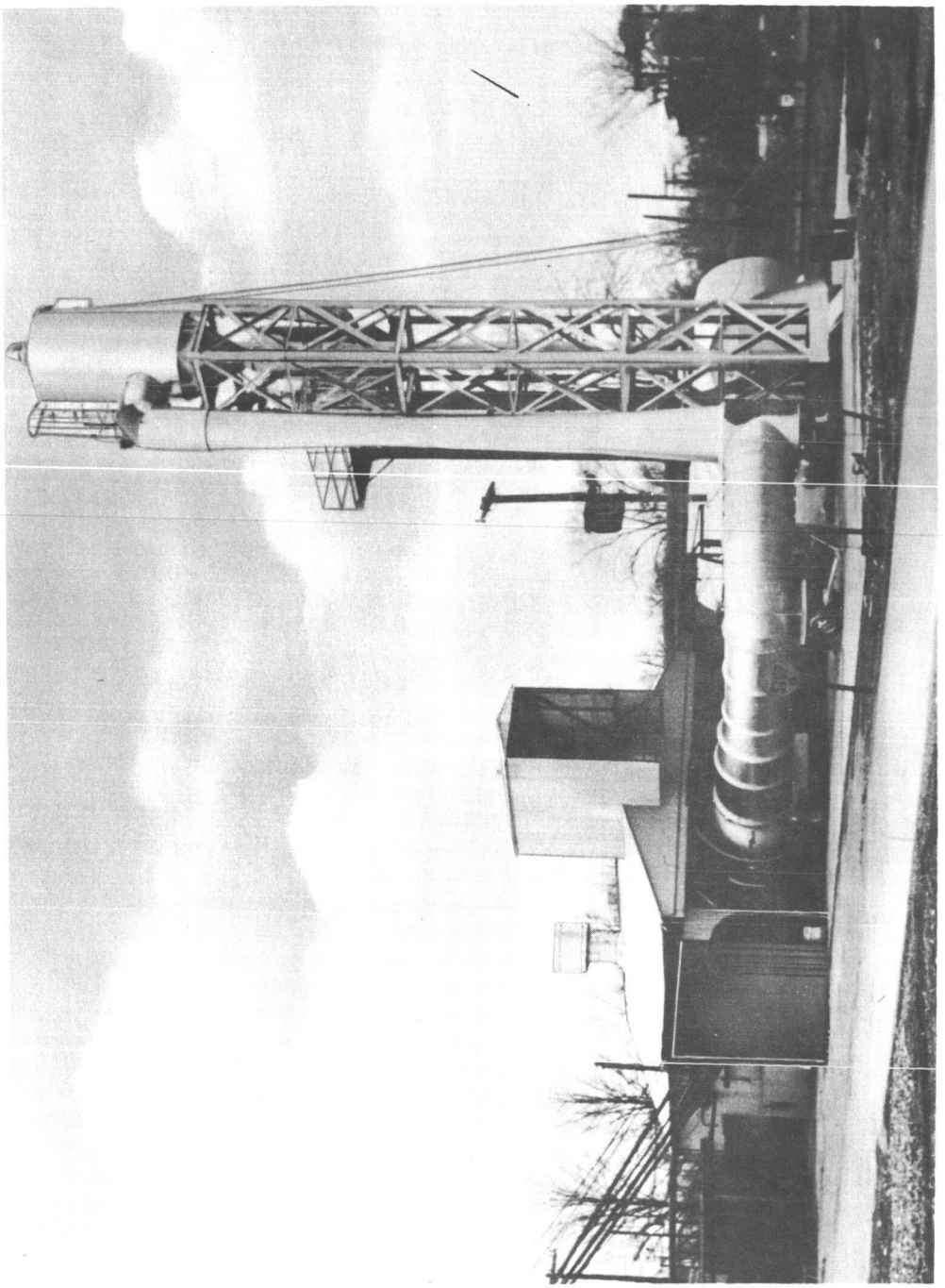

ALTITUDE TEST FACILITY

FIGURE 22

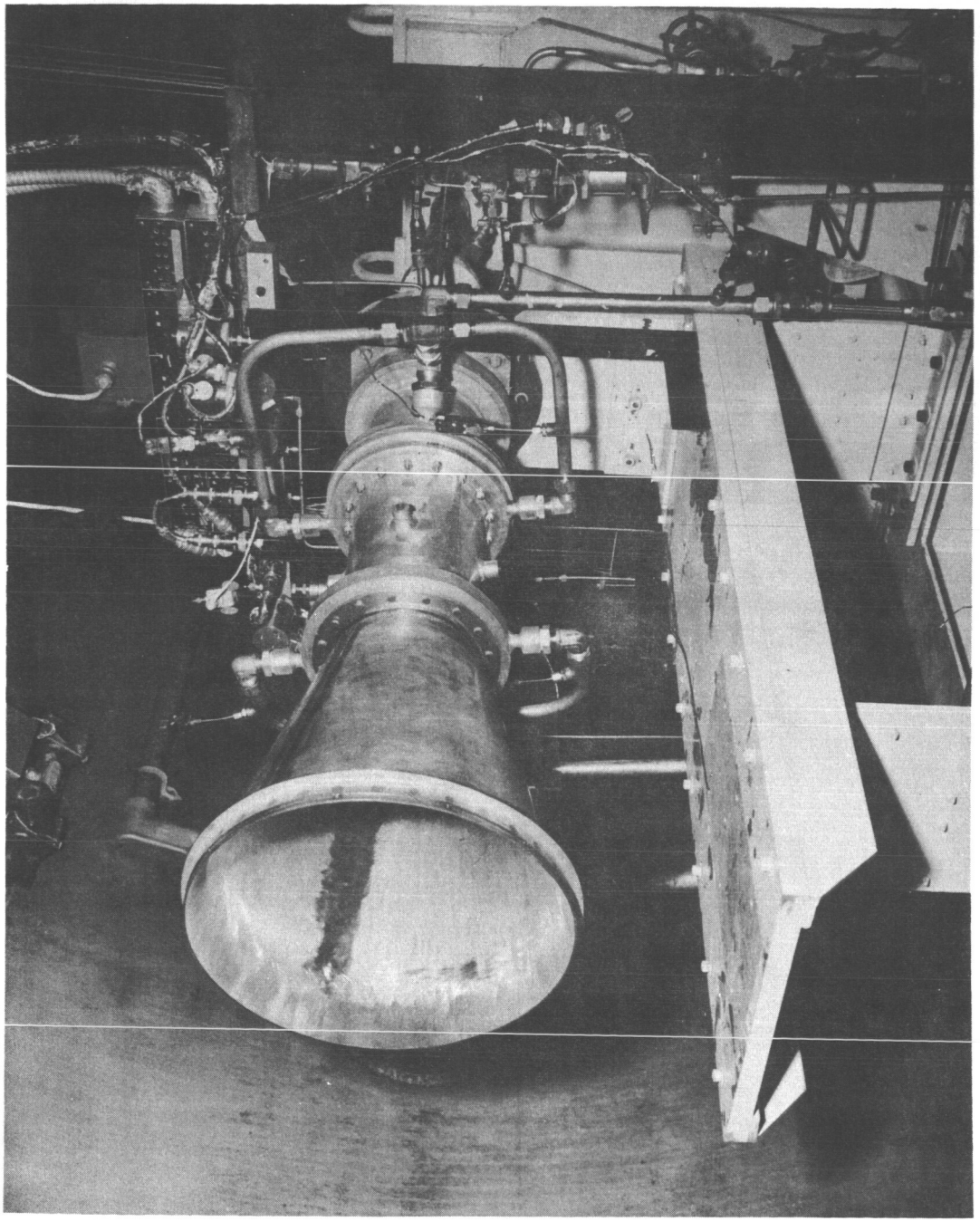

15° CONICAL NOZZLE (ϵ=40) INSTALLATION
FIGURE 23

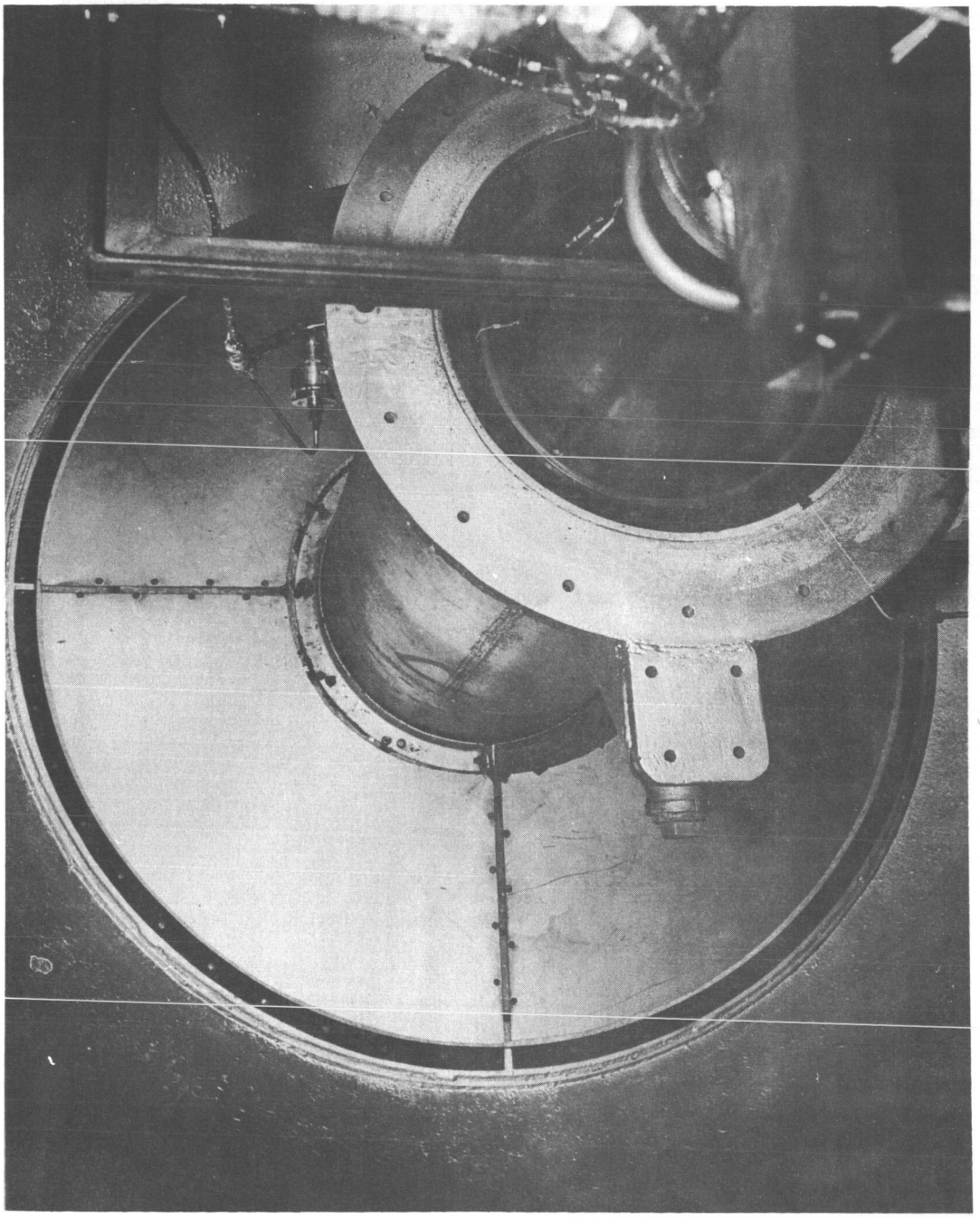

ALTITUDE FACILITY INTERIOR (DUCT SECTION)
FIGURE 24

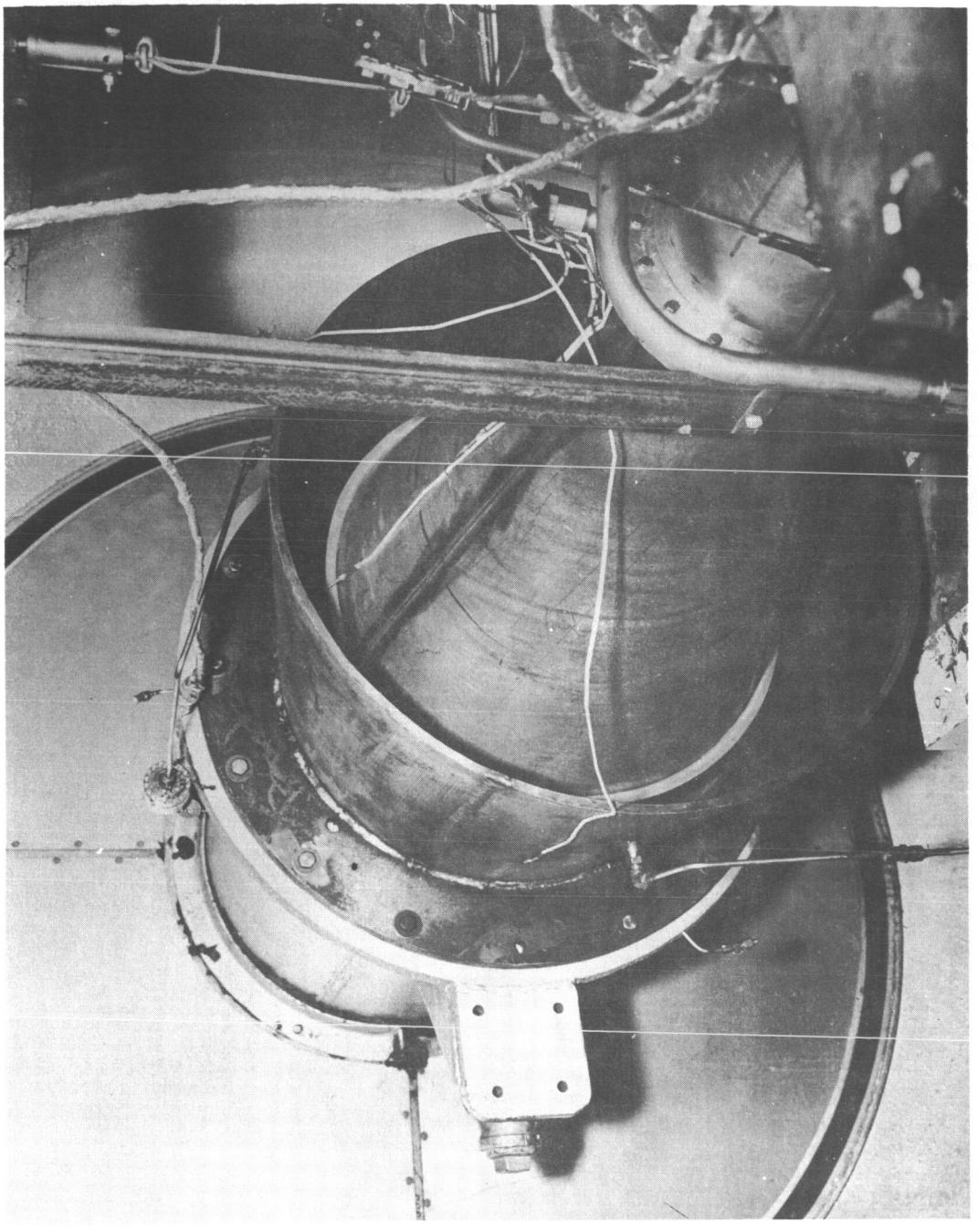

15° CONICAL NOZZLE (ϵ=60) DUCT INSTALLATION
FIGURE 25

MODEL _____

DATE 2-24-64

BELL AEROS

T

ALTITUDE TEST DATA -

	Test Number	Duration (sec)	P_a (psia)	$\bar{P}_o$ (psia)	$R_{o/f}$	W_T (lb/sec)	
29	2ES-1603	44.3	0.126	102.49	1.801	3.216	9
30	-1604	30.5	0.110	102.06	1.626	3.198	9
31	-1605	14.2	0.078	99.02	2.089	3.145	9
32	-1606	30.3	0.092	98.93	1.573	3.108	9
33	-1607	29.4	0.124	98.60	1.765	3.102	9
34	-1608	29.8	0.112	99.25	1.994	3.144	9
35	-1609	30.0	0.088	100.16	1.781	3.142	9
36	-1610	30.6	0.087	99.58	1.916	3.135	9
37	-1611	30.0	0.102	100.86	1.607	3.160	9
38	-1612	31.1	0.094	96.68	1.654	3.010	9
39	-1613	30.3	0.109	100.05	1.826	3.151	9
					ALTITUDE TEST DATA -		
40	2ES-1614	30.1	0.100	100.45	1.596	3.159	9
41	-1615	31.5	0.113	98.72	1.772	3.094	9
42	-1616	31.5	0.117	99.68	2.016	3.161	9
43	-1617	30.5	0.119	99.74	1.560	3.134	9
44	-1618	30.8	0.104	101.96	1.750	3.195	9
45	-1619	30.7	0.116	100.26	1.950	3.159	9

Form 0345 Rev. 1258 Sheet 1

ABLE III

15° CONICAL NOZZLE ϵ=40

F_∞ (lb)	c* (ft/sec)	C_{f_∞}	I_{sp_∞} (sec)	η_{c^*}	ηC_{f_∞}	ηI_{sp_∞}	Remarks
75.9	5516	1.772	303.5	0.971	0.968	0.940	
76.4	5524	1.780	305.3	0.966	0.974	0.941	
48.4	5449	1.782	301.6	0.977	0.971	0.949	Facility overheating
37.7	5509	1.764	301.7	0.963	0.966	0.930	
42.9	5502	1.779	304.0	0.967	0.972	0.940	
48.7	5464	1.779	301.7	0.973	0.970	0.944	
54.7	5517	1.774	303.9	0.970	0.969	0.940	
52.6	5498	1.780	303.9	0.974	0.971	0.946	
59.7	5524	1.771	303.7	0.966	0.970	0.937	
20.4	5559	1.772	305.8	0.973	0.969	0.943	
51.3	5496	1.769	301.9	0.969	0.966	0.936	
15° CONICAL NOZZLE ϵ=60							
55.7	5504	1.789	305.7	0.962	0.968	0.931	
54.3	5523	1.799	308.4	0.971	0.971	0.943	
55.9	5458	1.803	305.6	0.973	0.970	0.944	
51.5	5508	1.794	306.8	0.963	0.971	0.935	
78.8	5524	1.786	306.4	0.970	0.964	0.935	
56.6	5493	1.794	306.0	0.975	0.966	0.942	

MODEL _____

DATE _____

BELL AERO

ALTITUDE TEST DA

Test Number		Duration (sec)	P_a (psia)	$\overline{P}_o$ (psia)	$R_{o/f}$	W_T (lb/sec)	F_∞ (lb)
46	2ES-1620	30.8	0.110	98.64	1.644	3.159	945.9
47	-1621	29.4	0.109	99.27	1.779	3.174	948.0
48	-1622	28.4	0.110	99.08	2.021	3.190	952.3
49	-1623	30.8	0.118	99.04	1.626	3.151	946.0
50	-1624	30.0	0.114	99.51	1.875	3.174	956.4
51	-1625	30.0	0.115	100.31	2.015	3.226	962.8

ALTITUDE TEST DATA

52	2ES-1626	30.4	0.120	99.45	1.608	3.179	954.1
53	-1627	31.5	0.123	100.77	1.812	3.223	973.6
54	-1628	16.6	0.058	100.04	1.978	3.216	962.7
55	-1629	21.1	0.120	99.84	2.011	3.213	969.4
56	-1630	30.8	0.110	100.01	1.612	3.192	958.4
57	-1631	30.4	0.110	100.88	1.798	3.218	966.8
58	-1632	29.6	0.116	100.02	1.982	3.212	965.7

TABLE IV

TA - RAO NOZZLE ϵ = 40

	c^* (ft/sec)	C_{f_∞}	I_{sp_∞} (sec)	η_{c^*}	$\eta_{C_{f_\infty}}$	$\eta_{I_{sp_\infty}}$	Remarks
	5496	1.754	299.4	0.962	0.960	0.923	
	5505	1.747	298.7	0.968	0.955	0.924	
	5467	1.758	298.5	0.975	0.959	0.935	
	5532	1.747	300.2	0.968	0.956	0.925	
	5518	1.758	301.3	0.975	0.960	0.936	
	5473	1.756	298.5	0.976	0.958	0.935	
- 80% BELL NOZZLE ϵ = 40							
	5497	1.758	300.1	0.961	0.962	0.925	
	5494	1.771	302.1	0.968	0.967	0.936	
	5466	1.764	299.3	0.972	0.962	0.935	Loss of altitude
	5460	1.779	301.7	0.973	0.970	0.944	Erroneous skin thermocouple indicating extension overheating
	5505	1.756	300.3	0.963	0.961	0.925	
	5509	1.756	300.4	0.970	0.959	0.930	
	5472	1.769	300.7	0.974	0.965	0.940	

The injector combustion efficiency (based on equilibrium composition) is shown in Figure 27 as a function of reactant ratio. The combustion efficiency varies linearily from approximately 0.965 at a reactant ratio of 1.60 to 0.976 at a reactant ratio of 2.00. Both sea-level and altitude data are included in this Figure 27.

Figures 26 and 27 represent the final performance for this injector-thrust chamber assembly. Comparison of the combustion efficiency (ηc^*) data in Figures 17 and 26 show that the final data has shifted 0.2 to 0.3% from the previously quoted sea-level performance data.

The vacuum thrust coefficients ($C_{f\infty}$) for the four nozzles tested are shown in Figure 28 and the nozzle efficiencies (based upon theoretical frozen composition for ϵ=40 and 60) are shown in Figure 29. Statistical analysis indicates the nozzle efficiency ($\eta C_{f\infty}$) values of the respective nozzles are independent of reactant ratio. An examination of the three ϵ=40 nozzle data indicates that, with decreasing % Bell (nozzle length), the nozzle efficiency decreases. An indication that additional losses are associated with the larger area ratio nozzles can be seen by a comparison of the respective nozzle efficiencies of the two conical nozzles.

The thrust chamber altitude specific impulse ($I_{sp\infty}$) corrected to vacuum conditions is plotted as a function of reactant ratio in Figure 30. Best fit curves through the individual data points indicate that the 80% Bell nozzle maximum vacuum specific impulse occurs at a slightly different reactant ratio than the other three nozzles (where the maximum values occur approximately at the same reactant ratio). Examination of the over-all thrust chamber efficiencies shown in Figures 32 and 33 will be helpful in explaining how this difference occurs. From these figures, it can be seen that the three nozzles that have similar maximum $I_{sp\infty}$ values

(in Figure 30) have essentially the same I_{sp_∞} versus R_o/f slopes. The 80% Bell nozzle η I_{sp_∞} best fit curve, however, has a slightly steeper slope. This indicates that the characteristic velocity values of the 80% nozzle tests are not distributed evenly about the best fit characteristic velocity line, but have a slightly greater slope as a function of reactant ratio.

Figure 31 presents the same data (I_{sp^∞} versus R_o/f) shown in Figure 30, except now the individual data points were not plotted nor were the best fit curves established. The curves shown in Figure 31 were obtained using the best fit c* and C_{f_∞} values from Figures 26 and 28 to determine the I_{sp_∞} for each nozzle at any particular reactant ratio (R_o/f). This figure represents a more-accurate comparison and shows the four nozzle vacuum specific curves having similar shapes and with maximum values (of I_{sp_∞}) occurring at approximately the same reactant ratio ($R_o/f = 1.75$).

The maximum vacuum specific impulse values from Figure 31 are as follows:

Nozzle Type	Maximum Experimental I_{sp_∞} (sec)
15° Conical, ϵ=40	304.0
15° Conical, ϵ=60	307.5
80% Bell, ϵ=40	302.2
Rao, ϵ=40	300.4

Additional corrections were made to the experimental vacuum specific impulse data so that a comparison could be obtained for the analytical predicted performance values. The experimental data were to be compared to the theoretical equilibrium and frozen composition data, the Bray predicted data, and the theoretical performance data based upon the gas composition becoming frozen at the nozzle throat. To obtain the desired comparisons, the following corrections were applied to either the experimental or theoretical data.

(1) Combustion efficiency correction

(2) Correction for nozzle three-dimensional losses

(3) Correction for energy losses (by heat transfer) during the gas expansion process

(4) Nozzle friction (drag) losses

The combustion efficiency correction was, during initial data analysis, accomplished by simply multiplying each experimental data point by the reciprocal of its respective combustion efficiency ($1/\eta\, c^*$). During subsequent evaluation of the data, it was decided that it would be more valid to make this correction to the theoretical data. This was accomplished by adjusting the theoretical combustion gas enthalpy (in the chamber) to obtain characteristic velocities equal to those obtained experimentally at each reactant ratio. The theoretical equilibrium, frozen, Bray, and frozen at the throat data were revised by this method.

The nozzle three-dimensional corrections were based on the previously determined three-dimensional nozzle efficiencies computed during the design phase of the program (see Section G of the Appendix).

The performance loss due to heat rejection during the expansion process was computed for each nozzle configuration utilizing an incremental Rayleigh line solution. The experimental heat rejection rates were used for these calculations which were conducted on the IBM 7090 computer.

Calculations were also conducted on the computer to assist in the evaluation of the nozzle friction (drag) losses. The absolute magnitude of this friction loss (pounds drag) could not be accurately computed. However, the relative drag associated with different area ratios of a particular nozzle contour can be computed. This was done for the 15° conical nozzle at ϵ=40 and 60. Since the absolute frictional losses are unknown, a value of 1% was assumed for all nozzles with ϵ=40. The friction losses at the ϵ=60 conical nozzle were computed based upon using the

previously calculated relative drag and the assumed 1% friction for the ϵ=40 nozzles.

The appropriate corrections for nozzle three-dimensional, heat transfer and friction losses were applied to the experimental data. These correction factors, assumed to be independent of reactant ratio, are summarized (for the various nozzles) in Table V.

The corrected experimental vacuum impulse data are tabulated in Table VI. The specific impulse symbols are defined as follows:

Symbol	Correction Applied
I_{sp_∞}	Experimental vacuum specific impulse
$I_{sp_{\infty 1}}$	Three-dimensional losses
$I_{sp_{\infty 2}}$	Heat Transfer losses
$I_{sp_{\infty 3}}$	Friction (drag)

The final corrected experimental specific impulse ($I_{sp_{\infty 3}}$) values for the four nozzles are shown in Figures 34 through 37. Also shown in these figures are:

(1) The theoretical equilibrium composition vacuum specific impulse (for 100% η c*).

(2) The theoretical equilibrium composition vacuum specific impulse revised for actual combustion efficiencies.

(3) The Bray analytical vacuum specific impulse revised for actual combustion efficiencies. (The Bray analytical date for the four nozzles was supplied by NASA-MSC.)

(4) The theoretical vacuum specific impulse assuming the gas composition becomes frozen at the throat (revised for actual combustion efficiencies).

(5) The theoretical frozen composition vacuum specific impulse revised for actual combustion efficiencies.

The Bray analytical vacuum specific impulse data depend upon the individual nozzle contours, while the other theoretical data are independent of contour. However, the Bray curves for the 15° conical nozzles are identical to the 80% Bell nozzle Bray data. This occurs because the nozzle throat contours are identical to an area ratio larger than the calculated Bray "breakpoint" area ratios.

The 15° conical nozzle data are slightly above the Bray predicted (at the lower restart ratios) and between the Bray and frozen at the throat data at the higher reactant ratios. The 80% Bell nozzle experimental curve lies slightly below the theoretical frozen at the throat curve. The Rao nozzle data lies between the theoretical frozen composition and frozen at the throat analytical data.

Table VII shows the difference (in seconds I_{sp}) between the revised Bray analytical data and the corrected experimental data for the four nozzles.

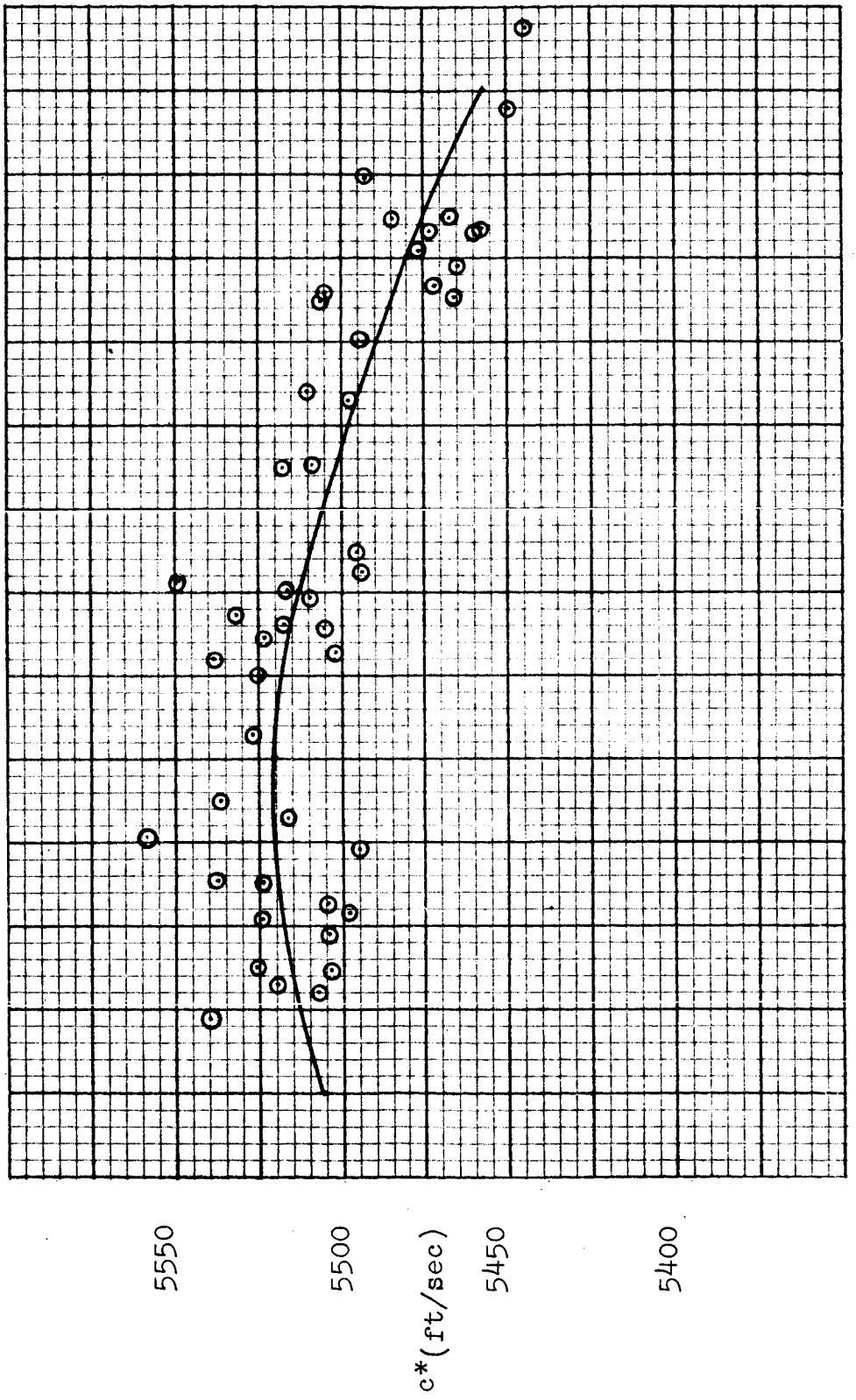

INJECTOR CHARACTERISTIC VELOCITY
(COMBINED SEA LEVEL AND ALTITUDE DATA)

FIGURE 26

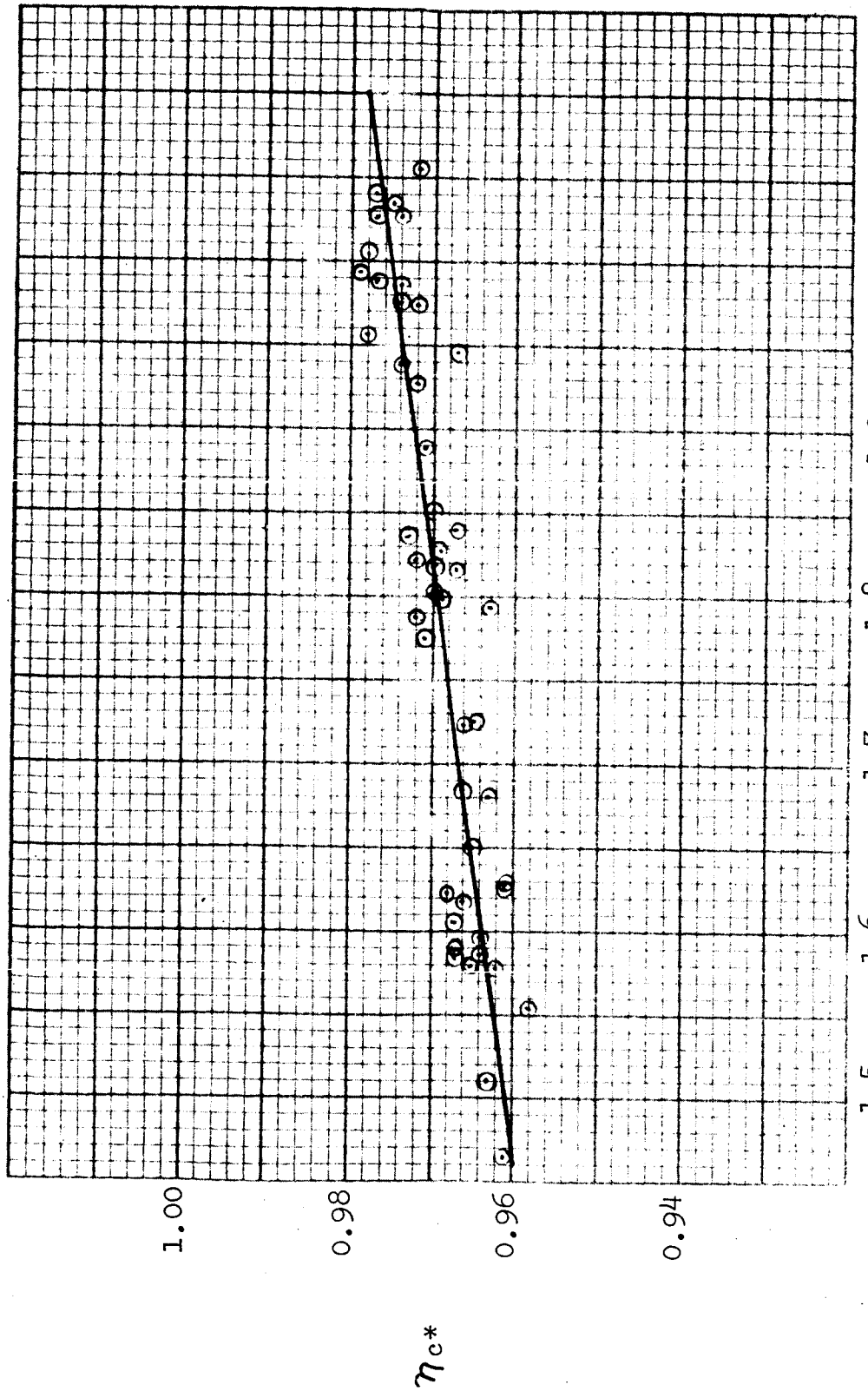

INJECTOR COMBUSTION EFFICIENCY (COMBINED SEA LEVEL AND ALTITUDE DATA - BASED ON THEORETICAL EQUILIBRIUM COMPOSITION)

FIGURE 27

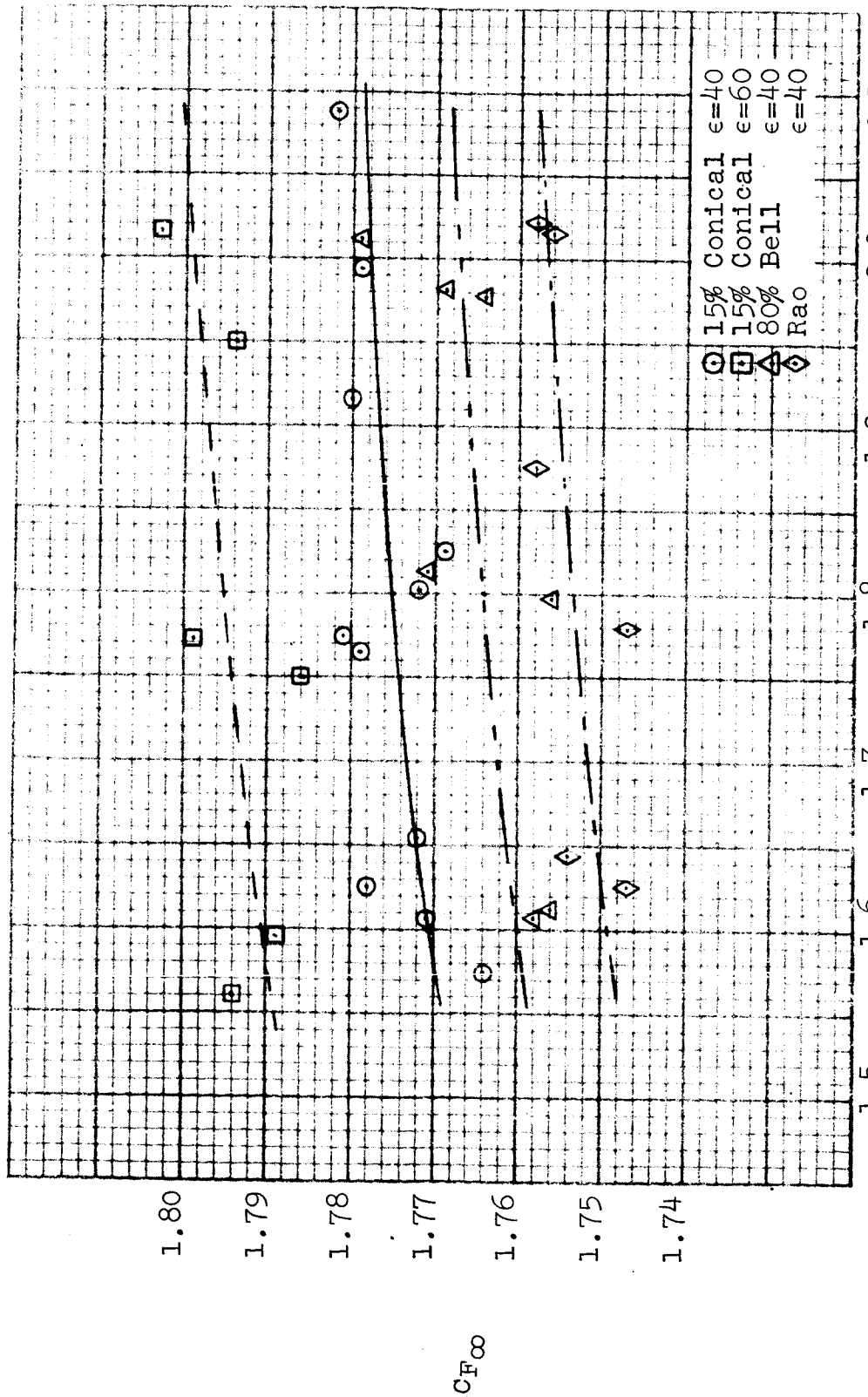

ALTITUDE NOZZLE VACUUM THRUST COEFFICIENTS

FIGURE 28

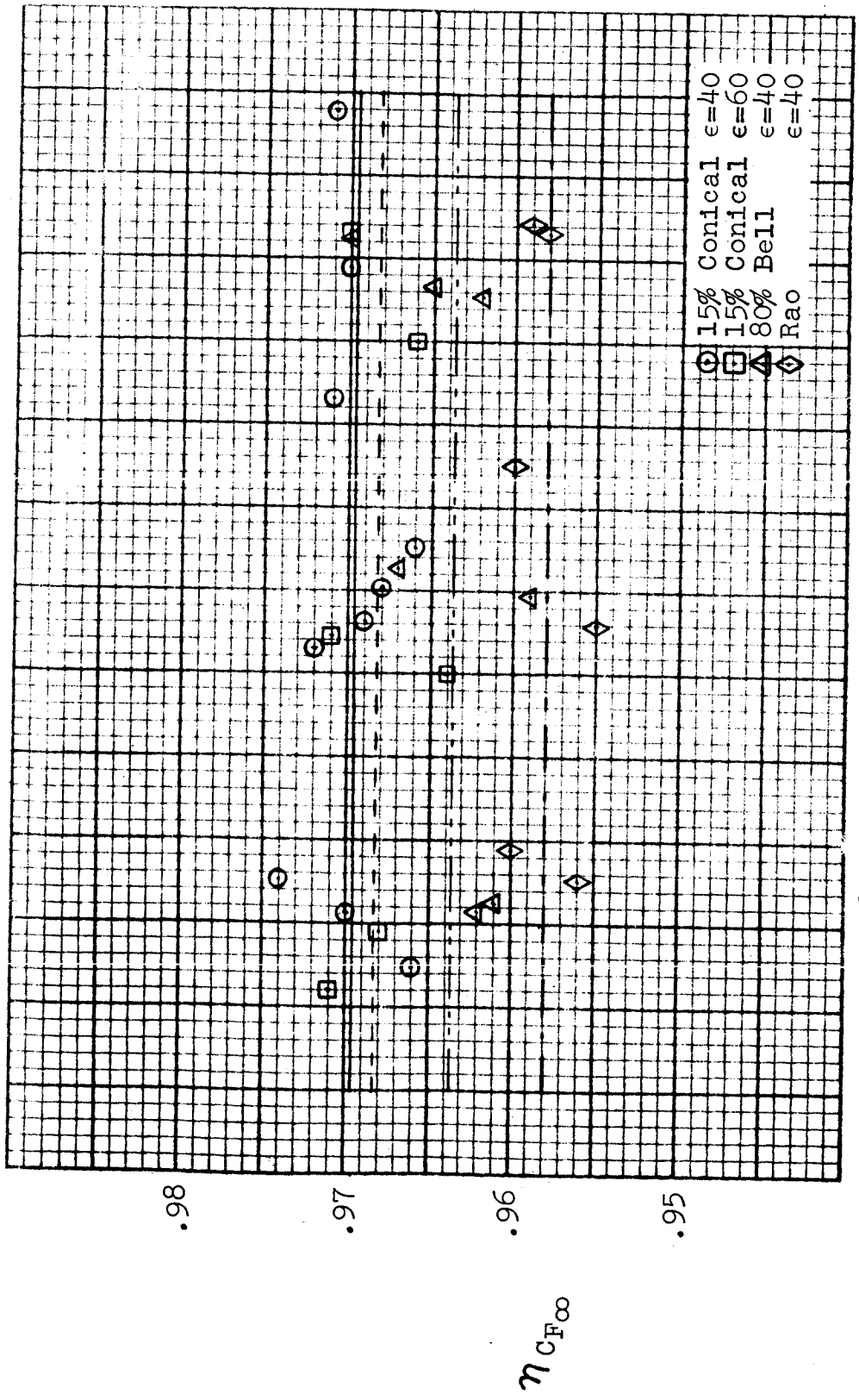

ALTITUDE NOZZLE EFFICIENCY (BASED ON THEORETICAL FROZEN COMPOSITION)

FIGURE 29

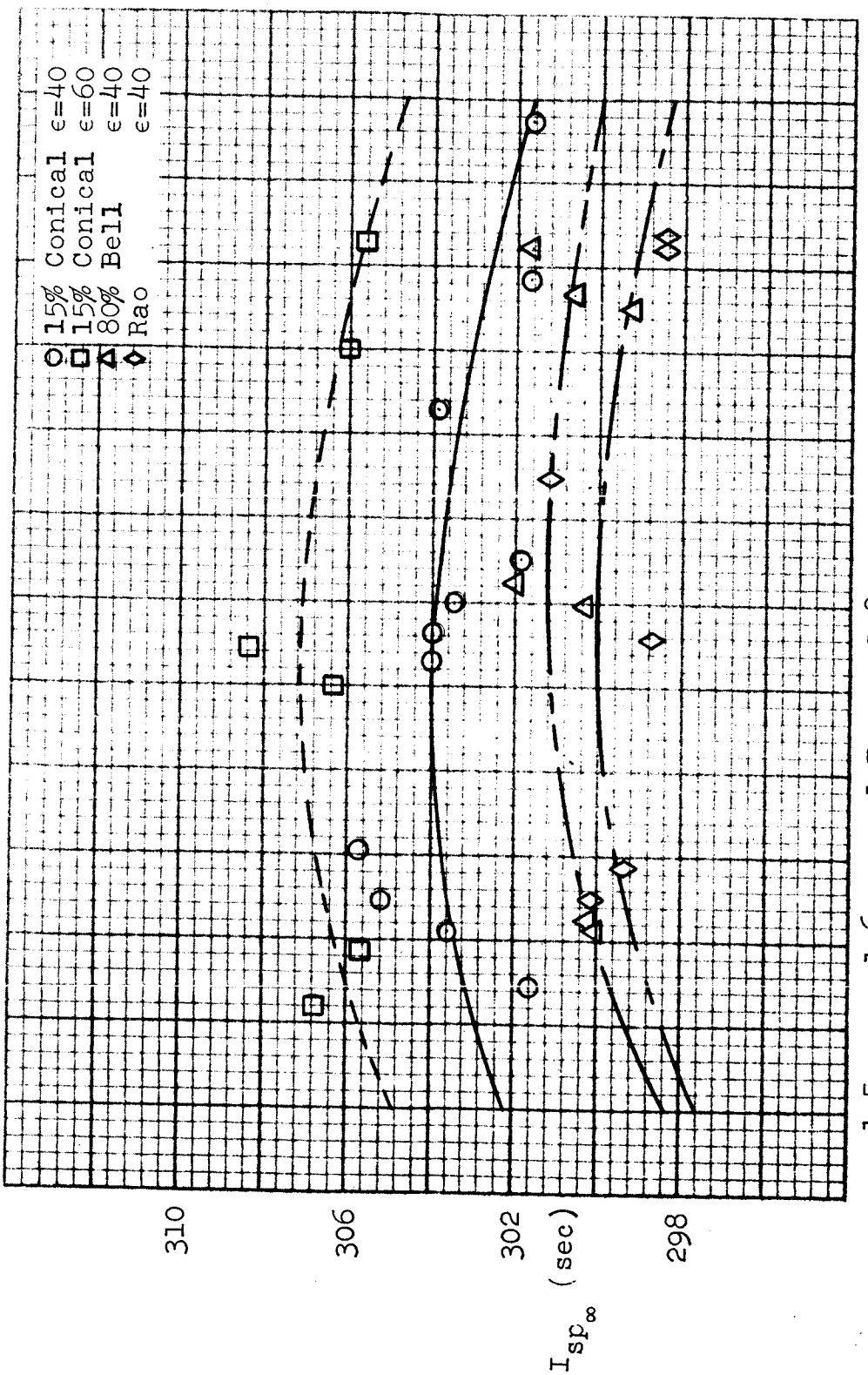

THRUST CHAMBER ALTITUDE SPECIFIC IMPULSE
CORRECTED TO VACUUM CONDITIONS (ACTUAL DATA)

FIGURE 30

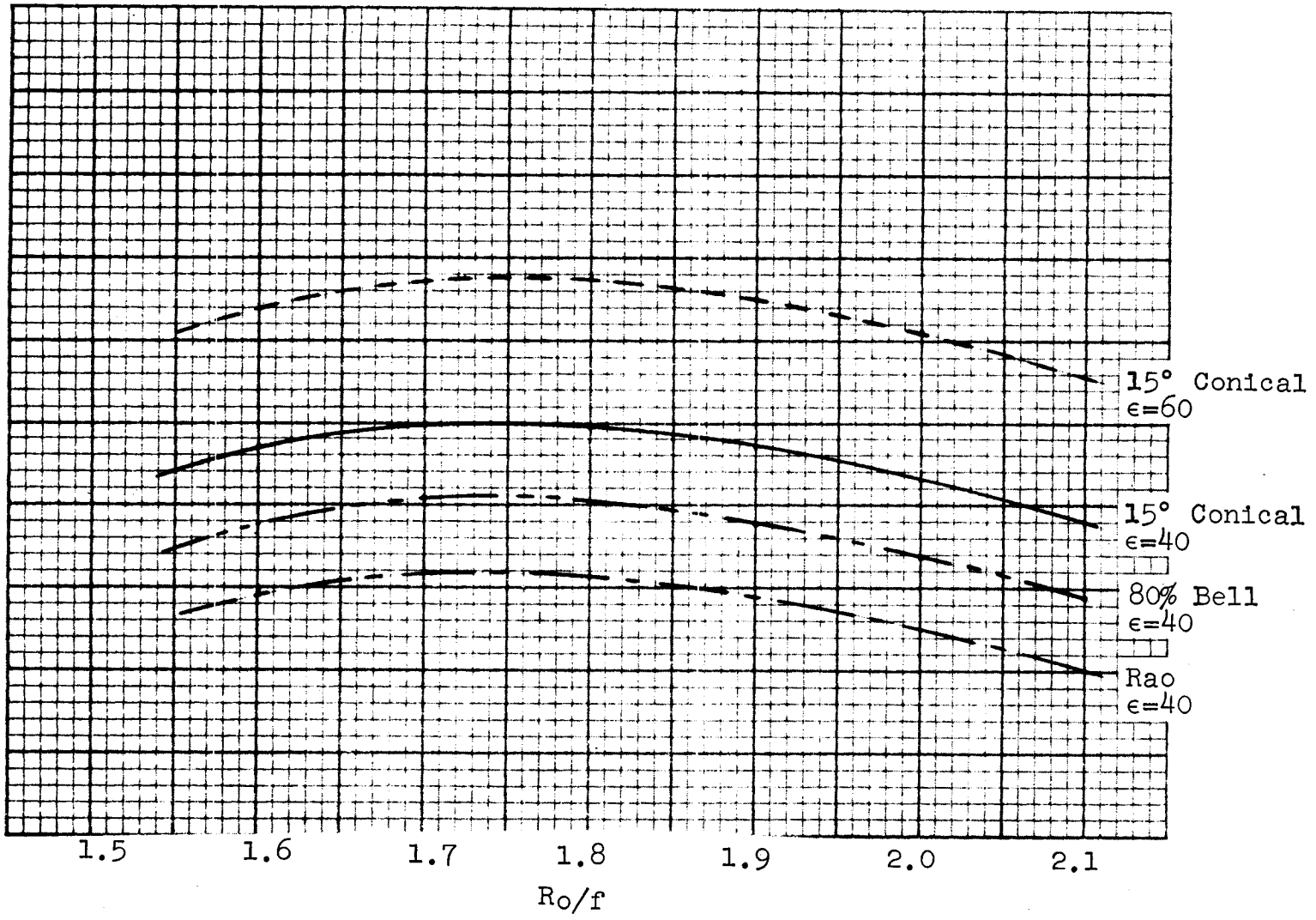

THRUST CHAMBER ALTITUDE SPECIFIC IMPULSE
CORRECTED TO VACUUM CONDITIONS (AVERAGE DATA)

FIGURE 31

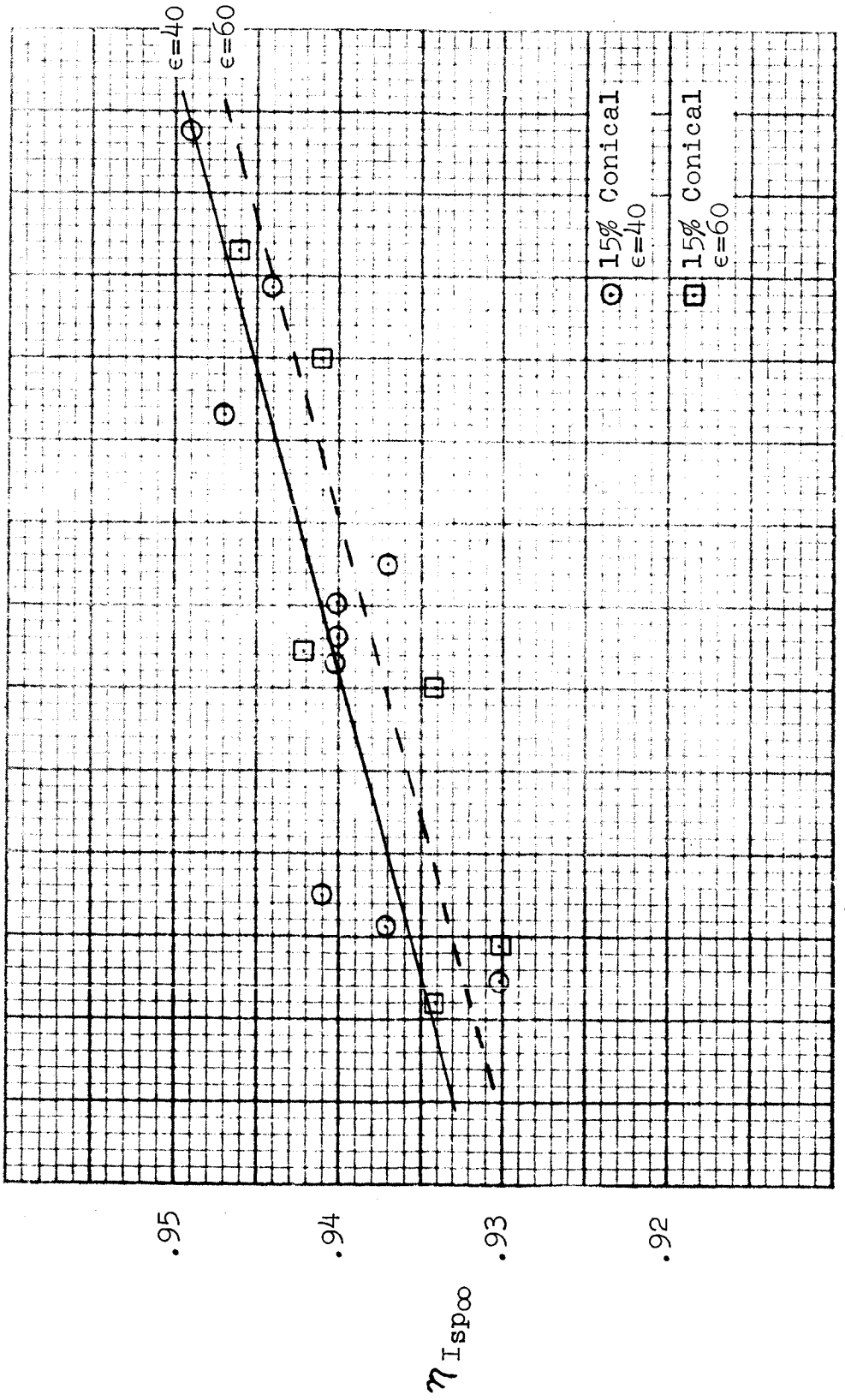

THRUST CHAMBER OVERALL EFFICIENCY 15° CONICAL NOZZLES (ALTITUDE DATA - BASED ON THEORETICAL EQUILIBRIUM C* AND THEORETICAL FROZEN $C_{F\infty}$ DATA)

FIGURE 32

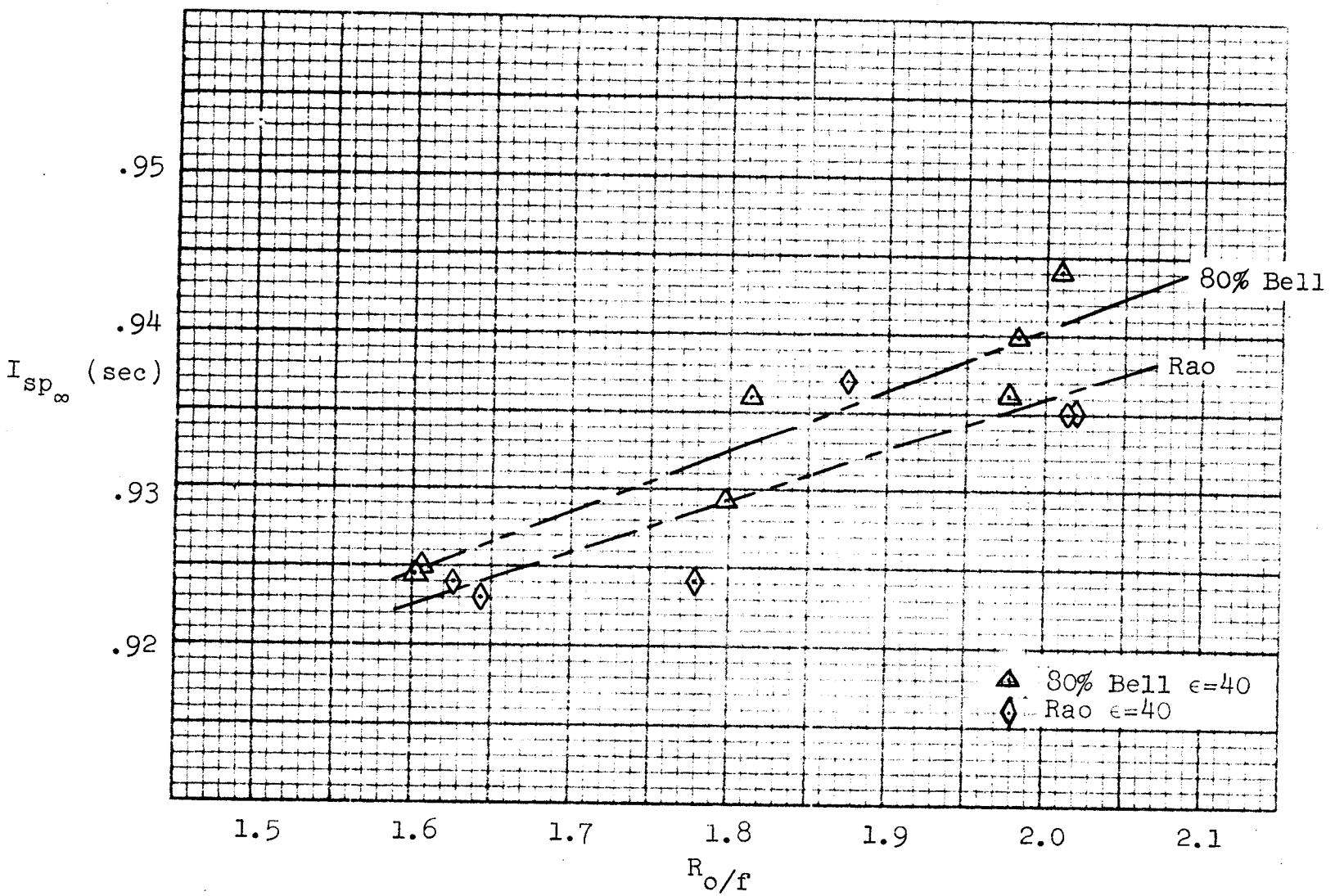

THRUST CHAMBER OVER-ALL EFFICIENCY CONTOUR NOZZLES (ALTITUDE DATA - BASED ON THEORETICAL EQUILIBRIUM c* AND THEORETICAL FROZEN C_{F_∞} DATA)

FIGURE 33

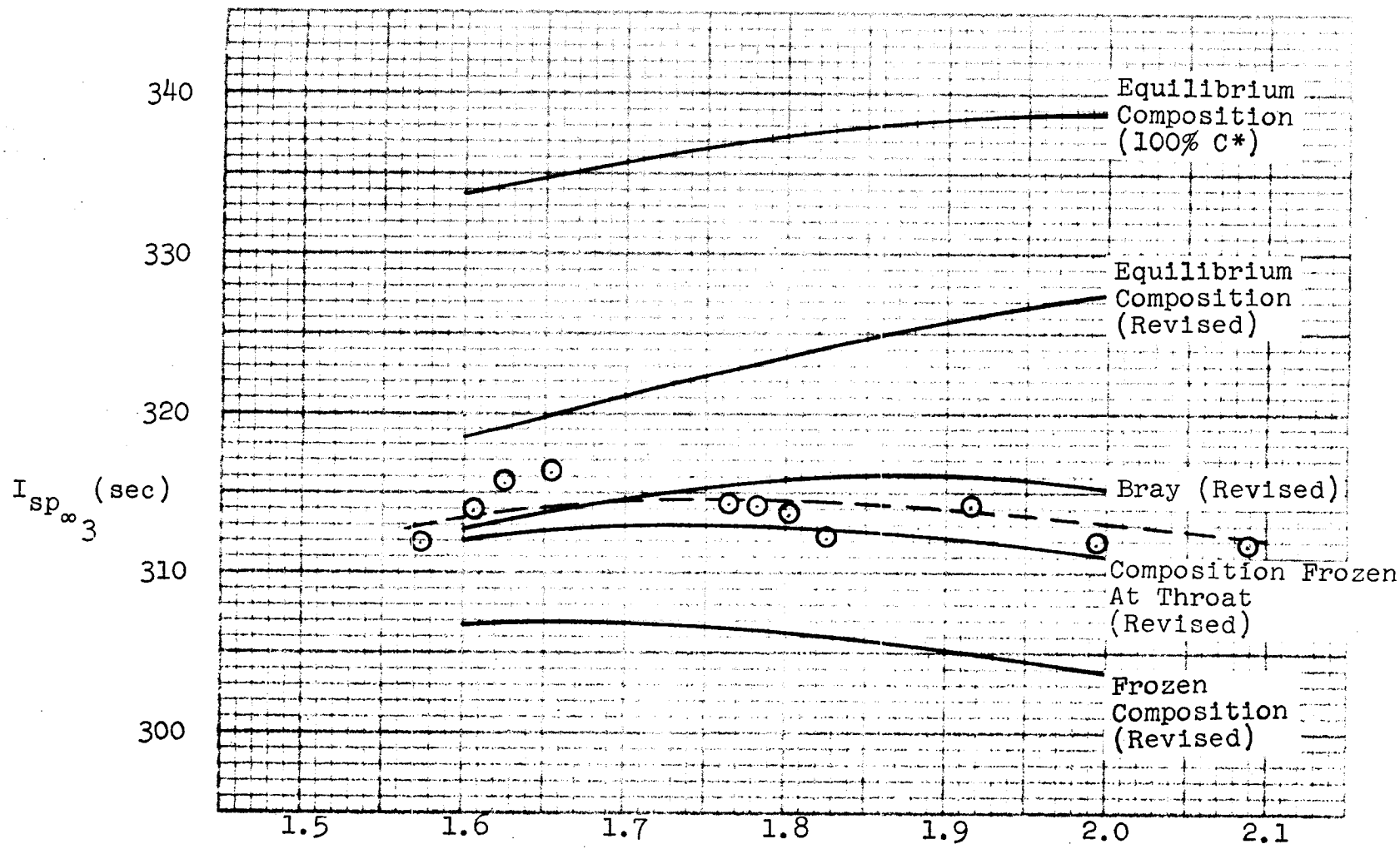

CORRECTED VACUUM SPECIFIC IMPULSE
15° CONICAL NOZZLE, ϵ =40

FIGURE 34

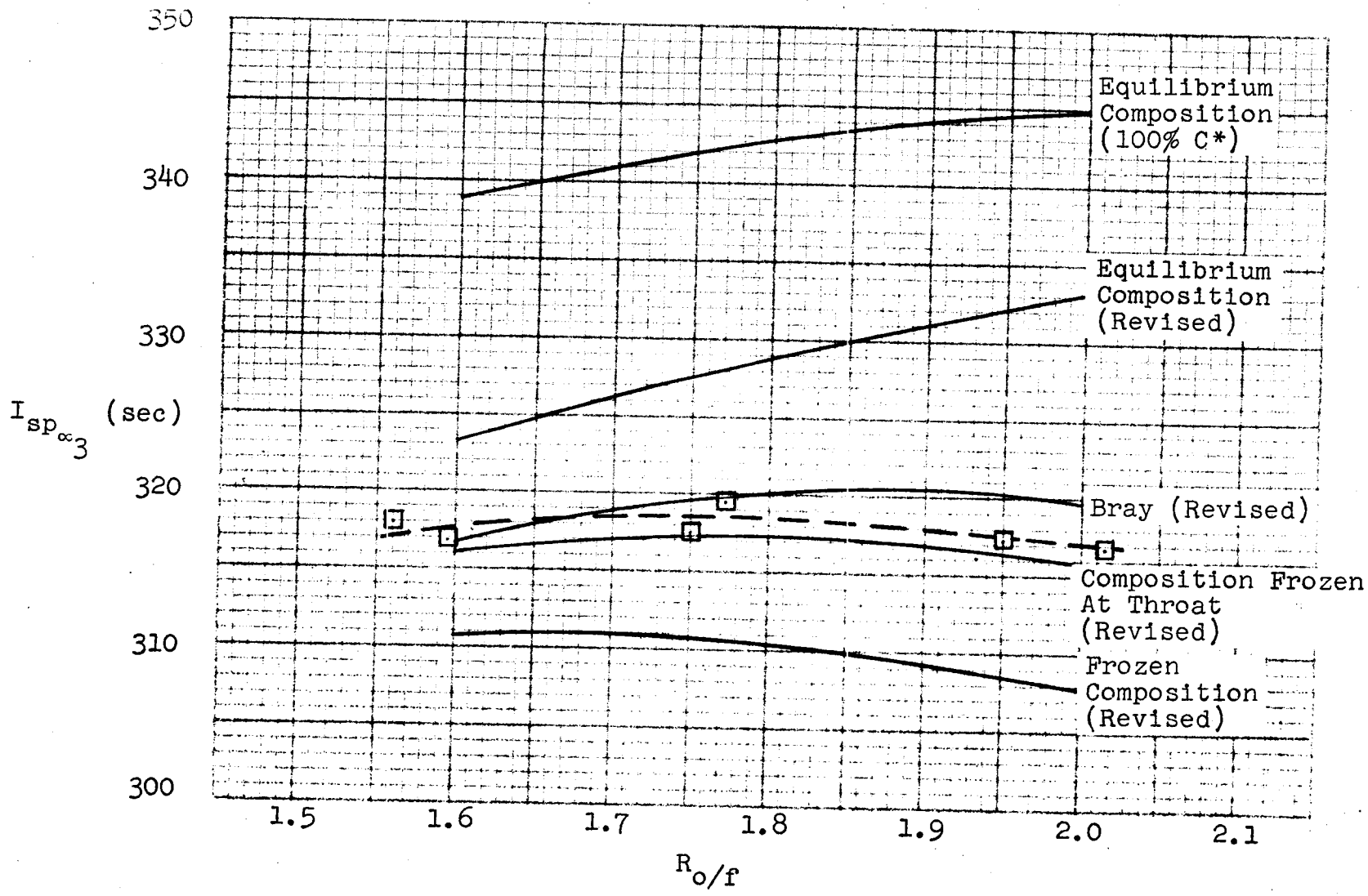

CORRECTED VACUUM SPECIFIC IMPULSE
15° CONICAL NOZZLE, ϵ =60

FIGURE 35

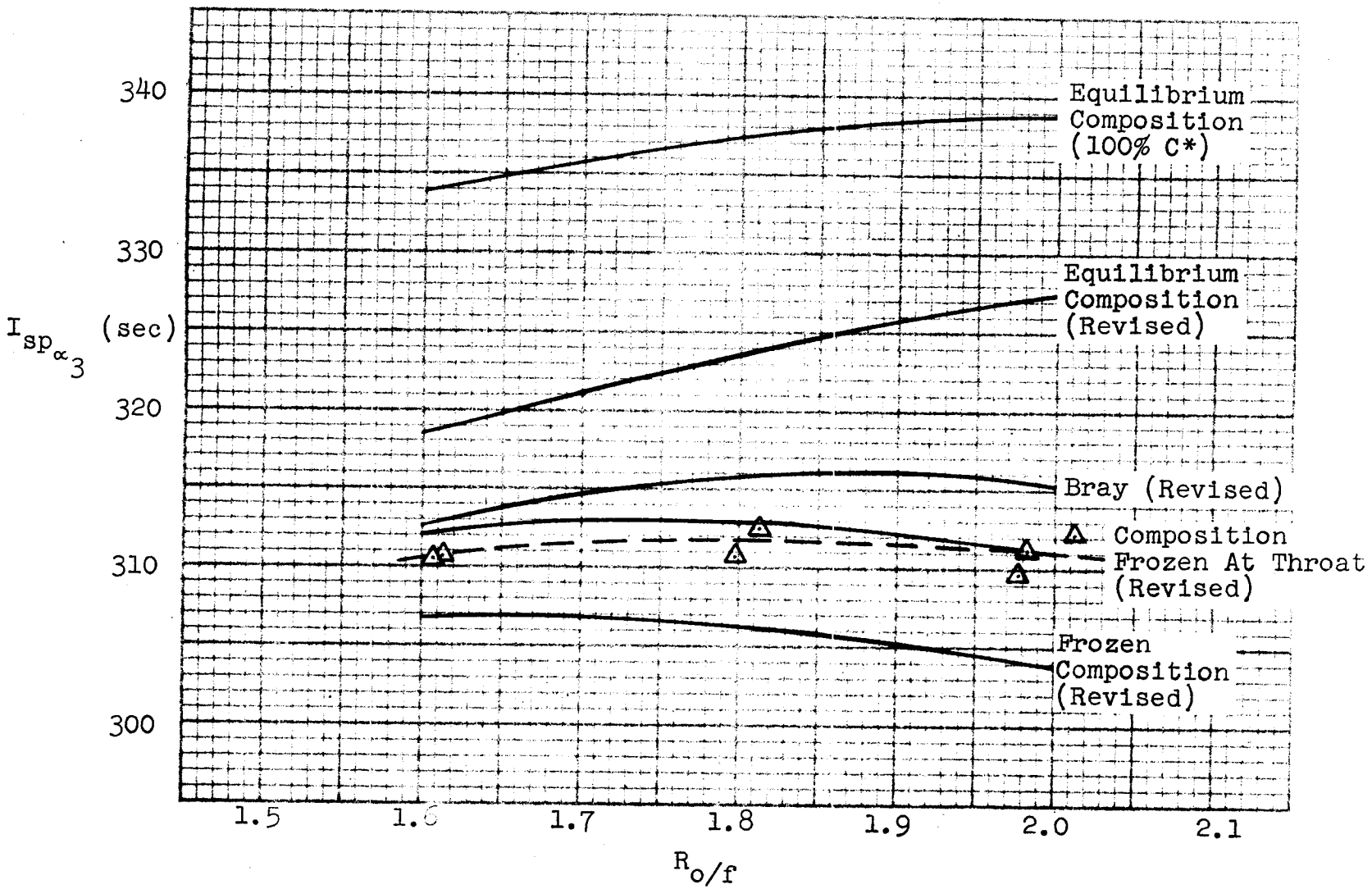

CORRECTED VACUUM IMPULSE
80% BELL NOZZLE, ϵ =40

FIGURE 36

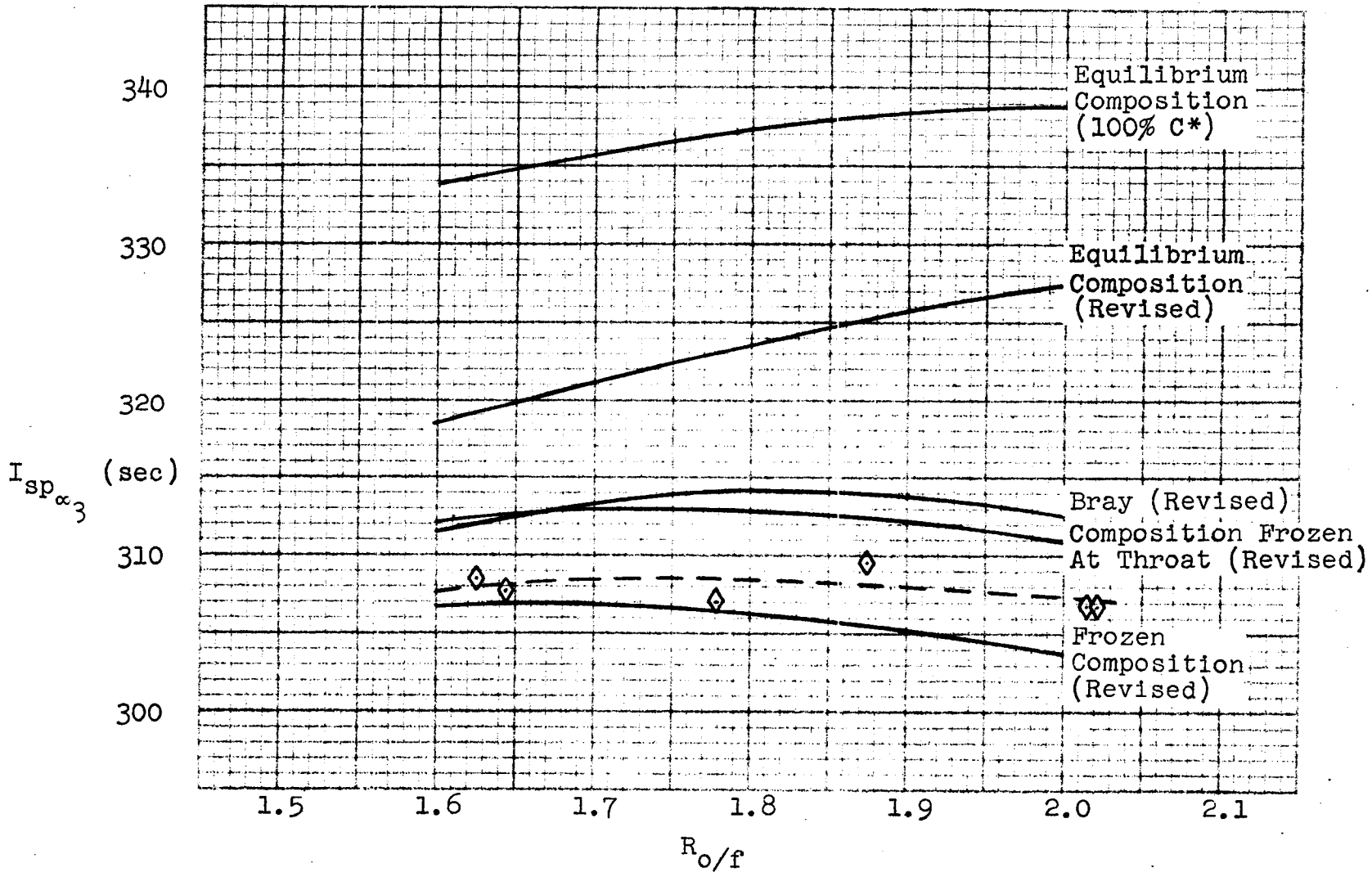

CORRECTED VACUUM SPECIFIC IMPULSE
RAO NOZZLE, ϵ =40

FIGURE 37

TABLE V

CORRECTION FACTORS FOR EXPERIMENTAL VACUUM SPECIFIC IMPULSE

	15° Conical ϵ=40	15° Conical ϵ=60	80% Bell ϵ=40	Rao ϵ=40
Three-Dimensional	1.537%	1.484%	1.668	1.018%
Heat Transfer	0.7813%	0.9242%	0.7293%	0.6930%
Friction (drag)	1.00%	1.16%	1.00%	1.00%

TABLE VI

CORRECTED VACUUM SPECIFIC IMPULSE DATA

15° Conical Nozzle, ϵ=40

Run Number	$R_{o/f}$	I_{sp_∞}	$I_{sp_{\infty_1}}$	$I_{sp_{\infty_2}}$	$I_{sp_{\infty_3}}$
2ES-1603	1.801	303.5	308.2	310.6	313.7
-1604	1.626	305.3	310.1	312.5	315.6
-1605	2.089	301.6	306.3	308.7	311.8
-1606	1.573	301.7	306.4	308.8	311.9
-1607	1.765	304.0	308.7	311.1	314.2
-1608	1.994	301.7	306.4	308.8	311.9
-1609	1.781	303.9	308.6	311.0	314.1
-1610	1.916	303.9	308.6	311.0	314.1
-1611	1.607	303.7	308.4	310.8	313.9
-1612	1.654	305.8	310.6	313.0	316.2
-1613	1.826	301.9	306.6	309.0	312.1

15° Conical Nozzle, ϵ=60

2ES-1614	1.596	305.7	310.3	313.2	316.9
-1615	1.772	308.4	313.0	315.9	319.6
-1616	2.016	305.6	310.2	313.1	316.8
-1617	1.560	306.8	311.4	314.3	318.0
-1618	1.750	306.4	311.0	313.9	317.6
-1619	1.950	306.0	310.6	313.5	317.2

Rao Nozzle, ϵ=40

2ES-1620	1.644	299.4	302.5	304.6	307.7
-1621	1.779	298.7	301.8	303.9	307.0
-1622	2.021	298.5	301.6	303.7	306.8
-1623	1.626	300.2	303.3	305.4	308.5
-1624	1.875	301.3	304.4	306.5	309.6
-1625	2.015	298.5	301.6	303.7	306.8

TABLE VI (Cont'd)

CORRECTED VACUUM SPECIFIC IMPULSE DATA

80% Bell Nozzle, ϵ = 40

Run Number	$R_{o/f}$	I_{sp_∞}	$I_{sp_{\infty_1}}$	$I_{sp_{\infty_2}}$	$I_{sp_{\infty_3}}$
2ES-1626	1.608	300.1	305.2	307.4	310.5
-1627	1.812	302.1	307.2	309.4	312.5
-1628	1.978	299.3	304.4	306.6	309.7
-1629	2.011	301.7	306.8	309.0	312.1
-1630	1.612	300.3	305.4	307.6	310.7
-1631	1.798	300.4	305.5	307.7	310.8
-1632	1.982	300.7	305.8	308.0	311.1

TABLE VII

UNDEFINED NOZZLE LOSSES (sec Isp)

COMPARED TO PREDICTED BRAY ANALYSIS

	$R_{o/f}$		
	1.6	1.8	2.0
15° Conical Nozzle, ϵ=40	+0.6	-1.2	-2.1
15° Conical Nozzle, ϵ=60	+1.0	-1.5	-2.4
80% Bell Nozzle, ϵ=40	-2.1	-4.0	-4.2
Rao Nozzle, ϵ=40	-3.8	-5.7	-5.2

Note: + and - indicate test data are above and below the BRAY predicted curve, respectively.

VI. DISCUSSION OF DATA ACCURACIES

A. GENERAL

The analyses discussed in this section of the report generally utilize test data from all firings conducted during the Nozzle Performance Evaluation Program. Exceptions will be noted and explained when they become significant.

All test data were statistically examined from two standpoints. An analysis was first conducted to establish the measurement error estimates for all significant independent parameters. These estimates were then used to compute resultant accuracy values for computed values of c* and C_{f_∞}. As a second approach, accuracy estimates for c* and C_{f_∞} were established by analyzing the actual test distributions of these parameters. The two methods are not strictly independent, but agreement in results confirms the validity of the methods and assumptions used in analyzing the test data. It is significant to point out that perfect agreement is rarely possible. This is especially true when instrument calibrations are not made prior to each test. Furthermore, certain types of bias error may never appear in an analysis of performance parameter errors even though their existence may be established by other methods. In general, however, a reasonable degree of agreement, especially in random errors, can be expected.

It will be observed that error values quoted in this report occasionally differ from values cited in previous reports. There are several reasons for these differences. In most cases sample sizes differ. As more test data are accumulated, error estimates will vary and will tend to approximate more closely the true values. Secondly, previous reports were of a preliminary nature so that, in some instances, the refined analytical methods utilized to establish values in this report were not considered justified at the time of their writing.

In all cases, the values quoted here are to be considered final best estimates.

B. ACCURACY OF MEASURED THRUST

Thrust error estimates were established by analyzing the calibration data from all test firings. The analysis consists of the following:

(1) A linearity check.

(2) Establishing 3σ limits for the measurement prediction interval.

(3) Establishing 3σ confidence intervals for the slope and intercept of the best fit line.

Since thrust calibration techniques are identical to those utilized in recording and reducing actual test data, an analysis of calibration data was considered justified.

With regard to linearity, all test calibration data distributions exhibited correlation coefficients in excess of 0.999. Since a value of 1.0 implies precise definition by a linear function, the linearity of all thrust calibrations can be considered excellent.

Examination of the 3σ confidence and prediction intervals showed a high degree of consistency in more than 90% of the test firings. It was, therefore, considered valid to obtain a general error estimate by computing pooled estimates of the over-all confidence and prediction intervals. It can be demonstrated that the few instances where significantly larger or smaller variations were observed contribute negligibly to the over-all estimate of performance parameter accuracy.

The best estimates of the random thrust errors for the sea-level and altitude test firings are as follows:

	3σ Error (lb)
Sea Level Tests	±6.5
Altitude Tests	±8.6

The differentiation between altitude and sea level test data was required because larger sensitivities must be used at higher thrust levels. A recording or reading error at higher sensitivities will, therefore, result in a greater absolute thrust error.

The observed random thrust errors are obviously comparable to the predicted value (±1%). However, an unexpected bias was observed between the pre-run and post-run coolant flow thrust deflections. The average error attributable to this bias was computed to be +1.4 pounds, with a 3σ random variation of ±3.6 pounds. Bias error such as this must be added directly to the random errors previously quoted. The random variation about this bias, however, has already been accounted for by the prediction interval used to estimate the random errors.

The resultant 3σ total error estimates for measured thrust then become:

	3σ Error (lb)	3σ Error (% F.S.)	3σ Error (% Rated Perf.)
Sea-Level Test	± 7.9	±0.79	±1.3
Altitude Test	±10.0	±1.0	±1.0

Both error estimates are conservative insofar as the bias estimate has been directly added to the random error values. The two estimates cannot, however, be randomly combined since a bias is not a random variable. The mean bias error represents one-half the difference between pre-run and post-run coolant thrust deflections. This is consistent with the normal data reduction procedure which consists in averaging the pre-run and post-run deflections. The error can, therefore, be no greater than one-half the difference between the two values. From a probability standpoint, an error actually this large is unlikely; however, no better means are available for properly estimating the total error.

C. ACCURACY OF MEASURED CHAMBER PRESSURE

Accuracy estimates for measured chamber pressure values were obtained by analyzing both calibration data and differences among simultaneous test measurements.

The calibration error was somewhat larger than anticipated. The computed 3σ error was ±0.28%, based upon the use of an average of five calibration values. (Calibration factors are established as the mean of the latest calibration factor, plus the four previously established values.)

The random run-to-run variation error was established as ±0.6% (3σ) by an analysis of the distribution of differences of simultaneous measurements. Statistically combined, the total 3σ error is ±0.68%. The predicted error was ±0.7%. The predicted and observed error values differ only with regard to the assumed sources of error. It was originally anticipated that random run-to-run variations (repeatability) were the primary contributors to error.

D. ACCURACY OF MEASURED FLOWRATE

In establishing accuracy estimates for the measurement of oxidizer and fuel flowrate, only test data from firings in Cell 2ES and the final four runs in Cell 1AW were utilized. This was due to the unreliability of flowrate measurements in earlier 1AW test firings as previously described.

Random run-to-run or repeatability errors were computed to be the following:

	% Error (3σ)
Oxidizer Flowrate	±0.27
Fuel Flowrate	±0.36

As in the case of chamber pressure, these values were obtained by an analysis of the distribution of differences of simultaneous measurements and are slightly larger than originally

anticipated. Calibration errors, however, were considerably lower. The computed 3σ error in calibration was established as ±0.32%. The R.S.S. (root sum square), or statistical combination of the two error estimates, yields the following 3σ estimates for total error:

	% Error (3σ)
Oxidizer Flowrate	±0.42
Fuel Flowrate	±0.48

The oxidizer calibration error was obtained by analyzing both test data from N_2O_4 calibrations and water calibration data. This approach was selected only after statistical examination established the similarity of the errors incurred by both methods of calibration.

E. ACCURACY OF MEASURED THROAT AREA

The accuracy of measured throat area was determined by analysis of the distribution of measurements (standard deviation). The best estimate of the 3σ error is ±0.11%. Measurements taken during the altitude test program were not utilized in this analysis. In fact, throat area values taken at this time were not used to compute final performance data because of the difficulity of measurement associated with the installation of the various nozzle extensions. Instead, bench measurements were made prior to and after each series of runs and were used to compute final performance values.

F. ACCURACY OF MEASURED ALTITUDE PRESSURE

At the initiation of the altitude test program, altitude pressures were computed as the best estimate (average) of two independent measurements. It was discovered, however, that one of these measurements was considerably unreliable. This conclusion was supported by an examination of calibration data which

showed a high degree of non-repeatability. Error estimates for the second instrument indicated that the use of the one instrument alone was sufficient to guarantee the specified accuracies for vacuum performance parameters. It was, therefore, decided to utilize the one instrument for altitude pressure measurements.

The 3σ error estimate for altitude pressure measurements is ±11.0%, which includes ±7.0% random error and ±4.0% bias in calibration standard.

G. ACCURACY OF COMPUTED PERFORMANCE PARAMETERS

This section and the following section are concerned with the statistical analyses conducted upon the computed values of c* and C_{f_∞}. In practice, it was found to be more convenient to treat combustion and nozzle efficiencies (η_{c^*} and $\eta_{C_{f_\infty}}$) rather than actual c* and C_{f_∞} values. The results obtained for the efficiency values are, however, directly applicable to test values of c* and C_{f_∞}.

1. Characteristic Velocity (c*)

Test values of η c* were found to exhibit a high degree of linear correlation (correlation coefficient $>$ 0.9) with propellant reactant ratio (see Figure 27). Thus, a regression analysis was conducted to establish a best fit line with 3σ confidence and prediction intervals. The confidence limits were computed as lying between ±0.1% and ±0.2%. A precise accuracy estimate cannot be quoted unless a particular reactant ratio value is specified since confidence limits are non-linear functions of the independent variable. The range of values quoted, however, represents operation in the reactant ratio range of 1.6 to 2.0.

2. Vacuum Thrust Coefficient (C_{f_∞})

Unlike the η c* data, no substantial correlation between ηC_{f_∞} and propellant mixture ratio could be found.

Consequently, regression analyses to establish accuracy estimates were not required. Accuracy estimates were obtained by establishing the standard deviation of the distribution of sample values.

The C_{f_∞} data obtained during the test program can be divided into five principal groups according to nozzle type:

(1) Start Chamber, ϵ=1
(2) 15° Conical Nozzle, ϵ=40
(3) 15° Conical Nozzle, ϵ=60
(4) Rao Nozzle, ϵ=40
(5) 80% Bell Nozzle, ϵ=40

The standard deviation values computed for each of the groups were found to be statistically equivalent. An over-all pooled estimate of the 3σ error was therefore computed. The accuracy of mean thrust coefficient data is given in the following table for each nozzle type. The differences between values are due entirely to the different number of tests conducted with each nozzle extension.

Nozzle Type	% Error (3σ)
Start Chamber, ϵ=1.0	±0.19
15° Conical, ϵ=40	±0.28
15° Conical, ϵ=60	±0.37
Rao, ϵ=40	±0.37
80% Bell, ϵ=40	±0.37

H. PERFORMANCE PARAMETER ACCURACY AS ESTIMATED FROM ERRORS IN INDEPENDENT VARIABLES

In the following two subsections accuracy values of c* and C_{f_∞} are given as established by a random combination of the observed errors in the variables upon which they depend. The error estimates used are as described in subsections B through F. The procedure used assumes that random errors are reduced by the square root of the number of measurements. Calibration errors are reduced

only by the number of calibrations made during the test period under consideration. Bias errors remain fixed regardless of the number of tests conducted.

In general, accuracy estimates of this type will be slightly larger than those quoted in the previous paragraphs. This is because normal statistical procedures for analyzing test data cannot account for bias errors. Furthermore, when several elements of variability such as calibration error and repeatability error do not appear with the same frequency, the observed standard deviations will tend to be smaller than the true values.

For these reasons, the accuracy values quoted in this section, though somewhat conservative, should be accepted as more valid estimates.

1. Characteristic Velocity (c*)

The accuracy of c* as obtained by a random combination of chamber pressure, throat area, and flowrate errors was computed to be ±0.20%. This estimate is slightly larger than that quoted in subsection G-1. In this particular case, the difference, although small, can be attributed to the fact that essentially only one calibration was conducted upon each of the two sets of oxidizer flowmeters (N_2O_4 calibration). As a result, a good estimate of the true variance cannot be obtained by examination of the c* data alone.

2. Vacuum Thrust Coefficient (C_{f_∞})

Vacuum thrust coefficient accuracies as established by randomly combining the errors in independent variables are listed in the following tabulation. The estimates represent the errors in mean performance values as a function of nozzle type.

Nozzle Type	% Error (3σ)
Start Chamber, ϵ=1	±0.49
Conical Nozzle, ϵ=40	±0.60
Conical Nozzle, ϵ=60	±0.64
Rao Nozzle, ϵ=40	±0.64
80% Bell Nozzle, ϵ=40	±0.64

The tabulated values are obviously larger than those quoted in subsection G-2. However, these estimates include thrust and, when applicable, altitude pressure bias, whereas the values given in subsection G-2 are based upon random error estimates only. If, for the purpose of comparison, the bias errors are removed from these tabulated values, the resulting 3σ random errors would be:

Nozzle Type	% Random Error (3σ)
Start Chamber, ϵ=1	±0.26
Conical Nozzle, ϵ=40	±0.36
Conical Nozzle, ϵ=60	±0.40
Rao Nozzle, ϵ=40	±0.40
80% Bell Nozzle, ϵ=40	±0.40

These values are obviously comparable to those established in subsection G-2.

I. Error in Vacuum Specific Impulse (I_{sp_∞})

Extimates of the error in vacuum specific impulse were also established by a random combination of the errors in thrust and propellant flowrate. The values, listed in the following tabulation as a function of nozzle type, include the bias errors in measured thrust and, when applicable, altitude pressure.

Nozzle Type	% Error (3σ)
Start Chamber, ϵ=1	±0.47
15° Conical Nozzle, ϵ=40	±0.49
15° Conical Nozzle, ϵ=60	±0.54
Rao Nozzle, ϵ=40	±0.54
80% Bell Nozzle, ϵ=40	±0.54

VII. CONCLUSIONS AND RECOMMENDATIONS

The sea-level testing in Cell 1AW and the sea-level and altitude testing in Cell 2ES established the injector characteristic velocity (with the previously described accuracy) over the reactant ratio range of 1.60 to 2.00.

The vacuum thrust coefficient and specific impulse was experimentally determined for the four nozzles: 15° conical (ϵ = 40 and 60), 80% Bell (ϵ = 40), and Rao (ϵ = 40).

The injector has accumulated a total run duration of 1327.9 seconds without any measurable change in performance. The front view of the injector (at the completion of the program) is shown in Figure 38. The apparent discoloration of the injector face is primarily the deposition of the tungsten carbide coating from the water-cooled chamber. Although essentially the entire coating was removed from the one water-cooled chamber, the base aluminum is still undamaged. All test hardware was in good condition at the completion of testing.

Difficulties with the oxidizer flow measurement during the earlier portion of the program indicates the desirability of calibrating the flowmeters in N_2O_4. Conducting these calibrations in the actual test cell is desirable, but may not be essential if proper care is exercised in the flowmeter installation and calibration procedures.

The experimental vacuum thrust coefficients (C_{f_∞}) appear to follow the theoretical frozen composition data for all four nozzles. The vacuum specific impulse (I_{sp_∞}) for the nozzles tested have maximum values occurring (with this particular injector) at a reactant ratio of approximately 1.75.

Comparison of the corrected experimental vacuum specific impulse data with the theoretical performance values illustrate the following:

(1) The theoretical equilibrium composition data alone is not adequate for defining nozzle performance at the 100 psia chamber pressure level.

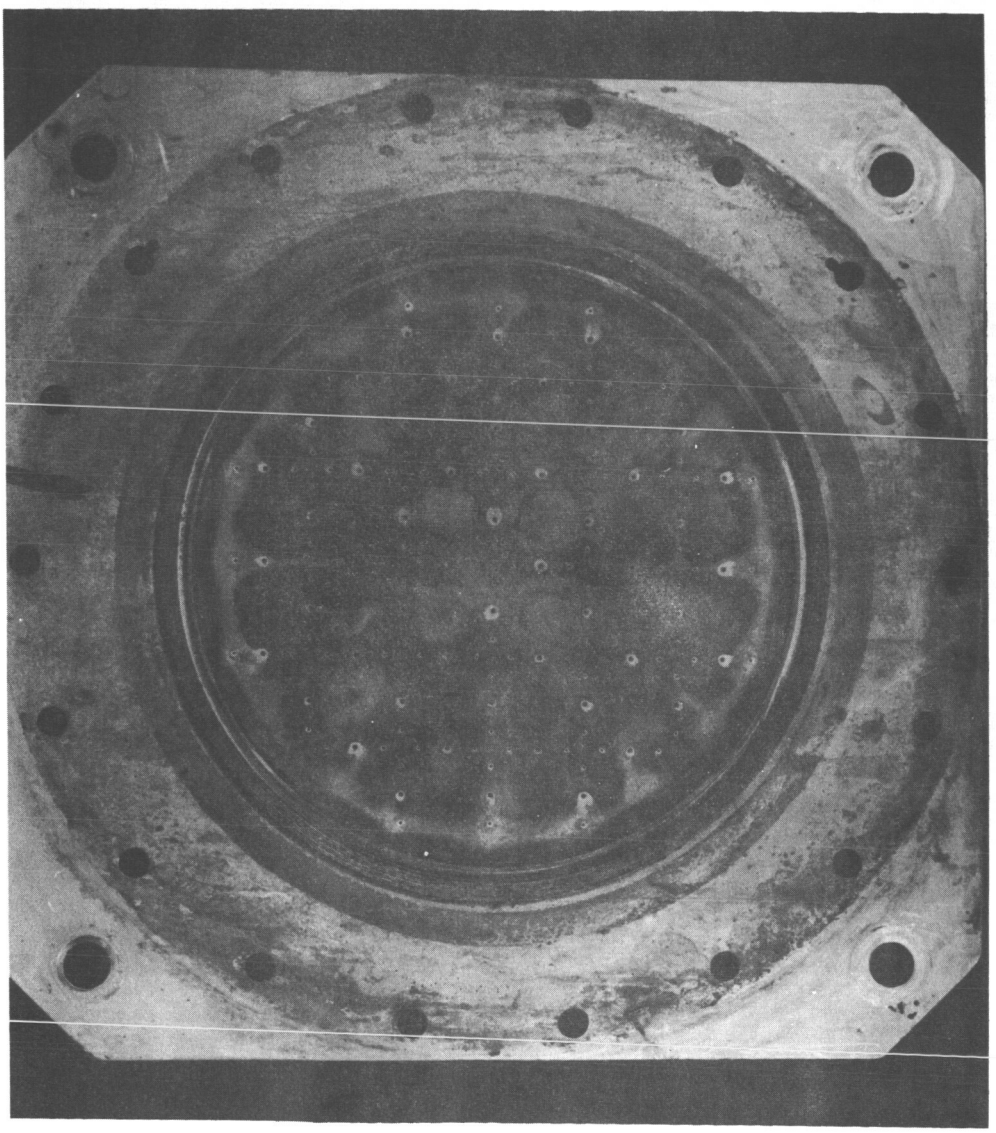

INJECTOR FRONT VIEW (AFTER TESTING)

FIGURE 38

(2) The revised Bray analytical data predicts the performance level within approximately 2% for all nozzle contours tested.

(3) In general, the experimental performance levels lie between the revised Bray analytical and the theoretical frozen composition data. The exception to this is the low reactant ratio 15° conical data that fall slightly above the Bray data.

By comparing the corrected performance data of the various nozzles, the performance level (with respect to the Bray data) is a function of nozzle length (percent bell).

Apparently, there are additional gas dynamic losses which have not yet been defined. These losses are more severe with decreasing nozzle length and/or rate of gas expansion. This can be seen by examining the data obtained with the 15° conical (ϵ = 40) and 80% bell (ϵ = 40) nozzles. At all reactant ratios, the revised Bray predicted performance is identical for both nozzles (since they are geometrically identical up to the flow breakpoint). However, the experimental performance differs. Again, the accuracy of the various correction factors utilized must be considered.

Based upon the results obtained during this program, and with an over-all objective of better understanding of nozzle flow the following are recommended:

(1) Experimentally define nozzle friction losses.

(2) Experimentally define nozzle three-dimensional and other gas dynamic losses.

(3) Evaluate additional parameters such as chamber pressure, scaling effects, and other high-energy propellant combinations.

APPENDIX

A. INSTRUMENTATION

Multiple instrumentation was utilized on all critical performance parameters. As previously mentioned, six chamber pressure transducers were utilized. At Station 1, one pressure port was located very near the center of the injector and one approximately midway between the center (central axis) and the thrust chamber wall. The two separate ports were used to obtain the best average pressure value at the injector plane (since it is possible to have a slight variation in pressure across the injector face).

Stations 2 and 3 are located on the cylindrical chamber section. Station 2 is approximately one inch upstream of the entrance to the convergent portion of the nozzle and Station 3 is located just at the entrance to the convergent nozzle. One pressure transducer was located at each of the Station 1 ports and two transducers attached to each of the single ports located at both Stations 2 and 3.

Two turbine type flowmeters were utilized to measure each propellant flowrate. These flowmeters were mounted in series, with each set having upstream and downstream thermocouples to measure the respective propellant temperatures.

The pressure transducers utilized were Alinco* Series 151 having a range of 0-100 psia. These transducers utilize a metallic pressure-actuated diaphragm connected to a bonded strain gage element. The output of the pressure transducer was recorded on standard strip chart recorders.

The propellant flowmeters are the 10C1510 Series turbine type, manufactured by the Fisher and Porter Company. The signal

*NOTE: Alleghany Instrument Company, Cumberland, Maryland

output of each flowmeter was recorded directly on an oscillograph.

The thrust stand utilized for the Cell 1AW testing was fabricated at BAC and employed three 500-pound Baldwin load cells. These load cells directly supported two parallel plates; one of which was fastened to the main stand supports. The injector-thrust chamber assembly was mounted to the other plate. The output of these three load cells was electrically summed by means of an electronic summing balancing network. The single thrust output signal was recorded on a strip chart recorder. The thrust stand was calibrated before and after each test run by utilizing a hydraulic actuator to apply a load (along the central axis) and a master load cell as the reference standard.

The thrust stand assembly utilized in Cell 2ES is an Alinco single component thrust measuring system comprised of a thrust stand and calibrator unit. The thrust loads are transferred to the load cell through its monoaxial assembly which is supported on one end by the thrust chamber mounting yoke and on the other end by the headblock of the thrust stand frame. The calibration system employs a dead weight and amplification beam principle. The weights (adjusted and certified by NBS) employed with this calibrator consisted of five weights of twenty-five pounds. The beam has an amplification factor of ten to one, thus permitting calibration of the load cell from 0 to 1250 pounds. The amplification beam has an automatic leveling motor assembly and electrical controls. This system automatically maintains the beam level during each calibration point. The calibrator pull rods can be disengaged from the thrust stand during thrust chamber testing. The entire calibration sequence is conducted at altitude and controlled remotely from the test cell control room.

The thrust measuring load cell utilized with the thrust stand was the Alinco Series 36 unit which are the bonded strain gage type and hermetically sealed to permit operation under altitude conditions. The load cell has two electrically independent bridge

circuits thus providing two simultaneous thrust measurement outputs.

The altitude during the Cell 2ES testing was measured utilizing two 0-1 psi ΔP Statham pressure transducers (Model PL743TC) referenced to a vacuum. These transducers were mounted exterior of the altitude chamber (in a temperature controlled box) and measured the altitude pressures adjacent to the thrust chamber assembly.

B. DATA REDUCTION PROCEDURES

The following describes the data reduction utilized to obtain the final reported test data from the basic raw test data.

As previously mentioned, four chamber pressure measurements were utilized for performance determinations; two located at the injector face and two located directly at the entrance to the convergent nozzle. The chamber pressure measurements taken at the injector are corrected to total pressure at the entrance of the convergent nozzle by Equation 1:

$$\frac{P_{inj.}}{\bar{P}_o} = \frac{P_{sn}}{\bar{P}_o} + \frac{V_n - V_{inj.}}{c^*\left[\frac{A_c}{A_t}\right]} \qquad (1)$$

where

$P_{inj.}$ = pressure at injector face - psia

$\bar{P}_o$ = total pressure at nozzle entrance - psia

P_{sn} = static pressure at nozzle entrance - psia

V_n = velocity at nozzle entrance - ft/sec

$V_{inj.}$ = velocity at injector face - ft/sec

c^* = characteristic velocity - ft/sec

A_c = chamber cross sectional area - $in.^2$

A_t = throat area - $in.^2$

Calculations conducted over test run reactant ratio ($R_{o/f}$) and combustion efficiency (ηc^*) ranges indicated a value for $\bar{P}_o/P_{inj.} = 0.9952$.

The chamber pressure measurements taken at the entrance to the convergent nozzle were corrected to total pressure by

Equation 2:

$$\frac{\bar{P}_o}{P_{sn}} = \left[1 + \frac{\gamma - 1}{2} M_c^2 \right]^{\frac{\gamma}{\gamma - 1}} \qquad (2)$$

where

P_{sn} = static pressure at nozzle entrance - psia

γ = gas specific heat ratio

M_c = chamber gas Mach number

The calculated value for this correction factor is $\bar{P}_o/P_s = 1.0073$. The quoted chamber pressure values for the individual test runs were obtained by correcting each of the four measured chamber pressure values (with its appropriate correction factor) and arithmetically averaging the four corrected values.

The propellant flow rates were obtained by direct cycle count on the oscillograph of each flowmeter output. The flowrate could then be obtained by utilizing the individual flowmeter calibration factors and appropriate propellant specific gravities.* The quoted propellant flowrates were then obtained by averaging the two flowrates thus calculated.

The Cell 1AW thrust data was obtained by recording the summed output of the three load cells and employing the pre and post run thrust calibration data. In Cell 2ES, two independent thrust measurements were recorded. The quoted thrust for these runs is based on the average of the two readings (each of which is obtained by utilizing the respective pre and post run calibrations). Due to the thrust produced by the coolant water flowrate, the quoted

*NOTE: The propellant specific gravities for a given test run were based on propellant analyses conducted on a daily basis and the measured run propellant temperatures.

thrust values are based on the difference between the run thrust reading and the average of the pre and post run water thrust readings.

The throat area (for any given test run) was calculated from the average of four pre and post run throat diameter measurements during sea level testing. Due to the difficulties involved in accurately measuring throat areas during the altitude test program, bench measurements taken prior to and after each series of tests were utilized to compute performance.

The characteristic velocity (c*) was calculated by Equation 3:

$$c^* = \frac{g_o \quad \bar{P}_o \quad A_t}{W_T} \qquad (3)$$

where

c^* = characteristic velocity - ft/sec

$\bar{P}_o$ = average nozzle total inlet pressure - psia

g_o = gravitational constant

A_t = throat area - $in.^2$

W_T = total propellant flowrate - lb/sec

Combustion efficiency (ηc^*) was calculated by the ratio of the c* values calculated by Equation 3 and the theoretical equilibrium c* at the appropriate reactant ratio.

The corrected thrust coefficient (C_{f_∞}) was calculated utilizing Equation 4:

$$C_{f_\infty} = \frac{F_m + P_a A_e}{\bar{P}_o \quad A_t} \qquad (4)$$

where

$C_{f\infty}$ = thrust coefficient corrected to vacuum conditions

F_m = measured thrust - lb.

P_a = ambient pressure - psia

A_e = nozzle exit area - $in.^2$

For the sea level nozzle, the exit area is equal to the throat area ($\epsilon = 1.0$). The exit areas for the various altitude nozzle extensions were calculated from four pre and post-run exit diameter measurements.

The sea nozzle efficiencies ($\eta C_{f\infty}$) were obtained by the ratio of the corrected thrust coefficients (from Equation 4) and the theoretical equilibrium composition thrust coefficients for a nozzle area ratio (ϵ) of 1.00. The altitude nozzle efficiencies were computed by ratioing the altitude vacuum thrust coefficients to the theoretical frozen composition thrust coefficients at the appropriate reactant ratios.

The theoretical values were taken at exit area ratios (ϵ) of 40 and 60 even though the respective test hardware did not have these exact values. The calculated error from these differences was found to be less than 0.1%.

The thrust chamber corrected specific impulse was calculated by Equation 5:

$$I_{sp\infty} = \frac{C_{f\infty}\ c^*}{g_o} \qquad (5)$$

The over-all thrust chamber efficiency ($\eta I_{sp\infty}$) is, therefore, just the product of the combustion and nozzle efficiencies. It should be noted that both the sea level data combustion and nozzle efficiencies are based on theoretical equilibrium composition data. The altitude data, however, has

the combustion efficiencies based on theoretical equilibrium composition data, but the nozzle efficiencies are based on theoretical frozen composition data.

C. STATISTICAL DATA ANALYSIS METHODS

In general, the method used to establish the accuracy of test data depends to a large extent upon the type of test data obtained. Thus, for example, the procedure used to analyze data which is dependent upon variations in other parameters (e.g. product variability, test conditions) must of necessity be different from a method designed to analyze data influenced only by instrumentation error.

For the purpose of this report, the term 3σ signifies a probability level of 99.7%. As applied to random errors this means that the actual value of a test parameter can be expected to lie within the quoted accuracy interval about the measured value 99.7% of the time.

Described below are four basic methods of statistically determining instrumentation error. The methods described have all been used to establish the values quoted in this report.

1. Determination of the Standard Deviation

When measurements of a parameter are not influenced by the variations of any other parameters upon which it depends, the instrumentation accuracy is equivalent to the standard deviation of the distribution of measurements:

$$1\sigma \text{ error} = \left[\frac{\sum (x_i - \bar{x})^2}{(N - 1)} \right]^{1/2} \qquad (6)$$

where

x_i = individual measurement

$\bar{x}$ = mean measurement

N = sample size

This method was used to establish the accuracy of throat area.

2. Pooled Estimate of Standard Deviation

When various distinguishable groups of test data can each be assumed to have essentially the same standard deviation, the best estimate of this standard deviation can be obtained by computing a pooled estimate:

$$S = \left[\frac{(N_1 - 1)\, S_1^2 + (N_2 - 1)\, S_2^2 + \ldots + (N_k - 1)\, S_k^2}{\left[\sum_{i=1}^{k} N_1 \right] - k} \right]^{1/2} \quad (7)$$

where

$S_1, S_2, \ldots S_k$ = standard deviations for each of the k groups

$N_1, N_2, \ldots N_k$ = sample sizes of each group

Flowmeter calibration variances and C_{f_∞} error estimates were combined in this manner.

3. Distribution of Differences

It can be shown that the distribution of the differences of two normally distributed variables is also normal with zero mean and a variance equal to the sum of the variances of the two distributions. Let the standard deviations of each distribution be S_1 and S_2. Then if $S_1 = S_2$:

$$S_o = \left[S_1^2 + S_2^2 \right]^{1/2} \quad (8)$$

$$= S_1 \sqrt{2} = S_2 \sqrt{2} \quad (9)$$

where:

S_o = standard deviation of the population of differences

When dual instrumentation is utilized, a standard deviation of differences may easily be obtained by using formula (6). Equation (9) then shows that the standard deviation (or 1σ error) of the parameter in question can then be obtained upon dividing by the $\sqrt{2}$.

This procedure is useful when test data is influenced by test conditions or by hardware variations. Computing differences accomplishes the same result as normalizing the test data. For this reason the random run-to-run variations in flowrate and chamber pressure were estimated in this manner.

4. Regression Methods

When, as in the case of c*, a variable can be related to another independent parameter, the method for obtaining accuracy estimates consists in computing ordinate confidence intervals about a best fit curve. When this curve is linear, the equation defining the confidence intervals is:

$$C.I. = t_{\alpha/2\ (N-2)}\ S_{y/x} \left[\frac{1}{N} + \frac{(X-\overline{X})^2}{(N-1)\ S_x^2} \right]^{1/2} \qquad (10)$$

where

$T_{\alpha/2\ (N-2)}$ = the t variable taken at (N-2) degrees of freedom and at a probability level of α

$S_{y/x}$ = the standard deviation about the best fit line

X = the ordinate at which the confidence interval (C.I.) is to be obtained

$\overline{X}$ = mean of the X values

S_x = standard deviation of the X values

Similar expressions have been defined for a large number of relationships.

Regression analysis can be used to establish the accuracy of measured thrust by an examination of calibration data.

During calibration one can establish a best fit linear relationship defining observed deflections as a function of known applied loads:

$$S = m F + b \tag{11}$$

where

S = observed recorder deflection
m = slope of best fit line
F = applied load
b = intercept of best fit line

In practice, the inverse relationship is used to establish thrust values from recorded deflections:

$$F = \frac{1}{m} (S-b) \tag{12}$$

The accuracy of a thrust value as computed from equation (12) may be linearly approximated by differentiation:

$$\Delta F = \frac{1}{m} (\Delta S - \Delta b) - \frac{(S-b)}{m^2} \Delta m \tag{13}$$

Statistically, the random thrust error is obtained by computing the square root of the sum of the squares of the terms in equation (13):

$$\Delta F = \left[\frac{1^2}{m} (\Delta^2 S + \Delta^2 b) + \frac{(S-b)^2}{m^4} \Delta m^2 \right]^{1/2} \tag{14}$$

Δb and Δm can be obtained by computing 3σ confidence intervals for the slope and intercept of the best fit line; ΔS is equivalent to the 3σ prediction interval defined by the following expression:

$$\Delta S = t_{\alpha/2\,(N-2)}\; S_{y/x} \left[\frac{(N+1)}{N} + \frac{(X - \overline{X})^2}{(N-1)\, S_x^{\,2}} \right]^{1/2} \qquad (15)$$

The symbols are as defined for equation (10). The 3σ prediction interval defines that range of values within which one could expect to observe recorder deflections for the same applied load (99.7% of the time).

D. HEAT TRANSFER DATA

Theoretical heat transfer calculations were conducted on the water-cooled chamber and nozzle sections during the hardware design stage employing the Eckert Reference Enthalpy Method. The calculations utilized the theoretical combustion gas properties at the mean reactant ratio of 1.80 and at the nominal chamber pressure of 100 psia.

The theoretical heat transfer calculations predicted the following water-cooled hardware heat rejection rates:

Chamber Section	207.0 BTU/sec
15° Conical Nozzle	287.3 BTU/sec
80% Bell Nozzle	237.8 BTU/sec
Rao Nozzle	169.8 BTU/sec

Chamber experimental heat rejection data were obtained during both the sea level and altitude testing conducted in Cell 2ES. The instrumentation employed in obtaining these data included the following: one turbine type water flowmeter, two chamber section water inlet thermocouples, two chamber section water outlet thermocouples, and two nozzle water outlet thermocouples. The chamber section and nozzle coolant flows were in series, therefore, the chamber water outlet temperature corresponds to the nozzle water inlet temperature.

In the analysis of the experimental data, corrections were not made for the slight run-to-run variations in chamber pressure or for the actual variations in test data about the mean reactant ratio of 1.80.

Sea level experimental heat transfer data (obtained during tests 2ES-1589 through 1602) indicated an average chamber heat rejection rate of 234.8 BTU/sec.

During the altitude test program (tests 2ES-1602 through 1632), considerable run-to-run variations were obtained in the chamber water outlet thermocouple measurements. The run-to-run variations in both the chamber water inlet and nozzle outlet

temperatures were considerably less; therefore, the over-all heat rejection rates (chamber plus nozzle) were calculated for the three chamber-nozzle combinations. The maximum spread about the three average over-all heat rejection values was 15%.

The variations in chamber water outlet temperatures, although large, appeared random and, therefore, the altitude thrust chamber heat rejection rate was obtained by calculating an average heat rejection rate using all the altitude test data. The heat rejection rates for the three nozzle sections were obtained by subtracting the average chamber heat rejection rate from the previously obtained average over-all heat rejection rates (for the three chamber-nozzle combinations). Table VIII summarizes these water-cooled heat rejection data.

Good agreement was obtained with the theoretical predicted and experimentally measured chamber and 15° conical nozzle heat rejection rates. The 80% Bell and Rao nozzle experimental heat rejection rates are 12% and 18% less (respectively) than the theoretical predicted values. This is not unreasonable since the theoretical predicted values are based on the same ideal area ratio relationships where, in actuality, the wall pressure profile for the nozzles varies considerably.

Nozzle extension outer surface temperatures were measured during all altitude tests. Six thermocouples were utilized on each extension located two each at three area ratios (120° apart).

Table IX lists the area ratio locations of these thermocouples and the average reading of the two thermocouples located at the same area ratio. The time when the data point was taken is also listed.

TABLE VIII

WATER-COOLED HARDWARE HEAT TRANSFER DATA

	Q_{theo} (BTU/sec)	Q_{exp} (BTU/sec)	Q_{exp}/Q_{theo}
Chamber (Sea Level)	207.0	234.8	1.13
Chamber (Altitude)	207.0	203.1	0.98
15° Conical Nozzle	287.3	280.0	0.98
80% Bell Nozzle	237.8	209.5	0.88
Rao Nozzle	169.8	139.5	0.82
Chamber-15° Conical Nozzle Over-all	494.3	483.1	0.98
Chamber-80% Bell Nozzle Over-all	444.8	412.6	0.93
Chamber-Rao Nozzle Over-all	376.8	342.6	0.91

TABLE IX

NOZZLE EXTENSION OUTER SURFACE TEMPERATURES

15° Conical Nozzle, ϵ=40

Run Number	Time (sec)	Average Surface Temperature (°F)		
		ϵ=8.306	ϵ=21.70	ϵ=39.66
2ES-1603	29.0	1078	495	215
-1604	30.0	1068	582	296
-1605	13.2	595	298	152
-1606	29.3	1135	589	252
-1607	28.4	1039	552	321
-1608	28.8	1048	588	364
-1609	29.0	994	606	312
-1610	29.6	1009	615	322
-1611	29.0	1056	580	315
-1612	30.1	1056	616	334
-1613	29.3	1055	599	319

15° Conical Nozzle, ϵ=60

		ϵ=8.21	ϵ=27.65	ϵ=59.92
2ES-1614	28.6	1199	483	190
-1615	30.5	1228	495	186
-1616	30.5	1203	520	190
-1617	29.5	1229	500	175
-1618	29.8	1268	495	183
-1619	29.7	1274	532	199

Rao Nozzle, ϵ=40

		ϵ=10.00	ϵ=24.74	ϵ=36.72
2ES-1620	29.8	900	1037	603
-1621	28.4	902	1018	631
-1622	27.4	945	1051	654
-1623	29.8	918	1039	679
-1624	29.0	940	986	630
-1625	29.0	1000	947	672

TABLE IX (Cont'd)

NOZZLE EXTENSION OUTER SURFACE TEMPERATURES

80% Bell Nozzle, ϵ=40

Run Number	Time (sec)	Average Surface Temperature (°F)		
		ϵ=9.33	ϵ=24.64	ϵ=36.82
2ES-1626	29.4	1231	869	592
-1627	30.5	1220	907	630
-1628	5.0	204	149	---
-1629	20.1	915	578	448
-1630	29.8	1245	866	625
-1631	29.4	1226	881	641
-1632	28.6	1234	808	675

E. INJECTOR DESIGN ANALYSIS

The injector was deisgned at the nominal reactant ratio ($R_{o/f}$) of 1.80 to have a velocity ratio (V_o/V_{fa}) and momentum ratio (M_o/M_{fa}) of 0.901 and 1.62, respectively. The velocity ratio is calculated by Equation 16:

$$\frac{V_o}{V_{fa}} = \frac{\dfrac{\dot{W}_o}{A_{ot}\ \rho_o}}{\left[\dfrac{\dot{W}_f}{A_{ft}\ \rho_f}\right] \cos \beta} \qquad (16)$$

where:

V_o = oxidizer stream velocity - ft/sec

V_{fa} = axial fuel stream veolcity - ft/sec

$\dot{W}_o$ = average oxidizer flowrate - lb/sec

$\dot{W}_f$ = average fuel flowrate - lb/sec

A_{ot} = total area of oxidizer orifices - $in.^2$

A_{ft} = total area of fuel orifices - $in.^2$

ρ_f = fuel density - lb/ft^3

β = impingement half-angle-degrees

ρ_o = oxidizer density - lb/ft^3

The impingement half-angle is 28° and the stream impingement point is 0.532 inches from the injector face.

The stream momentum ratios were calculated by Equation 17a.

$$\frac{M_o}{M_{fa}} = \left[\frac{\dot{W}_o}{\dot{W}_{fa}}\right]\left[\frac{V_o}{V_{fa}}\right] \qquad (17)$$

or

$$= R_{o/f}\left[\frac{V_o}{V_{fa}}\right] \qquad (17a)$$

The effects of the stream velocity and momentum ratios on injector combustion efficiency are shown in Figures 39 and 40, reespectively. These data are based on the sea-level testing conducted in Cells 1AW and 2ES. Both curves present the same trend as the combustion efficiency data shown as a function of reactant ratio (Figure 17). The plotted data points were fitted with a best fit curve and, when checked for linearity, were found to be linear throughout the range of the available data. If this linear curve is extended (with the same slope) it will cross the $\eta c^* = 1.00$ point at a velocity ratio of 1.40. Since it is unlikely that the slope of this curve would increase (and in all probability would decrease) the optimum velocity ratio for this particular injector configuration would appear to be greater than 1.40. Thus, for this particular injector configuration, the higher velocity and momentum ratios result in better impingement and propellant atomization and, therefore, higher combustion efficiencies.

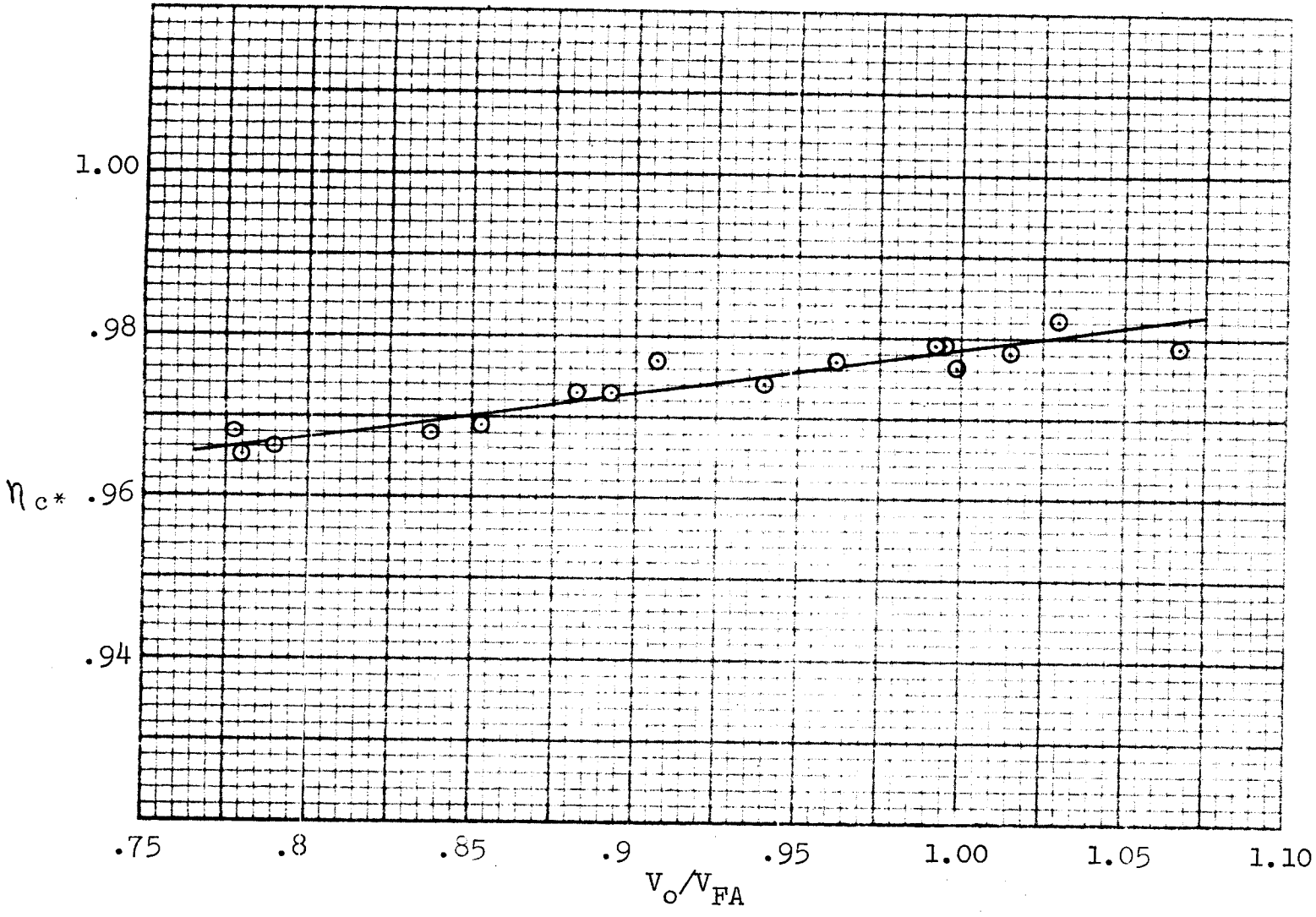

INJECTION VEOLICTY RATIO EFFECTS ON INJECTOR COMBUSTION EFFICIENCY
(SEA-LEVEL DATA - BASED ON THEORETICAL EQUILIBRIUM DATA)

FIGURE 39

Model
Date 2-24-64
BELL AEROSYSTEMS COMPANY
DIVISION OF BELL AEROSPACE CORPORATION
Page 98
Report 8289-933002

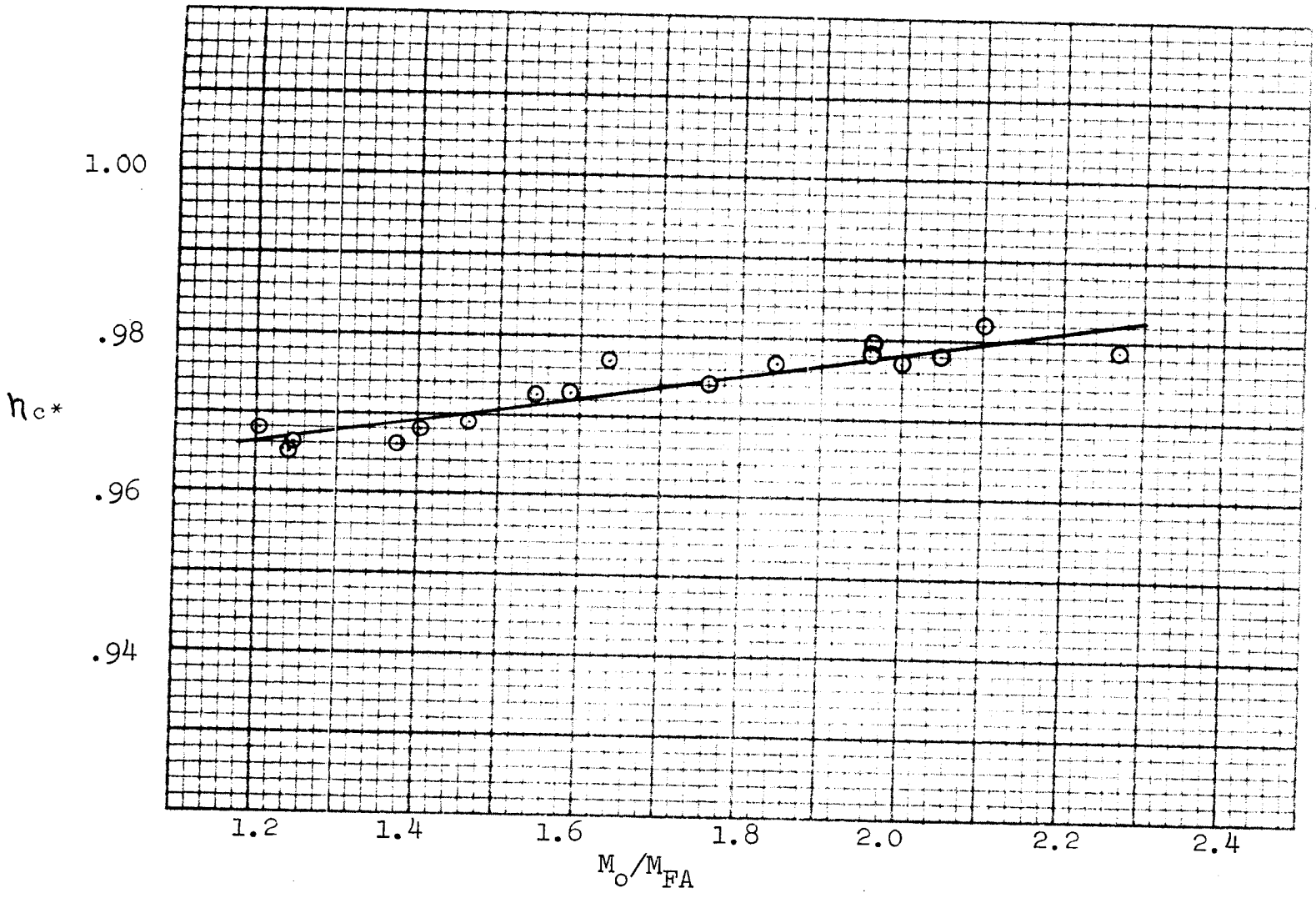

INJECTION MOMENTUM RATIO EFFECTS ON INJECTOR COMBUSTION EFFICIENCY
(SEA-LEVEL DATA - BASED ON THEORETICAL EQUILIBRIUM DATA)

FIGURE 40

F. FLOWMETER CALIBRATIONS

The fuel flowmeters were calibrated using water as the calibration fluid. Previous experience indicated that water calibrations gave accurate results for the 50/50 N_2H_4-UDMH propellant.

Initially, water calibrations were also conducted on the oxidizer (N_2O_4) flowmeters. Difficulties encountered in correlating test data obtained with the two flowmeter sets and disagreements experienced in simultaneous flow readings obtained from two flowmeters of the same set indicated that the water calibrations were not adequate with this propellant.

Calibration of the two oxidizer flowmeter sets with N_2O_4 was conducted utilizing the Cell 2ES system. By calibrating directly in the test cell system, any calibration errors caused by the upstream or downstream cell plumbing are automatically eliminated.

The calibration setup was a closed piping system consisting primarily of a collector tank and its associated valving, a scale, counters for determining total flowmeter cycles, an electronic timer and a cavitating venturi to maintain a constant flowrate. This venturi was sized to provide the same pressure level at the flowmeters as occurs during actual test conditions. The collector tank was evacuated prior to each calibration point to minimize back pressure effects.

The calibrations consisted primarily of flowing approximately 200 pounds of N_2O_4 and electronically counting the total cycle output of the two flowmeters being calibrated. The time interval for collecting this amount was also measured to determine rate of flow. Oscillograph and strip chart records were also taken to evaluate the start and shutdown transients of the individual flowmeters and to visually evaluate the flowrate during each calibration. Propellant temperatures were measured and propellant samples taken and utilized for determining the N_2O_4 specific gravity.

Each flowmeter set was calibrated over a propellant temperature range of 50° to 70°F and over flowrate ranges approximately ±25% about the nominal test run flow rate.

Final reduction of the oxidizer flowmeter calibrations with N_2O_4 indicated that there was no effect of propellant temperature on flowmeter calibration factors over this temperature range. Statistical analysis of these calibrations indicated that the same accuracies were being obtained during these calibrations as is normally obtained during water calibrations.

Following are listed the average calibration factors for the four oxidizer flowmeters obtained during the N_2O_4 calibrations. The average calibration factors obtained during previous water calibrations are also shown. The calibration factors are normalized to a specific gravity of 1.00 and represent pounds of flow per 100 cycles.

N_2O_4 Flowmeter Calibration Data

Set No.	Inst. No.	H_2O Calib. Factor	N_2O_4 Calib. Factor
1	330F-9	0.1750	0.1752
1	330F-10	0.1774	0.1777
2	300F-109	0.1785	0.1799
2	300F-110	0.1745	0.1747

Three of the flowmeters have a difference between the water and N_2O_4 calibration factors of less than 0.2%. One flowmeter (No. 330F-109) shows a difference in calibration factors of 0.78%. In all cases, the true propellant flowrates are greater than would be calculated by using the water calibration data.

G. ALTITUDE NOZZLES

The following four nozzles were designed, fabricated and tested:

Type of Nozzle	(Design) Area Ratio	(Actual) Area Ratio
15° Conical	40	40.04
15° Conical	60	59.96
80% Bell	40	39.44
Rao	40	39.46

The 15° conical nozzle has the identical convergent and throat as the 80% Bell throat to the point of tangency of the 15° line. This tangency point occurs at an area ratio (ϵ) of 1.243. The 80% Bell contour was designed with the long throat and is geometrically similar to the Agena nozzle contour. The Rao nozzle contour was designed based on the Rao criterion which is maximum performance for a given nozzle length. This contour was developed by computer programs utilizing the method of characteristics. The three dimensional performance of the 15° conical and 80% Bell nozzles is also determined using the three dimensional method of characteristics. The flow fields are utilized to determine the pressure distribution and integrated thrust produced on the divergent nozzle sections. This thrust was then combined with the three dimensional thrust produced by the throat sections to specify the total nozzle thrust. The nozzle aerodynamic characteristics were computed using a constant specific heat ratio (γ) of 1.18.

Table X summarizes the nozzle aerodynamic analysis conducted for the four nozzles.

Figure 41 shows the altitude nozzle contours tested during this program.

TABLE X

SUMMARY OF NOZZLE AERODYNAMIC ANALYSIS

Geometry								
Nozzle Type	15° Conical		15° Conical		80% Bell		Rao Optimum	
Exit Area Ratio	40		60		40		40	
% Bell	101.4		101.1		80		62.6	
Throat Diameter (in.)	2.622		2.622		2.622		2.622	
Exit Diameter (in.)	16.573		20.310		16.573		16.573	
Max. Wall Angle	15°		15°		27.86°		38.33°	
Exit Wall Angle	15°		15°		9.34°		7.01°	
Aerodynamic Performance	Throat	Exit	Throat	Exit	Throat	Exit	Throat	Exit
Theo 1 Dimen. C_{f_∞} (γ =1.18)	1.2391	1.907	1.2391	1.941	1.2391	1.907	1.2391	1.907
Computer 3 Dimen C_{f_∞} (γ =1.18)	1.2376	1.8777	1.2376	1.9122	1.2376	1.8752	1.2359	1.8876
Nozzle Efficiency % (γ = 1.18)		98.463		98.516		98.332		98.982
Exit Mach Number		4.00		4.38		3.82		3.59
Exit Pressure Ratio, P_t/P_e		393.0		717.0		242.0		156.7
Theo 1 Dimen. C_{f_∞} (Shift.Equi.)*	1.233	1.910	1.233	1.941	1.233	1.910	1.233	1.910
Theo 1 Dimen. C_{f_∞} (Frozen Flow)*	1.246	1.830	1.246	1.854	1.246	1.830	1.246	1.830

*NOTE: Values for the nominal reactant ratio ($R_{o/f}$) of 1.80

Model
Date 2-24-64

BELL AEROSYSTEMS COMPANY
DIVISION OF BELL AEROSPACE CORPORATION

Page 103
Report 8289-933002

MODEL _____

DATE _____

BELL AERO

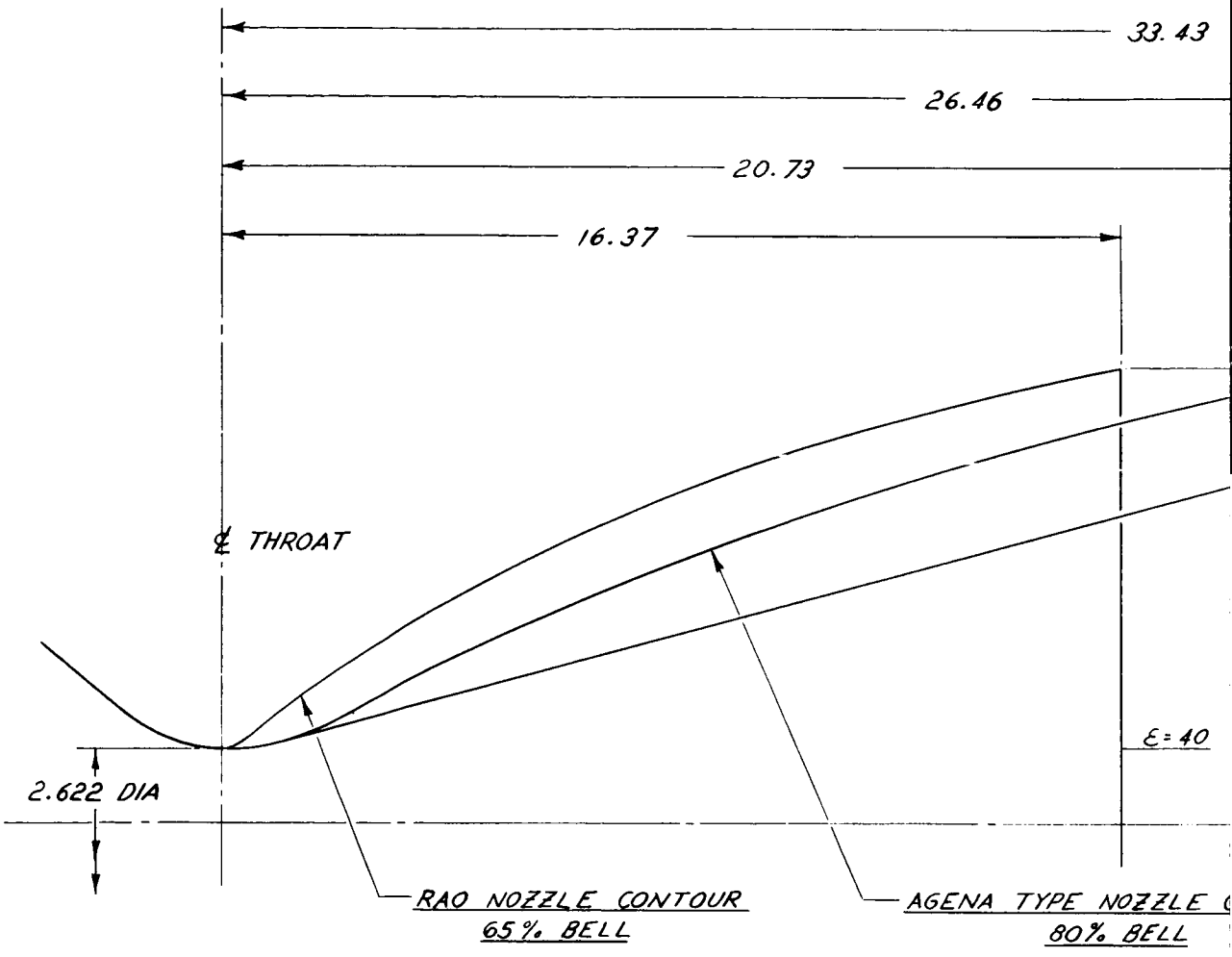

Form 0345 Rev. 1258 Sheet 1

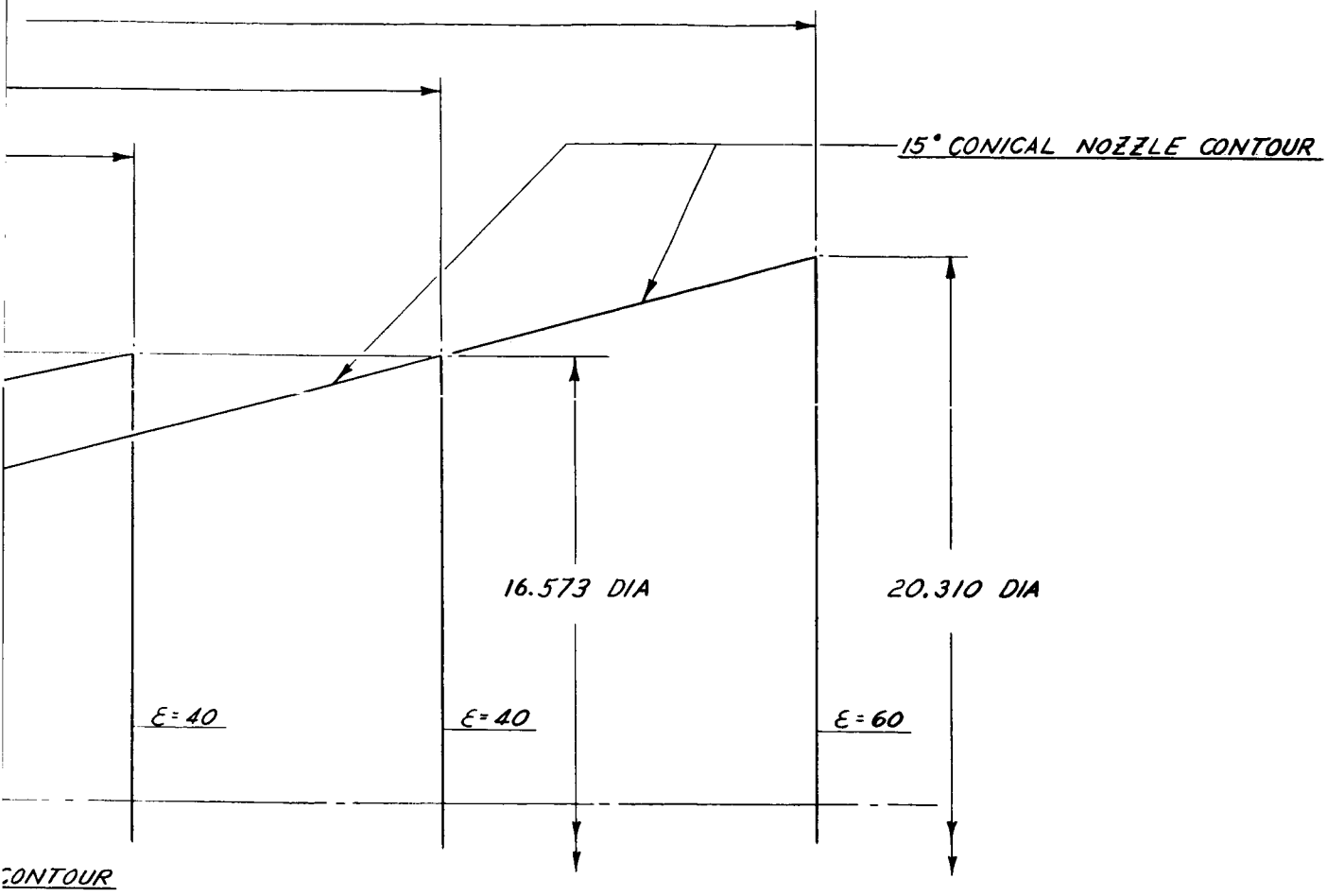

ALTITUDE NOZZLE CONTOURS

FIGURE 41